Research Square

Preprints are preliminary reports that have not undergone peer review.
They should not be considered conclusive, used to inform clinical practice,
or referenced by the media as validated information.

The developmental appearance of skeletal muscles in the human arm; their emergence as functional groups

Wouter Lamers

wh.lamers@maastrichtuniversity.nl

Maastricht University

Lisanne Sprik

https://orcid.org/0009-0009-6147-4924

Thomas Verlinden

Jill Hikspoors

Department of Anatomy & Embryology, Maastricht University https://orcid.org/0000-0003-2940-1812

Greet Mommen

Gabriela Morosan-Puopolo

Ruhr University Bochum

Eleonore Koehler

Article

Keywords:

Posted Date: November 16th, 2026

DOI: https://doi.org/10.21203/rs.3.rs-11469499/v1

License: This work is licensed under a Creative Commons Attribution 4.0 International License.
Read Full License

Additional Declarations: There is **NO** Competing Interest.

The developmental appearance of skeletal muscles in the human arm; their emergence as functional groups

Lisanne C. Sprik[1], Thomas J.M. Verlinden[1], Jill P.J.M. Hikspoors[1], Greet M.C. Mommen[1], Gabriela Moroşan-Puopolo[2], S. Eleonore Köhler[1], Wouter H. Lamers[1*]

1. Department of Anatomy & Embryology, Maastricht University, Maastricht, The Netherlands.

2. Department of Anatomy and Molecular Embryology, Ruhr University Bochum, Bochum, Germany

ORCID numbers:

Lisanne C. Sprik	0009-0009-6147-4924
Thomas J.M. Verlinden	0000-0002-0102-451X
Jill P.J.M. Hikspoors	0000-0003-2940-1812
Gabriela Moroşan-Puopolo	0000-0002-3135-0156
S. Eleonore Köhler	0000-0003-1977-9977
Wouter H. Lamers	0000-0003-3032-7824

Correspondence:

Wouter H Lamers MD, PhD

wh.lamers@maastrichtuniversity.nl

Acknowledgements

We express our gratitude to Drs. Maurice van den Hoff (AMC), Marco de Ruiter (LUMC), Annelieke Schepens (RadboudMC), Christoph Viebahn (Göttingen) and Beate Brand-Saberi (Bochum) for providing access to their institutional collections of human embryos and foetuses. We also extend our thanks to Dr. John Cork (New Orleans) for supplying additional digitized sections from the Virtual Human Embryo project. Special acknowledgment is given to Els Terwindt (Maastricht University) for her valuable technical assistance. Our appreciation goes to the bachelor students who contributed to this research during their academic internships. We are also thankful for the financial support provided by the 'Stichting Rijp'.

Author contributions

L.C.S. participated in data collection, analysis, and visualization, wrote the manuscript, and was responsible for formatting the figures. G.M.C.M. participated in the visualization of the structures in 3D. T.J.M.V., J.P.J.M.H., G.M.P., and S.E.K. participated in the data analysis and interpretation and edited the manuscript. W.H.L. conceived the study and supervised the interpretation of the data and the preparation of the manuscript.

Abstract

This study describes the morphogenesis and topography of the muscles, bones, nerves, and vessels that form in the upper extremity of human embryos. Between 4.5 and 5.5 weeks of development, myoblasts originating in somites C5-T1 migrate into the forelimb and start primary myogenesis. The ingrowth of a terminal nerve branch distinguishes pre-muscle from other nearby cell masses. We identified four dorsal and two ventral pre-muscle masses. Each pre-muscle mass differentiates into a functionally related set of muscles (e.g., flexors or extensors). The first pre-muscle mass appears at 5.5 weeks, and the first individual muscles at 6 weeks. Splitting of pre-muscle masses proceeds in a proximal-to-distal and superficial-to-deep sequence, but all muscles initiate secondary myogenesis simultaneously at 8 weeks. Resolving the sequence and topography of the splitting events allowed the composition of a dendrogram of the lineages of muscle masses. Too many or too few terminal-splitting steps account for adult variations.

Extended abstract

A comprehensive account of the timeline of the morphogenesis and topography of the individual muscles of the upper extremity of human embryos is presently not available. During Carnegie stages (CS) 13-16 (4.5-5.5 weeks of development), myoblasts originating in somites C5-T1 migrate into the forelimb and start primary myogenesis. Morphologically, these myoblasts are indistinguishable from the local lateral-plate cells. In addition to their position relative to the developing bones, arteries, and veins, the innervation of pre-muscle masses by the terminal branches of the brachial plexus proved a highly selective early marker for skeletal muscle identity. We observed the first pre-muscle mass at CS16. This mass split into dorsal and ventral pre-muscle masses at CS17. From these, four secondary dorsal and two secondary ventral pre-muscle masses emerged. Each of these masses differentiated into a functionally related set of muscles (flexors, extensors, endorotators, or exorotators). At CS17-18 (~6 weeks), the first individual muscles appeared in the shoulder region. In the arm, individual muscles became distinguishable between 6.5 and 8 weeks (CS19-23). In addition to this proximo-distal gradient in development, a superficial-to-deep gradient in pre-muscle mass differentiation exists in e.g. the endorotators of the arm, and the extensors and flexors of the wrist. In these cases, the largest, most superficial component first split off from such pre-muscle masses. Resolving the sequence and topographical location of the splitting events enabled construction of a dendrogram of the lineages of the arm's muscle masses. Variations in muscles are common. We observed an embryo with an extra biceps head and two embryos in which the terminal splitting event did not occur in 3 different muscle groups. Since muscles form between 5.5 and 8 weeks, most adult variations originate at this developmental stage. All muscles initiated secondary myogenesis at CS23.

1. Introduction

The cranial limb bud, or arm, develops from a fairly homogeneous, dividing cell mass into a highly organized structure in only 3.5 weeks (1). The mesenchymal cells that differentiate into cartilage, bone, and tendon are recruited locally from the lateral plate mesoderm (2), whereas myocytes originate from the dermomyotomal part of the somites. The neurons originate from the neural crest, and endothelium from mesodermal angioblasts (3). The pectoral/shoulder girdle (scapula and clavicle) derives from the dermomyotome, somatopleure, and neural crest (4). All these cells except those of the lateral plate must, therefore, migrate into the limb (5). This tightly regulated mechanism is not flawless, and variations between individuals have been described, especially regarding the limb muscles. Usually, these variants concern supernumerary muscle heads or muscles (6-9). Understanding the development of the muscular pattern in the embryonic limb bud and the interaction of this process with its environment may explain how, and perhaps why, variants can develop.

An early step in limb muscle development is the formation of metameric somites from the non-segmented paraxial mesoderm (10-12). The newly formed somites give rise to the sclerotome and the dermomyotome (13). The medially located non-migratory sclerotomes form the axial bones, tendons, and joints (14, 15), while the dermomyotomes give rise to dermis and myotomes. It should be kept in mind that the skeleton of the limbs, as opposed to the axial skeleton, derives from the lateral plate mesoderm. The epaxial (mediodorsal) part of the myotomes will give rise to intrinsic back muscles, and the hypaxial (ventrolateral) myotomes to the muscles of the trunk and limbs (16, 17).

The formation of the limb muscles starts with the migration of PAX3-positive muscle-progenitor cells from the ventrolateral dermomyotomal lip into the limb bud (17). The

myogenesis of the limb muscles can be subdivided into primary (Carnegie stage (CS)15-20; 5-7 weeks of development) and secondary myogenesis (7.5-10 weeks) (18). During primary myogenesis, the muscle-progenitor cells will invade the limb bud. Here they proliferate, differentiate, and fuse to form primary myofibres, which produce the muscle template of the limb (19). During secondary myogenesis, the primary myofibres fuse with other primary myofibres or foetal muscle-progenitor cells, and express PAX7 to form secondary myofibres (10-12). Muscle growth is an important part of secondary myogenesis. This description implies that the formation of individual muscles occurs during primary myogenesis. It was reported that after migration into the limbs, muscle-progenitor cells will form dorsal and ventral pre-muscle masses (12), but how these masses develop into individual muscles has only been addressed in a few studies (1, 20, 21).

In the present study, we report the timeline and topographic aspects of muscle formation in the upper limb, including the simultaneous development of bones, nerves and vessels. We show how the individual muscles in the developing human arm attain their shape, relative size, and position. We were able to identify and follow muscles from their earliest migration into the limb bud and their subsequent myogenesis by studying 32 embryos between 4 and 10 weeks of development with only small increments of development between them. We established that the muscle precursors ("pre-muscle cell masses") differ from the beginning from adjacent non-muscular cell masses in that their innervating nerve is present at a very early stage. Three-dimensional reconstruction of the respective cell masses, nerves, and vessels revealed that the topography of the forming muscle and bone masses is stable and predictable. The major outcome of our study is that the muscles of the upper extremity form by splitting into functional groups before the individual muscles have formed. The splitting is more extensive in the dorsal than the ventral pre-muscle masses. All arm muscles form between 5.5 and 8 weeks (Carnegie

stages 16-23). The splitting pattern is not flawless, and we have observed both too few and too many splits of muscle bellies. Importantly, the surrounding structures, such as nerves and arteries, are not affected by these variations.

2. Methods

2.1. Specimens

Stained serial sections of anonymized human embryos and foetuses were obtained from the Departments of Anatomy and Embryology of Leiden University Medical Centre (LUMC), Amsterdam University Medical Centre (AUMC, location AMC), Radboud University Medical Centre (RadboudUMC), Nijmegen, The Netherlands, the Georg-August-Universität, Göttingen (GOE) and the Ruhr University in Bochum, Germany. In addition, digital images were obtained from the Digitally Reproduced Embryonic Morphology (DREM) project (https://www.ehd.org/virtual-human-embryo/about.php; https://virtualhumanembryo.lsuhsc.edu/DREM/OnlineDisks.html), which are part of the Carnegie collection, Washington D.C., USA. The use of historical collections of anonymous human embryos and foetuses is exempt from ethical approval according to the Dutch regulations for the proper use of human tissue for (bio-)medical research purposes.

In this study, 32 well-preserved human embryos and foetuses between 4 and 10 weeks of development were studied (Table 1). Selection criteria for digitization were the histological quality of the sections [embryos undergo autolysis (maceration) soon after death], developmental stage, and plane of sectioning (almost exclusively transverse or sagittal). The criteria of O'Rahilly and Müller were used to correlate Carnegie stages of human development with days of development after fertilization (22). We have used the DREM embryos as

reference embryos, because they were specially selected from the Carnegie collection for that purpose (Virtual Human Embryo Project; https://virtualhumanembryo.lsuhsc.edu/). The ranking of the embryos was based on their correspondence to the DREM reference embryos, and on comparisons of heart, ear, lung, kidney, diaphragm and gut development.

2.2. Image acquisition, 3D-reconstruction and visualization were carried out as described previously (23, 24). Briefly (Figure S1), structures of interest were segmented manually and reconstructed three-dimensionally with Amira3D reconstruction software (version 2020.2; base package; ThermoFisher Scientific). Small deformations of individual sections due to the histological processing and stepwise stacking of sections were removed with Cinema4D software (MAXON Computer GmbH, Friedrichsdorf, Germany) and remodelled using the Amira model as template. The accuracy of the remodelling process was safeguarded by the simultaneous visualization of the original output from Amira in Cinema4D and the remodelled Cinema model. The Adobe Acrobat version 9 program (https://www.adobe.com) was used to transform the Cinema4D models into interactive 3D Portable Device Format (PDF) files.

2.3. Segmentation

We have studied the muscles of the arm, including the muscles that extend between the humerus, radius, or ulna on the one hand and the clavicle, scapula, ribcage, or spine on the other. The pectoralis major and latissimus dorsi muscles differ from the other included muscles in that they form in two steps, known as the “in-out” mechanism (25, 26). In addition to the muscles, bones, nerves, arteries, and veins were segmented in the embryos when present. A timeline of the reconstructed muscles in Amira was created (Figure S2). Comparing the reconstructions of the different embryos allowed us to establish the changes in size, shape, and position as a function of developmental time (Figure S3). Bones, nerves, arteries, and veins

functioned as local landmarks (Figure S4). Nerves were followed from their dorsal and ventral roots to their penetration into pre-muscle masses or muscles. Arteries entering the limbs were traced back to their origin from the dorsal aorta, and veins were followed to the point where they drained into the cardinal veins. A specific embryo is named in the text when we observed something for the first time or when a deviation from the other embryos within the same Carnegie stage was observed.

2.4. Growth of the bones

Length measurements of the humerus, radius and ulna were performed in Cinema 4D using the spline-pen function. A line was drawn along the entirety of the bone length and placed in the centre of the bone. The "coordinate manager" in Cinema 4D was used to determine the length of the line.

2.5. Orientation

The body axis is defined as the axis passing through the thoracic and lumbar vertebral column and is assumed to be perpendicular to the transverse plane (at the stages of development studied, the lumbar lordosis has not yet formed). To describe (changes in) the position of a structure relative to another structure or the observer, we use the terms cranial or caudal (equivalent to superior or inferior in adult human anatomy) for differences in position along the body axis, and ventral or dorsal (equivalent to anterior or posterior) for differences in position perpendicular to the body axis. Proximal (shoulder) and distal (fingers) refer to changes in position relative to the axis of the extremity (arm).

2.6. Nomenclature

Muscles are described in a proximal-to-distal order. Pre-muscle masses are used to describe the early stages in muscle development when the individual muscles must still split off from these masses, and the names of individual muscles are used when a muscle has separated from other (pre-) muscle (masses).

2.7. Three-dimensional reconstructions presented in PDF format.

In addition to the Figures, the evidence for our descriptions can be inspected in the corresponding interactive 3D-PDFs (Figures S5-10). The reader is, therefore, encouraged to read the text and inspect the corresponding interactive PDFs simultaneously. This is because their rotational options ("live" images) allow a much better understanding of the complex local topography than do "still" images and text. The 3D-PDFs can also be used to verify the identity of a structure in a Figure: after opening and positioning the reconstruction in the same view as in the Figure, marking or unmarking a structure in the model tree will link the structure to a name. Each of the stages of human development we studied is represented by a 3D-PDF reconstruction.

Table 1. Overview of embryos studied. Embryos are identified by their Carnegie stage (e.g., CS15), and the presence of advanced features (embryo CS15-4 has, for example, more advanced features than embryo CS15-3). The DREM embryos were considered as reference embryos, because they were selected as typical examples of their stage (https://virtualhumanembryo.lsuhsc.edu/DREM/OnlineDisks.html). CRL: Crown-rump length, CS: Carnegie stage; AMC: Academic Medical Centre, Amsterdam; DREM: Carnegie collection from the Digitally Reproduced Embryonic Morphology project; GOE: Göttingen; LUMC: Leiden University Medical Centre; H&E*:* Haematoxylin and Eosin; H&A: Haematoxylin and Azophloxin; HMH: Held's Molybdenum Hematoxylin; D-e-g: Delafield-eosin-gold orange; X: indifferent. Both arms were reconstructed in all models except the embryos with a postfix^{+} where only one arm is (partially) reconstructed, *Crown rump length estimated based on the number of sections in CS14-1 and CS16-2 and the longest section in CS17-2.

Age	Embryo	Collection	Plane	Staining	CRL (mm)	Sex	Section thickness (µm)	3D-pdf
CS12-1	1954-08-10	GOE	Sagittal	HMH	2.6	X	10	No
CS12-2	S8943	DREM	Transversal	H&E	3.9	X	8	No
CS13-1	S836	DREM	Transversal	Alum cochineal	4.0	X	15	No
CS13-2	1949-08-22	GOE	Sagittal	H&E (D-e-g)	4.2	X	10	No
CS14-1	S2201	AMC	Transversal	H&A	4.5*	X	10	No
CS14-2	S5029	AMC	Sagittal	H&E	7.0	X	7	No
CS14-3	1950-09-13	GOE	Sagittal	H&E (D-e-g)	6.5	X	10	No
CS14-4	S6502	DREM	Transversal	H&E, silver	6.7	X	10	No
CS15-1	1958-12-22	GOE	Sagittal	H&E (D-e-g)	7.8	X	10	No
CS15-2	1958-06-10	GOE	Sagittal	H&E (D-e-g)	7.2	X	10	No
CS15-3	S721	DREM	Transversal	H&E	9.0	X	15	No
CS15-4	1954-09-15	GOE	Sagittal	H&E (D-e-g)	9.0	X	10	No
CS15-5	1952-06-08	GOE	Sagittal	H&E (D-e-g)	8.9	X	10	No
CS16-1	S6517	DREM	Transversal	Alum cochineal	10.5	X	8	No
CS16-2^{+}	S2213	AMC	Transversal	H&A	6.8*	X	10	Yes
CS16-3	1946-07-20	GOE	Sagittal	H&E (D-e-g)	10.0	X	10	No
CS17-1	S6520	DREM	Transversal	Alum cochineal, Silver	14.2	X	10	Yes
CS17-2	S5032	AMC	Sagittal	H&E	8.5*	X	7	No
CS17-3	1950-12-08	GOE	Sagittal	H&E (D-e-g)	13.5	X	10	No
CS18-1	S4430	DREM	Transversal	Alum cochineal	14.0	Female	15	Yes
CS18-2	1947-06-19	GOE	Sagittal	H&E (D-e-g)	14.0	Female	10	Yes
CS18-3	S34	LUMC	Sagittal	H&E	19.0	Female	10	No
CS19-1	EYO-226	Bochum	Sagittal	H&E, Trichrome and Azan	16.0	Male	10	No
CS19-2	1949-06-22	GOE	Sagittal	H&E (D-e-g)	17.5	Female	10	Yes

CS20	S462	DREM	Transversal	Alum cochineal	20.0	Male	40	No
CS21^{+}	EYO-283	Bochum	Sagittal	H&E, Trichrome and Azan	21.0	Female	10	No
CS23-1	S9226	DREM	Transversal	Azan	31.0	Male	12	No
CS23-2^{+}	EYO-295	Bochum	Sagittal	H&E, Trichrome and Azan	32.0	Male	10	No
CS23-3	S4141	AMC	Transversal	H&A	35.0	Female	10	Yes
9 weeks	S57	LUMC	Transversal	H&E	50.0	Female	10	No
10 weeks-1^{+}	S4908	AMC	Transversal	H&A	50.0	Female	10	No
10 weeks-2^{+}	S1507	AMC	Transversal	H&A	40.0	Male	10	No

3.1 Results

From mesenchymal condensations to pre-muscle masses

Before describing the formation of individual muscles and their topography in the human embryonic arm, we briefly describe their temporal development as a group, from the establishment of a single central mesenchymal mass to the onset of separately identifiable muscles. Key additional structural features in this development are the nerves, bones, and vessels. We could identify (pre-)muscle masses because they become innervated immediately after formation, whereas non-muscle masses (primarily forming bones) attract nerves only later. We could subsequently follow individual muscles in embryos because of their unique topographic position.

3.1.1. The early formation of the upper limb and its nerves, muscles, and vessels

In Carnegie stage 12 (CS12-2; 26 somites formed; Figure 1A1-C1), the coelomic epithelium at the site of the emerging limb bud (arrow in Figure 1B1) is thick and begins to bulge outward but does not yet define the boundary of the upper limb bud. This bulge is not yet visible in an earlier CS12 embryo (CS12-1; 23 somites) but becomes recognizable as a ridge (red dotted line, Figure 1C2) on the lateral side of the embryonic body when ≥30 somites have formed (early CS13; Figure 1A2-C2). At this stage, the limb bud extends between somites C5 and Th1. Histologically, the anlage consists of a central dense, near-homogeneous mesenchymal mass that is covered with a well-developed epithelial layer. Medially, the dense mesenchyme does not have a well-defined boundary, and no signs of a penetrating nerve, artery, or vein are apparent. Cranial (arrow in Figure 1B2) and caudal (not visible in the Figure) to the limb bud, the periodic epithelial lips of the ventrolateral dermomyotomes are visible, but the muscle-progenitor cells entering the limb bud no longer show a visible segmental organization. In CS14 (Figure 1A3-C3), the now visible limb bud resembles a pebble (Figure 1C3). Its mesenchymal

mass is densely packed compared to the loose mesenchyme of the embryonic trunk, and the periphery of the limb bud has a denser staining (Figure 1A3-B3). The nerves, veins, and forming artery enter the limb bud (Figures 2A, 3A). At their penetration into the dense mesenchyme of the limb bud, the brachial plexus has formed its lateral, posterior, and medial cords (Figure 1A3-B3, D3).

In CS15 embryos, the limb bud (Figures 1A4-D4 and 4A1-C1) has undergone axial elongation. Its central mesenchyme remains a dense mass, which is bordered by loose mesenchyme of the trunk. The axillar region contains a prominent portion of the dense mesenchyme that is found in the limb bud (Figure 1B4-1B6). The marginal vein delineates the limb bud, and the artery penetrates the proximal part of the limb bud (Figure 2B).

3.1.2 The forming of separate pre-muscle masses

The outer appearance of the limb bud in CS16 embryos (Figures 1C5, 4C1-C2 and S5) resembles that in CS15. The dense central mesenchyme remains present but is now deeply penetrated by the artery and the large nerves (Figures 2C and 3C). The cords of the brachial plexus can be distinguished more easily due to the greater distance between them (Figure 3C). However, the major distal nerve branches, such as the radial nerve, still need to develop. Dorsally, loose mesenchyme has appeared between the dense central mesenchymal mass and the skin. A single very dense mesenchymal mass at the base of the pebble (asterisk in Figures 1A5, 1B5 and 4A2) is the cartilaginous precursor of the humerus. The precursors of ulna and radius have also formed but are still noticeably shorter than the humerus (Figure 4B2). Between 6 and 10 weeks of development, the humerus, ulna, and radius all grow exponentially, meaning they have a fixed growth fraction (Figure 5). Muscle-mass precursors first become identifiable at this stage (Figures 1B5 yellow contour, 4A2 and B2). They can be distinguished from the

developing bones by their histological architecture, topographical location and presence of nerves: the bones occupy a central position in the limb; their cells are more compactly arranged than myocytes and appear brighter in the available stainings. The pre-muscle mass is more elongated along the humerus, where it only covers the dorsal part of the bone and ends around the proximal part of the ulna (Figure 4B2). Note that part of the pre-muscle mass precursor does not enter the limb bud but extends caudally in the back towards the ribs (arrows in Figure 4B2).

In CS17 embryos (Figures 1C6, 4B3, 4C3 and S6), the limb bud extends outward, with flexion in the elbow. The central dense mesenchymal mass and the dorsal subcutaneous patch of loose mesenchyme are still present. The nerves distal to the brachial plexus have all formed and extend throughout the limb (Figure 3D). The vessels look similar as in the previous stage (Figure 2D). A pre-osseous tissue mass has developed in the hand, but separate hand bones cannot yet be identified (Figure S11). Pre-muscle masses have formed along both the ventral and dorsal sides of the humerus. The dorsal mass, which covers most of the scapula, extends between the shoulder region and the hand (red coloured structure, Figure 4B3). The ventral mass, which is absent from the scapula, is only present between the humerus and the hand (blue structure, Figure 4B3). The cells making up these pre-muscle masses can now be even better distinguished from the surrounding tissues by the presence of nerves and their higher contrast between muscle and surrounding connective tissue (compare inserts of Figure 4A2 and 4A3). In the shoulder region, the pre-muscle mass retains the shape it had in CS16, but its caudal extension in the back projects towards the dorsal side of the thorax (Figure 4B2 and 4B3, arrows). The dorsal pre-muscle mass contains holes in the shoulder region and near the transition of the upper arm into the forearm, whereas the ventral mass does not (Figure 4B3). We hypothesize that the holes reflect splitting activity in the dorsal pre-muscle mass. The

ventral mass shows invaginations on its most proximal and most distal parts, again probably precluding its splitting.

The carpals, metacarpals, and proximal phalanges are visible from CS18 (Figure S7) onwards, while the middle and distal phalanges appear at CS20. In this period (7^{th} week), the dorsal and ventral forearm pre-muscle masses split into multiple smaller masses (Figures 4A4, B4, 6 and Table 2). The nerves are present in the pre-muscle masses before their splitting into individual muscles (Figure 3E and 3G). The vessels generate a more complex network in the hand (Figure 2E and 2F). In the shoulder region, the dorsal mass splits into an endorotator mass (deltoid, supraspinatus, teres minor and infraspinatus muscles) and an exorotator mass of the arm (latissimus dorsi, teres major and subscapularis muscles). The dorsal mass alongside the humerus will form the extensor mass of the elbow (triceps muscle) and that corresponding to the extensor muscles of the wrist and digits. The ventral pre-muscle mass on the forearm splits into three masses: the mass on the ventral side of the humerus forms the flexors of the elbow (biceps brachii, coracobrachialis and brachialis muscles), that in the forearm the flexors of the wrist and digits, and that in the palm the intrinsic muscles of the hand. The development of individual muscles proceeds in a proximal-to-distal direction over a period of 2 weeks (7 Carnegie stages: CS16-CS23; Figure 6, Table 2). Virtually all muscles described in adult anatomy have, therefore, formed at the end of the embryonic period. By that time, joint cavities have formed in the shoulder and elbow joints, but not yet in those of the wrist or hand. Only the extensor carpi radialis longus and brevis have split into separate muscles in one of the 2 available 10-week-old foetuses (10-week-1), while the abductor pollicis longus and the extensor pollicis brevis muscles remain one mass in both 10-week-old foetuses.

3.2 From pre-muscle masses to topography and function

To describe the development of the muscles in more detail, we grouped them into the masses from which they derive. The muscles of a mass appear to represent the functional units around the joint they span.

3.2.2. Development of the exorotators of the arm

The first pre-muscle mass in the limb to completely split into individual muscles is that of the latissimus dorsi, teres major, and subscapularis muscles, all exorotators of the arm. Based on its definitive position and innervation, this muscle group can first be localized in embryo CS17-1 (Figure 7A1-C1), although the split is still incomplete, but has progressed in the more advanced embryo CS17-2 (Figure 7C2). In embryo CS18-1, the three muscles are individually identifiable, but their contours still touch (Figure 7C3). At this stage, the muscles have formed a cone towards the humerus, but do not yet attach to the bone (Figure 7A2 and B2). In embryos CS18-2 (Figures 7A3 and B3, and S8) and CS18-3 (not shown), the latissimus dorsi has attached to the humerus. In embryos CS19-2 (Figure S9) and CS20 (not shown), loose connective tissue has formed between the muscles, so that boundaries are better distinguishable (dotted lines, Figure 7A4-C4). In the CS23 embryos (Figure S10), myofibres and a perimysium become identifiable, indicating that the transition of primary into secondary myogenesis has started (Figure 7A5-C5, Table 2).

3.2.3. Development of the pectoralis major, minor and subclavius muscles

At CS16, the pectoral nerves have penetrated the pre-muscle mass of the pectoralis muscles on their medial side (Figure 8A1-A3). In embryo CS17-1 (Figure 8B1-B3), the subclavius muscle is present between the scapula and the first rib, whereas the pectoralis muscles still form a single mass between the humerus and the lateral part of the rib cage (27). In embryo CS17-3 and all CS18 embryos, the pectoralis major and minor are separately identifiable (Figure 8C1-C3). The

triangular pectoralis major has attachments to the clavicle and the humerus and extends over the first four ribs. The smaller pectoralis minor extends between the scapula and the second rib. In CS23 embryos, both muscles occupy their definitive position (Figure 8D1-D3).

3.2.4. Development of the endorotators of the arm

The pre-muscle mass of the deltoid, teres minor, infraspinatus and supraspinatus muscles is innervated by the suprascapular and axillary nerves (both originating in cervical roots 5 and 6 (Figure 9C1 and C4). Its composing muscles follow a superficial-to-deep temporal gradient in splitting. In embryo CS17-1 (Figure 9A1 and B1), the dorsal mass wraps around the scapula and humerus to acquire its definitive position. Two days later, in CS18, the deltoid has become a separate muscle that covers the 3 remaining, still unsplit muscles (Figure 10A1-C1). Its 3 heads do, however, not yet attach to the scapular spine, acromion, and clavicle (Figure 9A2-C2 and A3-C3). All muscles can be identified individually in embryo CS19-2 (Figures 9A4-C4 and 10A2-C2). The endorotator muscles in the CS23 embryos hardly differ from those at CS20 (Figure 9A5-C5).

3.2.5. Development of the flexors of the elbow

The mass of the biceps brachii, coracobrachialis and brachialis, which are commonly denoted as flexors of the elbow, derives from the ventral mass that is first seen in embryo CS17-1 (Figure 11A1). In the more advanced embryo CS17-3, this mass is already separate and encloses the musculocutaneous nerve (Figure 11B1 and C1). In embryo CS18-1, the still unsplit pre-muscle mass has acquired the approximate shape of the muscles it will form (Figure 11A2 and B2). In embryo CS18-2, the coracobrachialis has split from this pre-muscle mass (Figure 11A3-C3). Furthermore, the long and short heads of the biceps brachii are recognizable. Embryo CS19-2 resembles embryo CS18-2, except that the short head of the biceps has separated from the pre-

muscle mass near the radius and ulna (Figure 11A4-C4). The microscopic anatomy of embryos CS18-2 and CS19-2 shows that the short head of the biceps and the coracobrachialis are located close to each other, and that the musculocutaneous nerve courses in between. In embryo CS23-3, all three muscles have separated, and the brachialis and the biceps brachii can be identified (Figure 11A5-C5).

3.2.6. Development of the extensors of the elbow

Embryo CS17-1 (Figure 4B3) shows that, based on location, the triceps is derived from the dorsal pre-muscle mass. In the more advanced embryo CS17-3, the individual heads of the triceps cannot be identified yet (Figure 12B1). In embryo CS18-1, the triceps mass has acquired its adult shape, but its proximal part still does not reach the scapula (Figure 12A1). In embryo CS18-2, the triceps mass has separated into long (green), lateral (purple), and medial (pink) heads (Figure 12A2 and B2). In this embryo, the long head almost reaches the scapula, whereas the proximal part of the lateral head only reaches the middle of the humerus. The medial head is smallest and has a round shape. In embryo CS19-2, the medial and lateral heads have increased in size, and the distance between all three heads has increased. In this embryo, both the medial and long heads have further increased in size (Figure 12A3 and B3). In embryo CS23-3, the long and lateral heads have established their proximal attachments (Figure 12A4 and B4).

3.2.7. Development of the flexors of the wrist and digits

The flexor muscles in the forearm, like the flexors of the elbow, derive from the ventral pre-muscle mass (embryo CS17-1, Figure 4B3). The flexor carpi ulnaris is the first identifiable separate muscle in this group (embryo CS18-1, Figure 13B1) and already comprises the ulnar nerve. The muscle appears as a thin and elongated structure but has no attachments to the bones

yet. The remaining flexor muscles first form superficial and deep pre-muscle masses (Figure 13A1 and B1).

3.2.7.1. Superficial flexors

The superficial flexor mass in embryo CS18-1 extends from the humerus towards the hand region and still comprises the future distal head of the flexor digitorum superficialis, flexor carpi radialis, pronator teres and palmaris longus (Figure 6, Table 2). In the more advanced embryo CS18-2, the distal head of the flexor digitorum superficialis has split from the superficial mass and lies in the hand (Figure 13A2 and B2). The flexor carpi ulnaris now also reaches the hand (Figure 13B2). The palmaris longus has a proximal attachment on the humerus but still ends blind near the wrist. This configuration is also seen in embryo CS19-1 (Figure 13A3). In embryo CS19-2, the superficial mass has split into the flexor carpi radialis and pronator teres (Figure 13A4 and B4). The flexor carpi ulnaris already reaches the hand.

3.2.7.2. Deep flexors

The deep mass will give rise to the proximal head of the flexor digitorum superficialis, the entire flexor digitorum profundus, flexor pollicis longus, and pronator quadratus (Figure 6, Table 2). In all CS18 embryos, the deep mass is attached to the humerus and reaches digits II-V. In embryo CS19-2, the pronator quadratus and the proximal head of the flexor digitorum superficialis are distinguishable from the deep mass, which has formed an extra extension to digit I. In embryo CS21, the deep mass has split into the flexor pollicis longus and flexor digitorum profundus (Figure 13A5). In embryo CS23-2 and the 10-week-old-1 foetus, the distal head of the flexor digitorum superficialis has migrated into the hand and fused with the proximal head to form the flexor digitorum superficialis (Figure 13B5).

3.2.8. Development of the extensors of the wrist and digits

The extensors of the wrist and digits have, like the flexors, superficial and deep masses (embryo CS18-1; Figure 14A1). The superficial mass forms the extensor carpi ulnaris, anconeus, extensor digitorum and extensor digiti minimi, and extends from the humerus to the hand, where it reaches digits III-V (Figure 6, Table 2). The deep mass (the extensor indicis, extensor pollicis longus, abductor pollicis longus, extensor pollicis brevis, brachioradialis, supinator, and extensor carpi radialis longus and brevis) is covered by the superficial muscles (Figures 6 and 14A1, Table 2). The deep mass is proximally attached to the humerus and distally to the ulna and extends to the hand, where it has a small extension to digit II. In the more advanced embryo CS17-3, superficial and deep masses each split into two sub-masses (Figure 14B1). The extensor compartment of the right arm of embryo CS18-2 splits more slowly in the forearm , since only two extensor masses can be observed instead of the five masses found in the left arm (Figure 15).

3.2.8.1. Superficial extensors

The superficial mass-I ("Sup-I") generates the extensor carpi ulnaris and anconeus, while superficial mass-II ("Sup-II") splits into the extensor digitorum and extensor digiti minimi. In embryo CS18-2, mass Sup-I extends from the humerus to the wrist lateral of the ulna with the arm in pronation. Mass Sup-II, the biggest and most superficial mass, extends from the humerus to digits II-V, and has a hole near digit V (Figure 14A2 and B2, black arrow). In embryo CS19-2, the anconeus and extensor carpi ulnaris have become individual muscles (Figure 14A3 and B3). The Sup-II mass has developed an additional hole near digit III (Figure 14A3, black arrows). The extensor carpi ulnaris extends from the humerus to the hand. In CS23, the Sup-II mass has split into the extensor digiti minimi extending from the radius to the metacarpal of

digit V and the extensor digitorum which reaches from the humerus to the distal phalanges of digits II-IV (Figure 14A4-B4).

3.2.8.2. Deep extensors

The mass of the deep extensors has split into deep mass-I ("Deep-I") that will form the brachioradialis, supinator, and the extensor carpi radialis longus and brevis, and deep mass-II ("Deep-II") which will split into the abductor pollicis longus, extensor pollicis brevis, extensor indicis and extensor pollicis longus. In embryo CS18-2, the supinator is the first individual extensor muscle from mass Deep-I that can be delineated (Figure 14A2 and B2). Mass Deep-I attaches proximally to the humerus and extends across the radius to the wrist. Mass Deep-II has further split into Deep-IIa, which will develop the abductor pollicis longus and the extensor pollicis brevis, and mass Deep-IIb, which will split into the extensor pollicis longus and extensor indicis. Mass Deep-IIa is mostly located on the radius and extends from the humerus to the wrist and digits I and II, whereas mass Deep-IIb has a similar shape as Deep-IIa but is located mostly on the ulna and digits III and IV. In embryo CS19-2, the Deep-IIa mass has attached proximally between the ulna and radius and crosses the radius diagonally to the radial side of the wrist. The Deep-IIa and IIb masses still have a similar shape, but Deep-IIb is located more distally on the forearm and has two heads, one of which extends to digit I and the other to digit II (Figure 14A3 and B3). In embryo CS23-3, mass Deep-I has split into the brachioradialis and the extensor carpi radialis mass. The tendons of the extensor carpi radialis longus and brevis can already be identified, but the muscle bellies must still split. Mass Deep-IIa is still a single mass, but two tendons with different attachments to digit I have formed. Mass Deep-IIb has split into the extensor pollicis longus, which has a distal attachment to the distal phalanges of digit I, and the extensor indicis with a distal attachment to digit II (Figure 14A4 and B4). In 10-week-old foetuses, the extensor carpi radialis longus and brevis have clearly

separated, but this was not yet the case for the abductor pollicis longus and extensor pollicis brevis, even though the tendons of these muscles are already two separate entities.

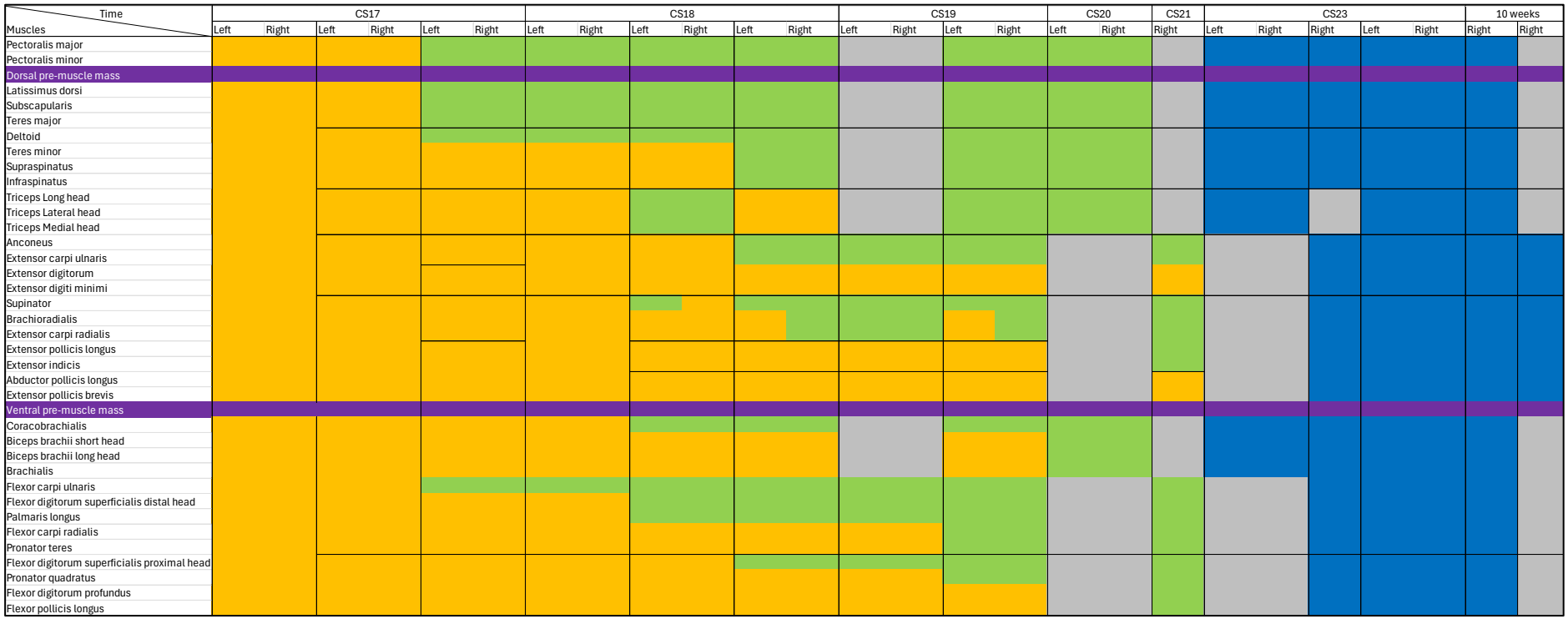
3.2.9. Variants in the development of the muscles of the upper extremity

During our analysis of the fate of the muscle (sub-)masses, we observed variants. These variants included differences in the developmental timing (retardation) and the number of splits in pre-muscle masses (too few or too many). These variants were observed between left and right sides, within one embryo or between embryos with comparable stages of development.

3.2.9.1. Several splitting variants in one embryo (CS23-3)

In embryo CS19-2, we identified the infraspinatus and teres minor as separate muscles for the first time (Figure 9A4-C4). In embryo CS23-3, in contrast, the infraspinatus and teres minor are still present as a single pre-muscle mass on both sides of the body (Figures 16 and S12). Comparison with embryo CS19-2 shows that these muscles should have split at that stage. We, therefore, conclude that splitting of the endorotator pre-muscle mass in the left arm was retarded on both sides in embryo CS23-3 (Figures 16 and S12). This embryo also has a muscle mass that extends from the middle of the humerus and merges with the tendon of the biceps brachii (Figures 16 and S13). The muscle mass has separated from that of the brachialis muscle and represents a third head of the biceps muscle. In that same CS23 embryo, finally, the mass of the flexor digitorum profundus and flexor pollicis longus muscles has not split in either arm (Figures 16 and S14). Since splitting of this mass is observed in a CS21 embryo and in embryos of a similar developmental age, the flexor digitorum profundus and flexor pollicis longus have not or not yet split in embryo CS23-3. The absence of timely splitting in three different pre-muscle masses of a single embryo suggests a common, more general cause for the observed delays.

Table 2. Overview of muscle splitting. The X-axis represents the timeline, with less advanced embryos to the left and more advanced embryos to the right within one stage. The switch from orange to green indicates complete splitting of a muscle mass. Temporally, splitting proceeds from proximal to distal and superficial to deep. Blue indicates the initiation of secondary myogenesis (appearance of muscle fibres). Grey indicates no data available.



4. Discussion

In the present study, we provide a detailed account of the developmental timeline and topography of the pre-muscle masses that form in the shoulder girdle and arms of human embryos. We have also paid attention to the development of nerves, bones, and vessels. Between 4.5 and 5.5 weeks of development (Carnegie stages 13-16), myoblasts originating in somites C5-T1 migrate into the forelimb, and primary myogenesis starts (28, 29). Morphologically, these myoblasts are indistinguishable from the resident cells in the limb (Figure 1B2 and 1B3). The ingrowth of the nerves of the brachial plexus into the pre-muscle masses, therefore, proved a valuable early and permanent marker for the identification of cell groups as pre-muscle masses. The primary dorsal and ventral pre-muscle masses were observed first (Figure 4B2 and 4B3). From these, four secondary dorsal and two secondary ventral pre-muscle masses emerged (Figure 6). Each of these pre-muscle masses differentiated into a functionally related set of muscles, such as flexors, extensors, endorotators, or exorotators. The first pre-muscle mass was observed proximally at CS16 (~5.5 weeks). Soon thereafter (CS17-18, ~6 weeks), the first individual muscles in the shoulder region were identified. Distally in the arm, individual muscles became distinguishable between 6.5 and 8 weeks (CS19-23). In addition to this proximo-distal gradient in development, we also observed a superficial-to-deep gradient in pre-muscle mass differentiation in e.g. the endorotators of the arm and the extensors and flexors of the wrist. The superficially located and usually largest component first splits from the pre-muscle mass. Resolving the timing, sequence and topographical location of the splitting events then allowed us to construct a dendrogram of the lineages of the original dorsal and ventral pre-muscle masses of the arm. There was no fixed time between muscle splitting and the formation of muscle fibres since all muscles initiated secondary myogenesis at CS23 (Table 2). Notwithstanding the induction of myogenesis by sex steroid hormones (30), the differentiation of primary to secondary myoblasts is not influenced by the sex of the embryo,

probably because the “masculinization programming period” only starts at ~8 weeks of development (31, 32).

4.1. Reliability of the morphological method to identify and follow pre-muscle masses

The overall architecture of the forming limb remained largely unchanged between CS15 and CS17 (5-5.5 weeks), when the initial mesenchymal pre-muscle mass migrates to its destination in the forelimb, and between CS17 and CS23 (5.5 and 8 weeks), when primary myogenesis is completed. Immunological techniques show, however, that the limb bud already contains primary myoblasts at the migratory stage of development (33). The bones form in the centre of the limb bud, and the pre-muscle masses surround this skeletal primordium (34). The main artery of the forelimb is a central structure that courses in a distal direction close to the bone, possibly because bone formation requires oxygen (35). The artery and nerves penetrate the limb along the same timeline (36, 37). The veins of the limb bud drain into the marginal vein of the limb bud at CS14 (38). Before the completion of primary myogenesis, pre-muscle masses differ from pre-osseous masses by their innervation. Our 3D-reconstructions allow us to identify innervated structures even when the nerves are in a different plane of section than the pre-muscle masses (34). Finally, we could validate name assignments to pre-muscle masses, because 32 developmentally closely spaced embryos between 4.5 and 10 weeks of development were available for analysis.

4.2. Earlier studies

Although the study of limb development based on histological sections is not a novel approach, we added not only interactive 3D reconstructions to the existing studies but also studied the complete upper limbs from shoulder girdle to complete digits in a large number of embryos and foetuses over a wide time range (1, 21, 34). Recently, similar studies were also carried out with

newer techniques, such as whole-mount immunostaining and optical projection tomography (20, 39). Of these, Diogo *et al.* (20) based their description on 10 embryos and early foetuses between 5.5 and 9 weeks of development (Table 2 in (20)) that were obtained from Belle *et al.* (40). They emphasized that their data confirm their earlier reports on the transient presence of several atavistic muscles, whereas we interpreted the variations we observed only as either too many or too few splitting rounds in a particular pre-muscle mass. These interpretations are not necessarily mutually exclusive; however, the regulatory mechanisms underlying the number of consecutive splitting events can probably be clarified experimentally but establishing whether the effects of fewer or more splitting rounds reveal atavistic phenotypes may prove challenging. The example of the dorsoepitrochlearis muscle is a case in point. While Diogo et al (20) consider the proximal head of the flexor digitorum superficialis muscle a typical example of an atavistic muscle (the dorsoepitrochlearis), we and others (41-44) consider it to be an example of proximal and distal bellies of a long, possibly digastric muscle that fuses. Of interest, we did not observe variations in the final degree of fusion of both heads of the flexor digitorum superficialis in CS23, but variations have been described where fusion of the heads of this muscle was incomplete (41). Wilde *et al.* (21, 39) studied 7 human embryos between Carnegie stages 6.5 and 7.5 weeks of development and could show the progression of splitting between the extensor pollicis and the abductor pollicis longus. Gräfenberg's study (21, 39) focused on the forearm and hand with special attention to the formation of the bones. Lewis (1902 (1)) and Bardeen (1906 (45)) studied the arm and the leg in the same group of embryos and described them in great detail. While Lewis was interested in muscle, cartilage, and nerve development, Bardeen was more focused on innervation and variations in muscle development. Our study comprised the entire arm, including structures such as nerves, bones, and arteries, which provide additional topographic information. Together with the topographic information of our

3D reconstructions, this approach allowed us to determine the origin of the tissue mass of each muscle and, hence, to which lineage it belongs.

4.3. How predictable are the splitting patterns and what type of variants are observed?

Our study comprised 28 embryos and early foetuses between 5 and 10 weeks of development. This comparatively large study population allowed us to determine which developmental changes occurred at a particular age and to identify variations between different embryos of the same developmental age. The variants are presented as fewer or more muscle bellies in a composite muscle (Figure S12). Examples are the teres minor muscle, which either derives from the same mass as the infraspinatus and supraspinatus muscles ((1); present study) or, from the deltoid mass based on its muscle fibre direction and its distance from the infraspinatus (20). Our argument is based on the completion of the splitting of the large deltoid muscle well before the final split of the relatively small teres minor, infraspinatus and supraspinatus muscles and on the dual innervation of the teres minor by the axillary and suprascapular nerves (Figures 5, 8 and 9). The increasing distance of the deltoid muscle from the remaining pre-muscle mass due to the accumulation of connective tissue underscores this interpretation.

4.4. What type of variants are found?

Variants of arm muscles that can be ascribed to fewer or more splitting events than normal are fairly common (6-9) and were observed in our cohort in 1 of the 13 embryos that were old enough (≥6.5 weeks) to have undergone the developmental splitting event (Figures 6, 15, 16 and S12-15). Some variants arose in embryos that had been expected to undergo the final split based on their developmental age, such as embryo CS23-3, in which 2 splitting events had not yet taken place at Carnegie stages 19 and 21. Furthermore, embryo CS23-3 had an extra head of the biceps muscle due to an additional split. In this embryo, the two missing splitting events

were bilateral, whereas the supernumerary split was only present in the left arm (Figures 15, 16 and S15). Of note, this embryo did not suffer from splitting defects in the leg or intrinsic back muscles (unpublished observations). From these observations and arguments, we conclude that the definitive muscle pattern is determined in the 8th week of embryonic development. The development of embryos with too few or too many split muscle bellies proceeds not visibly different from that in embryos with the normal splitting pattern of their muscles (see below). We, therefore, also argue that each limb can be considered as a separate sample in an analysis of limb development.

4.5. Functional significance of muscle splitting in the arm (Figure 6)

Figure 6 shows that the number of splitting nodes is substantial, but the functional impact of the position in the splitting order seems limited (6, 8). We, therefore, hypothesize that more or fewer splitting events lead to small changes in the course of muscles and, hence, functionality. Of note, however, cases in which muscle variations cause clinically relevant problems have also been reported. Examples are nerve compression in the pronator teres syndrome and median compression syndrome (46, 47).

At first sight, a well-developed forearm muscle like the brachioradialis challenges our hypothesis. The muscle is primarily responsible for flexing the forearm. However, the brachioradialis muscle is also generally accepted to be part of the dorsal (posterior) compartment of the forearm muscles and is innervated by the radial nerve, which classifies the muscle as a component of the extensor pre-muscle mass (Figure 6). Rather than an exception to our hypothesis that muscle splitting enables adaptive topographic optimization for a modified function (the capacity to flex rather than extend the elbow), we hypothesize that the migration of the brachioradial mass into a ventral (anterior) compartment of the arm is a rather extreme

example that splitting of pre-muscle masses can optimize the topographic aspects of a new function.

4.6. What is the role of vessels and nerves in muscle development?

In chick embryos, the presence of vessels seems to facilitate muscle splitting, whereas inhibition of vessel formation has the opposite effect (48). In our study, we see a close relation between the presence of nerves and arteries in the centre of the arm and the presence of pre-muscle masses which are about to split. We emphasize the apparent importance of topography, because the dermomyotomal segments of the somites that participate in the development of the limb bud are no longer individually recognizable once their cells have started to migrate into the forming limb bud. In contrast, the dermomyotomes that border the limb-forming segments cranially and caudally temporarily retain the epithelial structure of their segmentally delimited ventrolateral lips. Starting at CS14, three main nerve branches penetrate the pre-muscle mass of the limb bud. Using our 3D-reconstructions, we have located the position of the entrance of the nerves into the limb bud to the level of the lateral, posterior (dorsal), and medial cords of the brachial plexus, that is, in the armpit. These nerves also split, since we observed that all pre-muscle masses are innervated by a separate nerve branch.

For proper development of a regenerating limb in salamanders (urodele amphibians), the presence of a nerve is mandatory (49, 50). In aneural duck embryos, muscle development is affected, with absent myofibre formation and extensive cell death. In paralyzed ducks, on the other hand, muscle development is slowed down, but myofibres are formed, and cell death is less abundant (51). Mammalian embryos show a more diverse picture. In aneural mouse embryos, nerves have a small effect on primary and secondary myotube formation (52), whereas the condition only affects secondary myotube formation in aneural rat embryos (53).

The cited findings in developing avian and mammalian muscles imply a primarily trophic effect of nerves on developing muscles. Our finding that nerves have a very stable relationship with pre-muscle masses may, therefore, indicate such a trophic effect.

4.7. The cranial and caudal muscle columns of the arm are innervated by nerves originating from the C5, C6 and C8, T1 roots, respectively

The appendicular pre-muscle masses that are innervated by nerves that originate in segments C5 and C6 form a cranial column in the elongating extremity, whereas those that are innervated by segments C8 and T1 form a caudal column (Figure S16). This configuration is still found in adult human anatomy. The relation between the spinal nerves and the somitic (myotomal) cells they innervate suggests that myotomal cells and nerves engage in an early bonding that determines the final size, shape, and position of the muscle. The tight association of the onset of primary myogenesis with innervation (54) also suggests a close interaction between both cell types. It is now well-established, however, that pattern formation of the limb muscle is controlled by local cues from the limb mesenchyme (55). The profound effects of Tbx5 and Tbx4 production in the connective tissue on the patterning of muscles and tendons in the arm and leg, respectively, are a striking example (56). Alternatively, therefore, cells in the lateral plate impose the final size, shape, and position of the muscle on the migrating myoblasts. In both scenarios, the definitive muscle architecture of the upper limb is established at the latest in the 8th developmental week.

The pectoralis and latissimus dorsi muscles do not obey our hypothesis that muscles in a pre-muscle mass have a common innervation. In the cited cases, the “foreign” nerve segments originate in caudal segments C8 and T1 instead of the expected more cranial segments C5 and C6. Both muscles develop according to the “In-Out” mechanism, meaning that myoblasts first

migrate towards their destination (the limb bud). From there, a subgroup migrates back towards the medial attachment side of the muscles (clavicle, ribcage, vertebral column) (25, 26, 57). We hypothesize that the complex course of these myoblasts, which first migrate laterally and then again medially, allows for a switch to an alternative nerve pathway. We recently described the peripheral nervous system as a connection matrix in which neurons can change course to a different, neighbouring nerve (Figure 4 in (58)). This finding suggests that neurons innervating the myoblasts of these 2 muscles change course to a different nerve mix or that their myoblasts mix with resident pre-muscle masses.

5. Conclusion

Our study has shown how the muscles in the upper extremity develop. A striking feature was the early and permanent association between nerves and pre-muscle cells. This early nerve-muscle association and the *in situ* differentiation of pre-muscle masses allowed us to determine the identity and the fate of developing muscles without additional experimental lineage analysis. Another striking feature was the short period between migration of pre-muscle cells into the limb and the finalization of size and shape of the striated muscles. Our study shows that variants in the number of muscle bellies most likely become established during this early embryonic phase of development.

Literature list

1. Lewis WH. The development of the arm in man. American Journal of Anatomy. 1902;1(2):145-83.

2. Prummel KD, Nieuwenhuize S, Mosimann C. The lateral plate mesoderm. Development. 2020;147(12):dev175059.

3. Christ B, Huang R, Scaal M. Formation and differentiation of the avian sclerotome. Anatomy and embryology. 2004;208(5):333-50.

4. Young M, Selleri L, Capellini TD. Genetics of scapula and pelvis development: an evolutionary perspective. Current Topics in Developmental Biology. 2019;132:311-49.

5. He L, Papoutsi M, Huang R, Tomarev SI, Christ B, Kurz H, et al. Three different fates of cells migrating from somites into the limb bud. Anatomy and embryology. 2003;207(1):29-34.

6. Mori M. STATISTICS ON THE MUSCULATURE OF THE JAPANESE. Okajimas Folia Anat Jpn. 1964;40:195-300.

7. Rodríguez-Niedenführ M, Vázquez T, Choi D, Parkin I, Sañudo JR. Supernumerary humeral heads of the biceps brachii muscle revisited. Clinical Anatomy. 2003;16(3):197-203.

8. Macalister A. Additional observations on muscular anomalies in human anatomy.(Third Series) With a catalogue of the principal muscular variations hitherto published. The Transactions of the Royal Irish Academy. 1875;25:1-134.

9. Vanhoenacker FM, Desimpel J, Mespreuve M, Tagliafico A. Accessory Muscles of the Extremities. Semin Musculoskelet Radiol. 2018;22(3):275-85.

10. Chal J, Pourquié O. Making muscle: skeletal myogenesis in vivo and in vitro. Development. 2017;144(12):2104-22.

11. Deries M, Thorsteinsdóttir S. Axial and limb muscle development: dialogue with the neighbourhood. Cell Mol Life Sci. 2016;73(23):4415-31.

12. Buckingham M, Bajard L, Chang T, Daubas P, Hadchouel J, Meilhac S, et al. The formation of skeletal muscle: from somite to limb. J Anat. 2003;202(1):59-68.

13. Tani S, Chung U-i, Ohba S, Hojo H. Understanding paraxial mesoderm development and sclerotome specification for skeletal repair. Experimental & Molecular Medicine. 2020;52(8):1166-77.

14. Gasser RF. Evidence that sclerotomal cells do not migrate medially during normal embryonic development of the rat. American Journal of Anatomy. 1979;154(4):509-23.

15. Bobzin L, Roberts RR, Chen H-J, Crump JG, Merrill AE. Development and maintenance of tendons and ligaments. Development. 2021;148(8):dev186916.

16. Christ B, Brand-Saberi B. Limb muscle development. Int J Dev Biol. 2002;46(7):905-14.

17. Buckingham M. Myogenic progenitor cells and skeletal myogenesis in vertebrates. Current opinion in genetics & development. 2006;16(5):525-32.

18. Stockdale FE. Myogenic cell lineages. Dev Biol. 1992;154(2):284-98.

19. Dietrich S, Abou-Rebyeh F, Brohmann H, Bladt F, Sonnenberg-Riethmacher E, Yamaai T, et al. The role of SF/HGF and c-Met in the development of skeletal muscle. Development. 1999;126(8):1621-9.

20. Diogo R, Siomava N, Gitton Y. Development of human limb muscles based on whole-mount immunostaining and the links between ontogeny and evolution. Development. 2019;146(20).

21. Gräfenberg E. Die Entwicklung der Knochen, Muskeln und Nerven der Hand und der für die Bewegungen der Hand bestimmten Muskeln des Unterarms. Anatomische Hefte. 1905;30(1):5-154.

22. O'Rahilly R, Müller F. Developmental stages in human embryos: revised and new measurements. Cells Tissues Organs. 2010;192(2):73-84.

23. Hülsman CJM, Köhler SE, Morosan-Puopolo G, Hikspoors J, Lamers WH. The Development of the Human Female Reproductive Tract. Part 1: Uterine Tube and Uterus. Clin Anat. 2025.

24. Hülsman CJ, Gao H, Kruepunga N, Mommen GM, Köhler SE, Hikspoors JP, et al. The development of the external genitals in female human embryos and foetuses. Part 1: Perineal thick skin, clitoris and labia. Journal of anatomy. 2025;246(2):190-204.

25. Evans DJ, Valasek P, Schmidt C, Patel K. Skeletal muscle translocation in vertebrates. Anatomy and embryology. 2006;211:43-50.

26. Masyuk M, Abduelmula A, Morosan-Puopolo G, Ödemis V, Rehimi R, Khalida N, et al. Retrograde migration of pectoral girdle muscle precursors depends on CXCR4/SDF-1 signaling. Histochemistry and Cell Biology. 2014;142(5):473-88.

27. Okuno K, Ishizu K, Matsubayashi J, Fujii S, Sakamoto R, Ishikawa A, et al. Rib Cage Morphogenesis in the Human Embryo: A Detailed Three-Dimensional Analysis. Anat Rec (Hoboken). 2019;302(12):2211-23.

28. Biressi S, Molinaro M, Cossu G. Cellular heterogeneity during vertebrate skeletal muscle development. Developmental biology. 2007;308(2):281-93.

29. Murphy M, Kardon G. Origin of vertebrate limb muscle: the role of progenitor and myoblast populations. Current topics in developmental biology. 2011;96:1-32.

30. Gharahdaghi N, Phillips BE, Szewczyk NJ, Smith K, Wilkinson DJ, Atherton PJ. Links between testosterone, oestrogen, and the growth hormone/insulin-like growth factor axis and resistance exercise muscle adaptations. Frontiers in physiology. 2021;11:621226.

31. Connan-Perrot S, Léger T, Lelandais P, Desdoits-Lethimonier C, David A, Fowler PA, et al. Six decades of research on human fetal gonadal steroids. International Journal of Molecular Sciences. 2021;22(13):6681.

32. Siiteri PK, Wilson JD. Testosterone formation and metabolism during male sexual differentiation in the human embryo. The Journal of Clinical Endocrinology & Metabolism. 1974;38(1):113-25.

33. Cinnamon Y, Kahane N, Kalcheim C. Characterization of the early development of specific hypaxial muscles from the ventrolateral myotome. Development. 1999;126(19):4305-15.

34. Streeter G. A Review of the Histogenesis of Cartilage and Bone. Developmental Horizons in Human Embryos: Age Groups XI-XXIII, Embryology Reprint. 1951;2:151-67.

35. Dunwoodie SL. The role of hypoxia in development of the Mammalian embryo. Developmental cell. 2009;17(6):755-73.

36. Miller RA. Observations upon the arrangement of the axillary artery and brachial plexus. American Journal of Anatomy. 1939;64(1):143-63.

37. Singer E. Embryological pattern persisting in the arteries of the arm. The Anatomical Record. 1933;55(4):403-9.

38. Rodríguez-Niedenführ M, Burton G, Deu J, Sañudo J. Development of the arterial pattern in the upper limb of staged human embryos: normal development and anatomic variations. The Journal of Anatomy. 2001;199(4):407-17.

39. Wilde S, Feneck EM, Mohun TJ, Logan MPO. 4D formation of human embryonic forelimb musculature. Development. 2021;148(4).

40. Belle M, Godefroy D, Couly G, Malone SA, Collier F, Giacobini P, et al. Tridimensional Visualization and Analysis of Early Human Development. Cell. 2017;169(1):161-73.e12.

41. Yamada TK. [Re-evaluation of the flexor digitorum superficialis]. Kaibogaku Zasshi. 1986;61(4):283-98.

42. Huang AH, Riordan TJ, Wang L, Eyal S, Zelzer E, Brigande JV, et al. Repositioning forelimb superficialis muscles: tendon attachment and muscle activity enable active relocation of functional myofibers. Developmental cell. 2013;26(5):544-51.

43. Wilde S, Feneck EM, Mohun TJ, Logan MP. 4D formation of human embryonic forelimb musculature. Development. 2021;148(4):dev194746.

44. Rodríguez-Vázquez JF, Jin ZW, Zhao P, Murakami G, Li XW, Jin Y. Development of digastric muscles in human foetuses: a review and findings in the flexor digitorum superficialis muscle. Folia morphologica. 2018;77(2):362-70.

45. Bardeen CR. Development and variation of the nerves and the musculature of the inferior extremity and of the neighboring regions of the trunk in man. American Journal of Anatomy. 1906;6(1):259-390.

46. Lacey SH, Soldatis JJ. Bilateral pronator syndrome associated with anomalous heads of the pronator teres muscle: a case report. J Hand Surg Am. 1993;18(2):349-51.

47. De Smet L. Median and ulnar nerve compression at the wrist caused by anomalous muscles. Acta Orthop Belg. 2002;68(5):431-8.

48. Tozer S, Bonnin MA, Relaix F, Di Savino S, García-Villalba P, Coumailleau P, et al. Involvement of vessels and PDGFB in muscle splitting during chick limb development. Development. 2007;134(14):2579-91.

49. Satoh A, Mitogawa K, Makanae A. Nerve roles in blastema induction and pattern formation in limb regeneration. Int J Dev Biol. 2018;62(9-10):605-12.

50. Wells KM, Kelley K, Baumel M, Vieira WA, McCusker CD. Neural control of growth and size in the axolotl limb regenerate. Elife. 2021;10.

51. Sohal GS, Holt RK. Role of innervation on the embryonic development of skeletal muscle. Cell and Tissue Research. 1980;210(3):383-93.

52. Ashby PR, Wilson SJ, Harris AJ. Formation of primary and secondary myotubes in aneural muscles in the mouse mutant peroneal muscular atrophy. Dev Biol. 1993;156(2):519-28.

53. Wilson SJ, Harris AJ. Formation of myotubes in aneural rat muscles. Dev Biol. 1993;156(2):509-18.

54. Hurren B, Collins JJ, Duxson MJ, Deries M. First Neuromuscular Contact Correlates with Onset of Primary Myogenesis in Rat and Mouse Limb Muscles. PLoS One. 2015;10(7):e0133811.

55. Duboc V, Logan MP. Regulation of limb bud initiation and limb-type morphology. Developmental Dynamics. 2011;240(5):1017-27.

56. Hasson P, DeLaurier A, Bennett M, Grigorieva E, Naiche L, Papaioannou VE, et al. Tbx4 and tbx5 acting in connective tissue are required for limb muscle and tendon patterning. Developmental cell. 2010;18(1):148-56.

57. Valasek P, Theis S, DeLaurier A, Hinits Y, Luke GN, Otto AM, et al. Cellular and molecular investigations into the development of the pectoral girdle. Developmental biology. 2011;357(1):108-16.

58. Verlinden TJ, Lamers WH, Herrler A, Köhler SE. The differences in the anatomy of the thoracolumbar and sacral autonomic outflow are quantitative. Clinical Autonomic Research. 2024;34(1):79-97.

59. Peterson Kendall F, Kendall McCreary, E., Geise Provance, P., McIntyre Rodgers, M., Romani, W. A. Segmentale oorsprong van zenuwen en spieren (appendix A: kaarten) [Segmental origin of muscles, appendix A] (maps). In: Hulsman H, editor. Spieren, tests en functies. 4 ed. Houten: Bohn, Stafleu, van Loghem; 2008. p. 427-33.

60. Carter H, Richer P, Vizniak NA. Quick reference evidence based muscle manual: Professional Health Systems; 2008.

61. Guttmann L. Spinal cord injuries; comprehensive management and research. 2 ed. Oxford: Blackwell Scientific Publications; 1973.

Legends

Table 3. List of colour and number codes of the muscles in the Figures.

	Skin
	(Precursor of) bones
	Somites
	Precursor muscle mass (pre-muscle mass)
	Dorsal muscle mass
	Ventral muscle mass
	Serratus anterior (8)
	Hand muscle mass (9)
Exorotators of the arm (1)	Latissimus dorsi (1.1)
	Teres major (1.2)
	Subscapularis (1.3)
Pectoral muscles and subclavius (2)	Subclavius (2.1)
	Pectoralis major (2.2)
	Pectoralis minor (2.3)
Endorotators of the arm (3)	Deltoid (3.1)
	Teres minor (3.2)
	Supraspinatus (3.3)
	Infraspinatus (3.4)
Flexors of the elbow (4)	Biceps long head (4.1a)
	Biceps short head (4.1b)
	Coracobrachialis (4.2)
	Brachialis (4.3)
	Biceps extra head (4.1c)

Extensors of the elbow (5)		■ Triceps lateral head(5a)
		■ Triceps long head(5b)
		■ Triceps medial head(5c)
Flexors of the wrist and digits (6)		■ Flexor carpi ulnaris (6.1)
		■ Flexor digitorum superficialis (6.2)
	Superficial flexors (6.3)	■ Flexor carpi radialis (6.3.1)
		■ Pronator teres (6.3.2)
		■ Palmaris longus (6.3.3)
		■ Flexor digitorum superficialis distal head (6.2b)
	Deep flexors (6.4)	■ Flexor digitorum profundus (6.4.1)
		■ Flexor pollicis longus (6.4.2)
		■ Pronator quadratus (6.4.3)
		■ Flexor digitorum superficialis, proximal head (6.2a)
Extensors of the wrist and digits (7)	Superficial mass-I (7.1)	■ Extensor carpi ulnaris (7.1.1)
		■ Anconeus (7.1.2)
	Superficial mass-II (7.2)	■ Extensor digitorum (7.2.1)
		■ Extensor digiti minimi (7.2.2)
	Deep mass-I (7.3)	■ Brachioradialis (7.3.1)
		■ Supinator (7.3.2)
		■ Extensor carpi radialis longus & brevis (7.3.3)
	Deep mass-II (7.4)	■ Extensor indicis (7.4.1)
		■ Extensor pollicis longus (7.4.2)
		■ Extensor pollicis brevis & Abductor pollicis longus (7.4.3)

Table 4. **List of abbreviations used in the Figures.**

A	Aorta
B	Brain
CRL	Crown-rump length
CV	Cardinal veins
DM	Dorsal pre-muscle mass
He	Heart
MV	Mesonephric vesicle
NT	Neural tube
OC	Occipital
Pa	Pharyngeal arches
Uc	Umbilical cord
VM	Ventral pre-muscle mass
Bones	
C	Clavicle
Ca	Capitate bone
H	Humerus
I-V	Digits I-V
R	Rib
RA	Radius
S	Scapula
Sc	Scaphoid bone
Ste	Sternum
T	Trapezium bone
Tq	Triquetrum bone
Tz	Trapezoid bone
U	Ulna
Nerves	
Ax	Axillary nerve
Cen	Cervical nerve
IT	Inferior trunk
LC	Lateral cord
LPec	Lateral pectoral nerve
LTh	Long thoracic nerve
MC	Medial cord
Me	Median nerve
MPec	Medial pectoral nerve
MT	Middle trunk
Mu	Musculocutaneous nerve
PC	Posterior cord
Ra	Radial nerve
ST	Superior trunk
Sub	Subscapular nerve
Sup	Suprascapular nerve
Thn	Thoracic nerve
Tho	Thoracodorsal nerve
Un	Ulnar nerve

Figure legends

General. For abbreviations of structure names and the colour codes of the contours and reconstructed objects in the sections, see Tables 3 and 4. The colour codes of the contours in the sections and 3D reconstructions are the same. Parallel dashed black lines indicate the location of the corresponding histological sections. Asterisks identify bones. Bars are 200µm unless mentioned otherwise.

Figure 1. **The development of the human arm between CS12 and CS17 (4.5-5.5 weeks).** Panels A1-A3 show overviews of the histology of the developing upper limb, with magnifications in the corresponding panels B1-B3. Panels C1-C3 show 3D models of the embryos' external surfaces (left) or the same embryo with transparent skin (right) to visualize the somites. Brain (B), pharyngeal arches (PA), heart (He), umbilical cord (UC), and occipital somite 1 (OC1) are indicated and serve as landmarks. Panels B3 and D3 show the nerve trunks entering the limb (yellow arrows). Note that the image of embryo CS13-2 (panel A2) is flipped horizontally. * Bone (panels 1A5-6, B5-6). In panels A1 and B1, a small bulge of the somatopleura identifies the location of the upper limb bud (arrow in panel B1). Vessels and nerves have not yet migrated into the limb bud. Panel B2 shows periodic epithelial lips of the ventrolateral dermomyotomes (arrow in B2). Panel C2 shows the external appearance of the limb bud in embryo CS13-2. Panels A3 and B3 show a CS14 embryo with a more advanced limb bud into which terminal branches of the brachial plexus and vessels are penetrating (yellow arrow in B3). Panels A4 to C4 show the axial elongation of the limb bud. Panels A5 and B5 show the beginning condensation of bone mesenchyme (*). A pre-muscle mass can be recognized in the limb bud (yellow contour in panel B5). Its innervation is indicated by green arrows (panels B5 and B6). Note that the external appearance of the limb bud at CS16 (panel C5) is like that at CS15 (panel C4). In CS17 (panels A6 and B6), bone (*) and pre-muscle

masses (red and blue contours) are better distinguishable. Sections B5 and B6 have a similar orientation and reveal the progressive demarcation of the first pre-muscle mass. Panels D3 to D6 show that the roots (D3), trunks (D4), divisions (D5), and terminal branches (D6) of the brachial plexus have formed. For abbreviations of structure names and the colour codes of the contours and reconstructed objects in the sections, see Tables 3 and 4.

Figure 2. **The development of arteries (red) and veins (blue) between CS14 and CS23 (5-8 weeks).** Panels A and B show the centrally and peripherally developing vessels of the limb, while panel C only shows the central arteries. In panel A (embryo CS14-1), the forming marginal vein (orange arrows) delineates the periphery of the limb bud. The yellow asterisk identifies the cut umbilical artery. Two days later (panel B, embryo CS15-3), the subclavian artery penetrates the bud (green arrows). In panels C-E (CS16-19), the branching network of the artery (red) extends distally and around the bones of the lower arm and hand. The marginal vein (blue) is present around the upper and lower arm and hand. In panel F (CS23), the topography of the brachial artery (green arrow) and the cephalic (orange arrow) and basilic veins is established. For abbreviations of structure names and the colour codes of the contours and reconstructed objects in the sections, see Tables 3 and 4.

Figure 3. **Ventral and dorsal views of the developing brachial plexus.** The nerve roots form in early CS14 embryos (panel A), while the trunks and divisions form in CS15 embryos (panel B). In CS16 embryos, almost all nerves except the long thoracic nerve have formed (panel C). In CS17 embryos, the nerves extend to the distal end of the ulna and radius (panel D). Note that the radius and ulna are still relatively short structures at this stage. The remaining elongation and branching of the nerves take place between CS18 and CS23 (panels E-G). The abbreviations are explained in Table 4, but for the colour codes of the nerves, which are only used in this

figure, see ■ Cen4, ■ Cen5,■ Cen6.■ Cen7, ■ Cen8, ■ Thn1,■ ■ ■ Trunks, ■ Fusion of all nerve segments, ■ Tho, ■ Sub, ■ Sup, ■ Ax, ■ Lpec, ■ Mpec, ■ Lth, ■ Mu, ■ Un, ■ Me, ■ Ra.

Figure 4. **The microscopic anatomy of developing muscles and bones of the arm.** From left to right, the columns show the histology and 3D models of the bones and (pre)muscle masses. Column C shows left-sided views of embryos with their skin rendered translucent to show the position of the bones (rows 2-3 only). Bones and muscles become simultaneously visible at CS16. Panel B1 shows a division of the brachial plexus that penetrates the limb bud. Also note the centrally located artery (yellow arrow). Single-colour structures in panels B4-6 represent individual muscles, whereas cross-hatched multi-coloured structures (orange arrows in e.g. panel B4) represent composite pre-muscle masses that must still split into separate single-coloured muscles (B4-5). This coding also applies to Figures 7-16 and S12-S14. Note that panel A1 does not yet show forming pre-muscle masses and bones, whereas panels A2-C2 reveal that the humerus, ulna, radius and the first pre-muscle mass have become identifiable, albeit with fuzzy boundaries. A caudal muscle extension can be seen in panels B2 and B3 (black arrow). Panels A3-A6 show that the boundaries between the visible pre-muscle masses and between bones and muscles have become more apparent. In panels C2-C6, the blueprints for the limb skeleton become visible. Panels A4 and B4 show that the muscles develop in a proximal-to-distal order, with the cross-hatched multi-coloured pre-muscle masses (orange arrows) becoming individual (single-colour) muscles in the shoulder, followed by the development of upper arm and then forearm muscles (panels B5 and B6). The carpal bones are visible in the hand (panel C4). Panels A5 and B5 show that the number of individual (single-coloured) muscles in the shoulder and arm regions have increased and that their boundaries have

sharpened. Panels C4-C6 show that the arm flexes between CS18 and CS23. Panel A6 shows that muscle fibres are forming in the muscles and that all limb muscles are present (panel B6). For abbreviations of structure names and the colour codes of the contours and reconstructed objects in the sections, see Tables 3 and 4.

Figure 5. **Growth of the long bones of the arm in embryos and foetuses between 5.5 and 10 weeks of development**. Developmental age is shown on the X-axis, bone length on the left Y-axis, and crown-rump length (CRL) on the right Y-axis. Humerus, ulna, and radius all grow exponentially, whereas the CRL (shown for reference) increases linearly.

Figure 6. T**imeline of muscle splitting in the upper extremity of embryos aged 5.5 to 8 weeks (CS16-23).** The X-axis shows the embryonic age at which the individual muscles form. Most of the splitting of the pre-muscle masses takes place between 6 and 6.5 weeks. The colours of muscle names (orange, light blue, red, purple, dark blue, green) reveal the muscles that become identifiable at the same period. Apart from a proximal-to-distal gradient, superficial pre-muscle masses split and differentiate earlier than deep pre-muscle masses. * The extensor carpi radialis can be identified at CS21, but the final split into the extensor carpi radialis longus and brevis is completed only at 10 weeks.

Figure 7. **Development of the exorotator muscles of the arm.** Humerus, scapula, and the preaxial vein (future cephalic vein; panel C1) indicate the topography of the muscles. The (pre-)muscle masses contain numbers which correspond to the numbers in Table 3; the first number corresponds to the pre-muscle mass, and the addition of a letter indicates a head of a muscle. Panels A1 and B1 show the dorsal pre-muscle mass (red) with a caudal extension near the scapula (blue arrow). Panel C1 shows the thoracodorsal nerve (Tho) entering the caudal extension of the muscle mass (DM, red), implying that it becomes the latissimus dorsi muscle.

Panel C2 shows a sagittal section (embryo 17-2) instead of a transverse section (embryo 17-1; panels C1, C3-C5). The caudal part (blue arrow in panels A1 and B1) has split from the dorsal pre-muscle mass. The pre-muscle mass (1) contains the posterior cord (PC) of the brachial plexus, which will split into the thoracodorsal and the subscapular nerves (Figure 7C2). In panels A2 and B2, the muscles that derive from the caudal mass can be identified as the latissimus dorsi (1.1, light orange), teres major (1.2, brown-orange (panels A2-5, B2-5) or red (panels C3-C5)), and the subscapularis (1.3, yellow) muscles. Panels A3-5 and B3-5 show only small differences between Carnegie stages 18 and 19, but the muscles show more contrast relative to the surrounding connective tissue (panels C3-C5). In addition, panel C5 (embryo CS23-1) shows that muscle fibres are accumulating in embryo CS23-1 (panel C5). For abbreviations of structure names and the colour codes of the contours and reconstructed objects in the sections, see Tables 3 and 4.

Figure 8. **Development of the adductor muscles in the shoulder girdle.** 3D views of the pectoralis major, pectoralis minor, and subclavius muscles during Carnegie stages 16-23 are shown in panels A1-D1. Ribs (R), scapula (S), and humerus (H) provide landmarks to facilitate muscle identification. Coloured contour lines in the sections shown in the middle and lower rows correspond with the dashed lines in the top row. In panels A1-A3 (CS16), the pre-muscle mass has not yet split. Panels B1-B3 (CS17-1) show the pectoralis mass (2.2+2.3) between the humerus and the ribs (cross-hatched in panel B1). The subclavius muscle (2.1) is encoded in green. In panels C1-C3, all muscles are present as individual muscles, but their attachments to bone form only at CS23 (panels D1-D3). Note that secondary muscle fibres can be observed in panels D2 and D3. For abbreviations of structure names and the colour codes of the contours and reconstructed objects in the sections, see Tables 3 and 4.

Figure 9. **Development of the endorotators of the arm.** The deltoid, teres minor, infraspinatus and supraspinatus muscles are the main endorotators of the upper arm. The scapula and humerus are visible in the 3D models of the CS18-CS23 embryos (left 2 columns), with their primordium first identifiable in embryo CS17-1. The pre-muscle mass of the endorotator muscles is part of the dorsal pre-muscle mass in CS17-1 (red; panels A1 and B1) and can be first identified at CS17-2 (panel C1). The deltoid (#3.1, cyan) is the first muscle to split away from the endorotator pre-muscle mass (#3.2+3.3+3.4) (panels A2-C2). Its form changes in later stages (panels A3, 4-C3, 4) and acquires its definitive shape at CS23 (panels A5 and B5). The teres minor (#3.2, pastel blue), supraspinatus (#3.3, khaki), and infraspinatus (#3.4, green) muscles form at CS19 (panels A4-C4). For abbreviations of structure names and the colour codes of the contours and reconstructed objects in the sections, see Tables 3 and 4.

Figure 10. **The teres minor muscle splits from the same pre-muscle mass as the infraspinatus and supraspinatus muscles.** The scapula and humerus are used as topographical references in the 3D models. The comparison of embryos CS18-2 (panels A1-C1) and CS19-2 (panels A2-C2) shows the formation of the teres minor (#3.2, pastel blue), supraspinatus (#3.3, khaki), and infraspinatus (#3.4, green) muscles. Their pre-muscle mass in embryo CS18-2 (panel C1, #3.2+3.3+3.4) contains the axillary nerve (Ax). In embryo CS19-2, the teres minor (#3.2) is innervated by the axillary nerve (panel C2; yellow arrow). Furthermore, the deltoid muscle (#3.1) and the remaining pre-muscle mass separate from each other due to the accumulation of connective tissue between them (panels B1-B2; double-headed red arrows). This demonstrates that the teres minor muscle derives from the pre-muscle mass that also contains the infraspinatus and supraspinatus muscles, but no longer the deltoid muscle. For abbreviations of structure names and the colour codes of the contours and reconstructed objects in the sections, see Tables 3 and 4.

Figure 11. **Development of the flexors of the elbow.** The coracobrachialis (#4.2, green), biceps brachii (#4.1a, blue and #4.1b, brown), and brachialis (#4.3, pastel green) muscles are the main flexors of the upper arm. Scapula, humerus, ulna, and radius are visible in the 3D models of the CS18-CS23 embryos. The left column shows the 3D reconstructions. In embryo CS17-1, the skeletal primordium of the hand is also shown (panel A1). The flexors of the elbow are derived from the ventral pre-muscle mass (bright blue; panel A1) and split from the forearm flexor mass in embryo CS17-3, which already contains the musculocutaneous nerve (Mu) (panels B1 and C1). Panels A2 and B2 show a histologically uniform pre-muscle mass (#4) that is stretching over the entire humerus, but the distal head of the coracobrachialis can already be observed. Panels A3-C3 show that the proximal part of this mass has split and forms the coracobrachialis muscle (#4.2, green), whereas the distal region remains unsplit (#4.2+4.3). The different heads of the biceps brachii are visible in panels A3 (blue and brown arrows) and B3 (long head: #4.1a, blue circle; short head: #4.1b, brown circle). The musculocutaneous nerve (Mu) is present between coracobrachialis (#4.2, green) and the biceps brachii short head (#4.1b, brown). In embryo CS19-2 (panels A4-B4), the muscles appear similar to those in embryo CS18-2, but the mass has assumed a more specific shape, although no splitting has taken place in the distal region (C4). In panels A5-C5, the splitting is complete, and all three muscles can be observed individually. For abbreviations of structure names and the colour codes of the contours and reconstructed objects in the sections, see Tables 3 and 4.

Figure 12. **Development of extensors of the elbow.** The lateral (#5a, purple), long (#5b, green), and medial (#5c, pink) heads of the triceps brachii are the main extensors of the elbow. The humerus, ulna, radius, and bones of the hand are present as topographic landmarks in the 3D models. In embryo 18-1, a uniform pre-muscle mass (#5, multicoloured structure) is still present

on the dorsal side of the humerus (panels A1 and B1), while all three muscle heads have formed in embryo CS18-2 (panels A2 and B2). In Carnegie stage 19 embryos, the triceps heads retain a similar appearance (panels A3 and B3). The attachments to the bones are present in Carnegie stage 23 embryos (panels A4 and B4). For abbreviations of structure names and the colour codes of the contours and reconstructed objects in the sections, see Tables 3 and 4.

Figure 13. **Development of the flexors of the wrist.** The flexor carpi ulnaris (#6.1, crème), flexor digitorum superficialis (#6.2, red), flexor carpi radialis (#6.3.1, yellow), pronator teres (#6.3.2, light brown), palmaris longus (#6.3.3, brown), flexor digitorum profundus (#6.4.1, purple), flexor pollicis longus (#6.4.2, green) and pronator quadratus (#6.4.3, dark brown) are the main flexors of the wrist. These will split into superficial and deep pre-muscle masses from which the individual muscles form, except for the flexor carpi ulnaris. Humerus, ulna, radius, carpal bones, and phalanges are visible in the 3D-models. The superficial layer (#6.3 + 6.2b) remains limited to the hand, whereas the deep layer (#6.4 +6.2a) extends into digits II-V in embryo CS18-1 (panels A1-B1). The flexor carpi ulnaris (crème) is already present at this stage (panel B1, blue arrow). Panel A2.1 shows that the distal head of the flexor digitorum superficialis (#6.2b, red), which has split off from the superficial pre-muscle mass (#6.3), is located on top of the deep mass (#6.4+6.2a) and that the deep mass, in turn, lies on top of the intrinsic muscles of the hand (#9). Panel A2.2 shows the median nerve (Me) penetrating both the deep (#6.4+ 6.2a) and superficial masses (#6.3.1+6.3.3). In panel B2, the superficial mass has split into three masses: the distal head of the flexor digitorum superficialis (#6.2b, red), palmaris longus (#6.3.3, brown), and a mass containing the pronator teres and the flexor carpi radialis (#6.3.1+6.3.2, cross-hatched light brown and yellow). Panel A3.1 shows that the median nerve (Me; yellow arrow) is more superficial and innervates the distal head of the flexor digitorum superficialis (#6.2b, red), whereas the ulnar nerve (Un, red arrow) is deeper and

innervates the hand muscles (#9, green). Panel A3.2 shows that the ulnar nerve lies between the deep mass (#6.4.1+6.4.2) and the flexor carpi ulnaris (#6.1, crème). The pronator quadratus (#6.4.3, light brown) and the proximal head of the flexor digitorum superficialis (#6.2a, red) can be identified here for the first time. In embryo CS19-2, all superficial muscles have developed (panels A4 and B4), but the flexor digitorum profundus (#6.4.1, purple) and flexor pollicis longus (#6.4.2, green) of the deep mass still need to split (panels A4.1-A4.2). Panel B5 shows that the proximal (#6.2a) and distal (#6.2b) heads of the flexor digitorum superficialis (#6.2) have fused and that all the flexor muscles can be seen. For abbreviations of structure names and the colour codes of the contours and reconstructed objects in the sections, see Tables 3 and 4.

Figure 14. **Development of the extensors of the wrist.** The extensor carpi ulnaris (#7.1.1, orange), anconeus (#7.1.2, purple), extensor digitorum (#7.2.1, pastel blue), extensor digiti minimi (#7.2.2, dark blue), brachioradialis (#7.3.1, dark green), supinator (#7.3.2, bright green), extensor carpi radialis longus + brevis (#7.3.3, khaki), extensor indicis (#7.4.1, red), extensor pollicis longus (#7.4.2, pink), extensor pollicis brevis + abductor pollicis longus muscles (#7.4.3, bright blue) are extensors of the wrist. Humerus, ulna, radius, carpal bones, and phalanges are visible in the 3D models. Panel A1 shows superficial (#7.1+7.2) and deep masses (#7.3+7.4) (the left model shows only the deep mass, and the right model shows the larger superficial mass on top of it). The yellow dotted line indicates the boundary between the superficial and deep layer on the lateral side. Panel B1 shows that the superficial and deep masses both have split into 4 separate masses each (#7.1 to #7.4). In embryo CS18-2 (panels A2 and B2), the extensor carpi ulnaris and anconeus mass (#7.1, orange and purple) is located laterally to the ulna (panels A2 and B2.2), and the extensor digitorum profundus and digiti minimi (#7.2, pastel and dark blue) cover almost the entire forearm (panel A3). Please note that

the ulna and radius are still very short structures. The supinator (#7.3.2, bright green) is the first separately identifiable muscle (panel B3.1), and the extensor indicis and extensor pollicis longus mass (#7.4.1+7.4.2, red and pink) is located mostly on the ulna, whereas the extensor pollicis brevis and abductor pollicis longus mass (#7.4.3, bright blue) centres on the radius (panels A3 and B3.1). The brachioradialis muscle and extensor carpi radialis mass (#7.3.1+ 7.3.3, green and khaki) are located mostly lateral of the radius. Panels A3 and B3.2 show that the extensor carpi ulnaris (#7.1.1, orange) and anconeus (7.1.2, purple) have split. The extensor indicis and extensor pollicis longus mass (#7.4.1+7.4.2, red and pink) has formed two distal attachments (blue arrows), whereas the extensor pollicis brevis and abductor pollicis longus mass (#7.4.3, bright blue) still has only one. The brachioradialis and extensor carpi radialis mass (#7.3.1+ 7.3.3, green and khaki) also has two distal bellies (panel A3, orange arrows). Panel A4-B4 shows that, at CS23, all muscles have split except for the extensor pollicis brevis, abductor pollicis longus (#7.4.3), and extensor carpi radialis muscles (#7.3.3). The final split of the extensor carpi radialis muscles had taken place in both 10-week-old foetuses (not shown). For abbreviations of structure names and the colour codes of the contours and reconstructed objects in the sections, see Tables 3 and 4.

Figure 15. **Variant of the extensor muscles in the forearm of the CS18 -2 embryo.** The left arm shows the normal development of the extensor muscles, with 5 extensor masses (7.1, 7.2, 7.3.1+ 7.3.3, 7.4.1+7.4.1, 7.4,3) and the supinator (7.3.2), whereas the right arm only has 2 extensor masses (7.1 and 7.2+7.3+7.4). Humerus, ulna, radius, and bones of the hand are visible in the 3D models. In panel A, three masses can be distinguished, while in panel D only two can be seen. In panels B and C, six masses can be observed, while in panels E and F they have not split, so only one mass is visible.

Figure 16. **Variations observed in embryo CS23-3.** Scapula and humerus are visible in the 3D models. Bars: 500µm. The top row (A1-C1) shows the variation that was observed, and the bottom panel (A2-C2) shows the normal development. Panel A1 shows an unsplit teres minor and infraspinatus, B1 shows an extra biceps head, and panel C1 shows an unsplit flexor digitorum profundus and flexor pollicis longus. For a more detailed view of how the variation appears, see Figures S12-14. For abbreviations of structure names and the colour codes of the contours and reconstructed objects in the sections, see Table 3.

Supplemental figures

Figure S1. **Protocol for generating 3D models of serial histological sections.** Histological sections were digitized (panels A and B). The digitized serial sections (panel C) were uploaded to Amira to segment the structures of interest (panel D). The segmented outlines were then stacked and aligned (panel E). Next, the stacked 3D outlines from Amira were imported into Cinema4D to serve as a reference (panel F) to create accurate but smooth 3D images (panel G). Note that in panel F, the irregular surfaces on the outside of contours were removed during surface modelling because the comparison of the Amira and Cinema renderings shows that they represent noise.

Figure S2. **Overview of Amira3D reconstructions that were used to deduce the dendrogram of appearance in time and topography of the skeletal muscles of the arm.** Panels A and B show the dorsal and ventral muscles, respectively. Legend Panel A: ■ Bones, ■ Dorsal muscle mass, ■ Deltoid + supraspinatus + infraspinatus+ teres minor, ■ Latissimus dorsi + teres major + subscapularis, ■ Supraspinatus+ infraspinatus+ teres minor,

■ Infraspinatus+ teres minor, ■ Deltoid, ■ Teres minor, ■ Infraspinatus, ■ Supraspinatus, ■ Latissimus dorsi, ■ Teres major, ■ Subscapularis, ■ Triceps mass, ■ Triceps brachii lateral head, ■ Triceps brachii long head, ■ Triceps brachii medial head, ■ Superficial extensor mass, ■ Deep extensor mass,■ All extensors (except extensor carpi ulnaris + anconeus), ■ Extensor carpi radialis longus + brevis + brachioradialis+ supinator, ■ Extensor carpi ulnaris + anconeus, ■ Extensor digitorum + extensor digiti minimi, ■ Extensor indicis + extensor pollicis longus + extensor pollicis brevis + Adductor pollicis longus, ■ Extensor carpi radialis longus + brevis + brachioradialis, ■ Extensor pollicis brevis + adductor pollicis longus ,■ Extensor indicis + extensor pollicis longus, ■ Brachioradialis, ■ Supinator, ■ Extensor carpi ulnaris, ■ Anconeus, ■ Extensor digitorum, ■ Extensor digiti minimi, ■ Extensor indicis, ■ Extensor pollicis longus, ■ Extensor carpi radialis longus + brevis, ■ unable to split the extensors further due to the thickness of the sections.

Legend Panel B: ■ Ventral muscle mass, ■ Biceps brachii + coracobrachialis + brachialis, ■ Biceps brachii + brachialis, ■ Coracobrachialis, ■ Brachialis, ■ Biceps brachii short head, ■ Biceps brachii long head, ■ Flexor muscles, ■ Flexor muscles (except flexor carpi ulnaris), ■ Flexor carpi ulnaris, ■ Palmaris longus + pronator teres + flexor carpi radialis +

flexor digitorum superficialis distal head, ■ Flexor digitorum profundus + flexor pollicis longus + pronator quadratus, + flexor digitorum superficialis proximal head, ■ Flexor digitorum superficialis, ■ Palmaris longus + pronator teres + flexor carpi radialis, ■ Flexor digitorum profundus + flexor pollicis longus + pronator quadratus, ■ Palmaris longus, ■ Pronator teres, ■ Flexor carpi radialis, ■ Flexor digitorum profundus + flexor pollicis longus, ■ Flexor digitorum profundus, ■ Flexor pollicis longus, ■ Pronator quadratus. X= Not able to differentiate the flexors of the lower forearm due to the thickness of the sections.

Figure S3. **A comparison of the shoulder region of 3 different embryos showing the splitting patterns of the muscle masses in the shoulder region.** The development of the main endorotators of the upper arm shows how the muscles of the upper limb develop by splitting from one pre-muscle mass. In embryo CS17-2 (left panel), one pre-muscle mass (colored slices) can be seen around the scapula and humerus. This mass splits into the deltoid muscle (C18-2, middle panel), and subsequently into the infraspinatus, supraspinatus, and teres minor muscles (CS19-2, right panel). Note that in embryo CS19-2 the muscles are separated by connective tissue, which was not yet present in embryo CS18-2.

Figure S4. **Reconstruction of the arteries and nerves in the arm and shoulder of embryo CS23-3.** Panels A-C show how vessels and nerves were used as landmarks to identify muscles. All panels show the scapula, humerus, ulna, radius, and digits. Panel A shows the bones and brachial plexus, and panel B shows the same bones and the artery of the arm. Panel C shows, in addition to the bones and nerves, the lateral head of the triceps brachii and its innervation by

the radial nerve. The left side of panel C shows the triceps as a solid mass, whereas on the right side it is rendered transparent. ■ Bones, ■ Cen4, ■ Cen5,■ Cen6.■ Cen7, ■ Cen8, ■ Thn1,■ ■ ■ Trunks, ■ Fusion of all nerve segments, ■ Tho, ■ Sub, ■ Sup, ■ Ax, ■ Lpec, ■ Mpec, ■ Lth, ■ Mu, ■ Un, ■ Me, ■ Ra,■ Arteries, ■ Triceps brachii lateral head.

Opening and visualizing the 3D-PDFs

To visualize a 3D-PDF, download it on a computer (required) with an Adobe PDF reader (*not* an equivalent reader). To activate the 3D-PDF, "click" with the mouse on the reconstruction. A toolbar appears at the top of the screen that includes the option "model tree". The model tree displays the material list of structures in the upper box and preset viewing options (cameras) in the lower box. The list of visible structures can be changed by marking or unmarking a structure. To manipulate the reconstruction, press the left mouse button to rotate it, the scroll button to zoom in or out, and the left and right mouse buttons simultaneously to move the embryo across the screen. A structure can be rendered transparent by selecting that option from the drop-down menu after selecting the structure with the right mouse button.

Figure S5. **3D-PDF of embryo CS16-2.** The right limb of the embryo was damaged. For that reason, only the left side was fully reconstructed.

Figure S6. **3D-PDF of embryo CS17-1.**

Figure S7. **3D-PDF of embryo CS18-1.**

Figure S8. **3D-PDF of embryo CS18-2.** Due to a variation on the right side of the forearm, there are only two extensor masses, whereas the left side contains five extensor masses.

Figure S9. **3D-PDF of embryo CS19-2.** The skin of the embryo was not fully available. For that reason, the lateral sides of the head are not reconstructed.

Figure S10. **3D-PDF of embryo CS23-3.** Two examples of incomplete splitting are present in both arms. The teres minor and infraspinatus have failed to split in the shoulder region, and the flexor digitorum profundus and pollicis longus have incompletely split in the forearm. An extra split (head) of the biceps brachii can be observed in the left arm of this embryo.

Figure S11. **Different appearances of cartilage in embryo CS17-1.** Scapula, humerus, ulna, radius and the bones of the hand are shown. The difference in appearance of the cartilage becomes evident when the shoulder and arm (panels A-C) are compared with the hand (panels D and E). The primordium of the large bones appears as bright cartilage cells in the centre of the bone with a darker lining surrounding it (panels A-C). This contrasts with the hand, where the forming metacarpal cartilage consists of uniformly dense cells (panels D-E).

Figure S12. **Variations of muscle splitting patterns of the infraspinatus and teres major muscles of embryo CS23-3.** The scapula and humerus are visible in the 3D models, and the level of sectioning in panels A–F is shown in the 3D models. The left panels show the variation of the unsplit infraspinatus and teres minor (#3.4+3.2, green pastel and blue), and the right panels show the normal development of the infraspinatus (#3.4) and teres minor (#3.2). Panels A-C show one mass, whereas in panels D-F the teres minor muscle (#3.4, blue) can be observed ventrally to the infraspinatus muscle (#3.4, green). Bars: 500µm.

Figure S13. **Variant with an extra biceps muscle head in the left arm of embryo CS23-3.** The right arm shows the normal development of the biceps brachii (#4.1), coracobrachialis #4.2), and brachialis (#4.3) muscles, whereas the left arm has formed an extra muscle. Scapula, humerus, ulna, and radius are visible in the 3D models, and the level of sectioning in A–F is

shown in the 3D models. Bars: 200µm. The left panels show the variation of the extra biceps head (#4.1c), and the right panels show the normal development without it. Panels A and D show a similar appearance of the muscles in their proximal region. Panel B shows that the extra head of the biceps (#4.1c, red) is located between the biceps brachii (#4.1, brown/blue) and the brachialis muscles (#4.3, green). The musculocutaneous nerve (Mu) is close to the extra muscle head (#4.1c). Panel F shows that the musculocutaneous nerve is between the brachialis (#4.3) and the biceps brachii (#4.1) muscles. In panel C, the musculocutaneous nerve passes between the extra head of the biceps brachii (#4.1c) laterally and the brachialis (#4.3) medially.

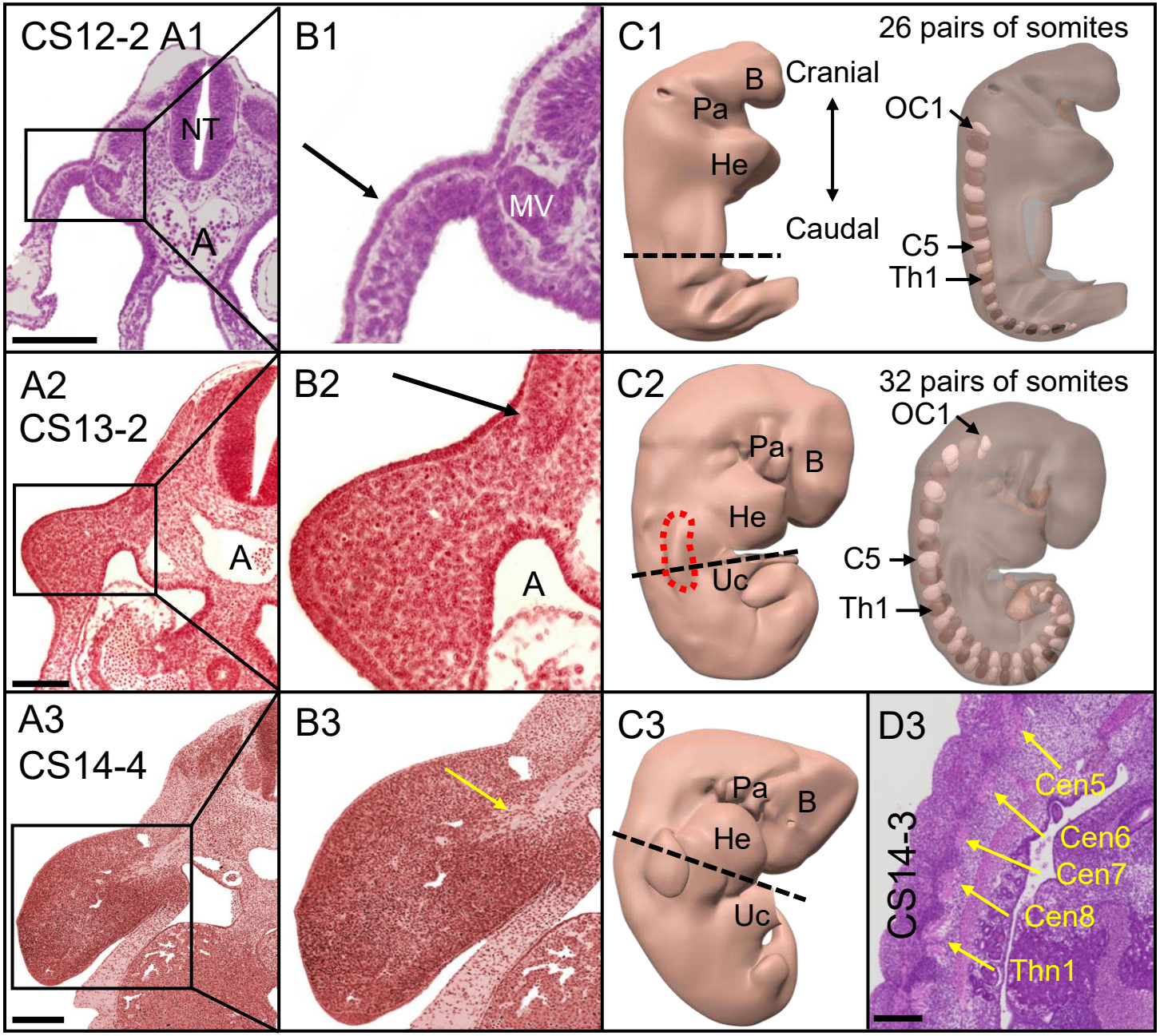
Figure S14. **Fusion variant of flexor digitorum profundus and flexor pollicis longus muscles in embryo CS23-3**. Due to the thicker sections of embryo CS23-1, it was not possible to reconstruct its lower arm in detail and, therefore, one of the 10-week-old foetuses was used for comparison. The scapula and humerus are visible in the 3D models, and the level of sectioning in panels A–F is shown in the 3D models. Bars: 200µm. The unsplit flexor digitorum profundus and flexor pollicis longus muscles (#6.4.1+6.4.2, green and purple) are visible in the right panels, and normal development is visible in the corresponding left panels. In panel A, the green and purple cross-hatched mass lies between the flexor digitorum superficialis (#6.2, red) and the pronator quadratus (#6.4.3, brown) muscles. Panel C shows a similar section plane except that the flexor pollicis longus muscle (#6.4.2, green) is the proximal muscle of the unsplit pre-muscle mass (#6.4.1+ 6.4.2, green and purple) in panel A, while the distal muscle is the flexor digitorum profundus (#6.4.1, purple). A similar situation is observed in the more proximal region of the forearm, where only the cross-hatched mass is visible in panel B. In panel D, two muscles are recognizable the distal muscle representing the flexor digitorum profundus and the proximal muscle representing the flexor pollicis longus.

Figure S15. **Correlation between the timeline of muscle splitting events and the postulated time of origin of the splitting variants that we identified.** The diagram is identical to that shown in Figure 6, with the addition of the deduced timepoints of missing splitting events as red crosses and the supernumerary split as a rectangle outlined in red.

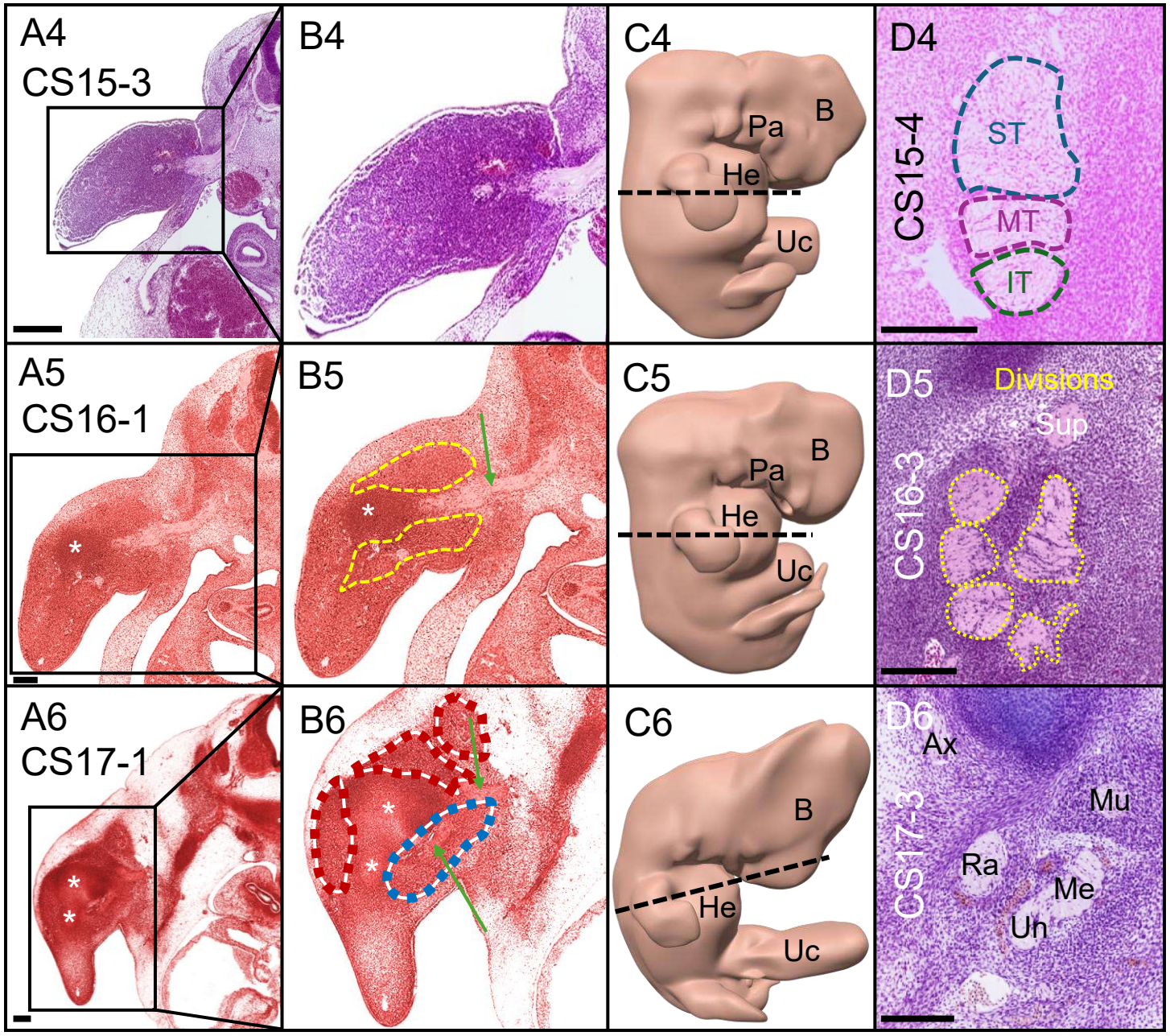
Figure S16. **Topographic positions of muscles innervated by nerves originating in cervical segments 5 and 6 (Cen5-Cen6), and those in cervical segment 8 and thoracic segment 1 (Ce8-Thn1)(59-61).** Both groups originate as cranial and caudal columns along the arm from the time muscle masses become identifiable. Their topography, therefore, is already established at Carnegie stage 18. The asterisks indicate the latissimus dorsi muscle. A part of the myoblasts of this muscle first migrates to their target on the arm and then back to the ribcage and spine (so-called “In-Out” mechanism (25, 26, 57)).

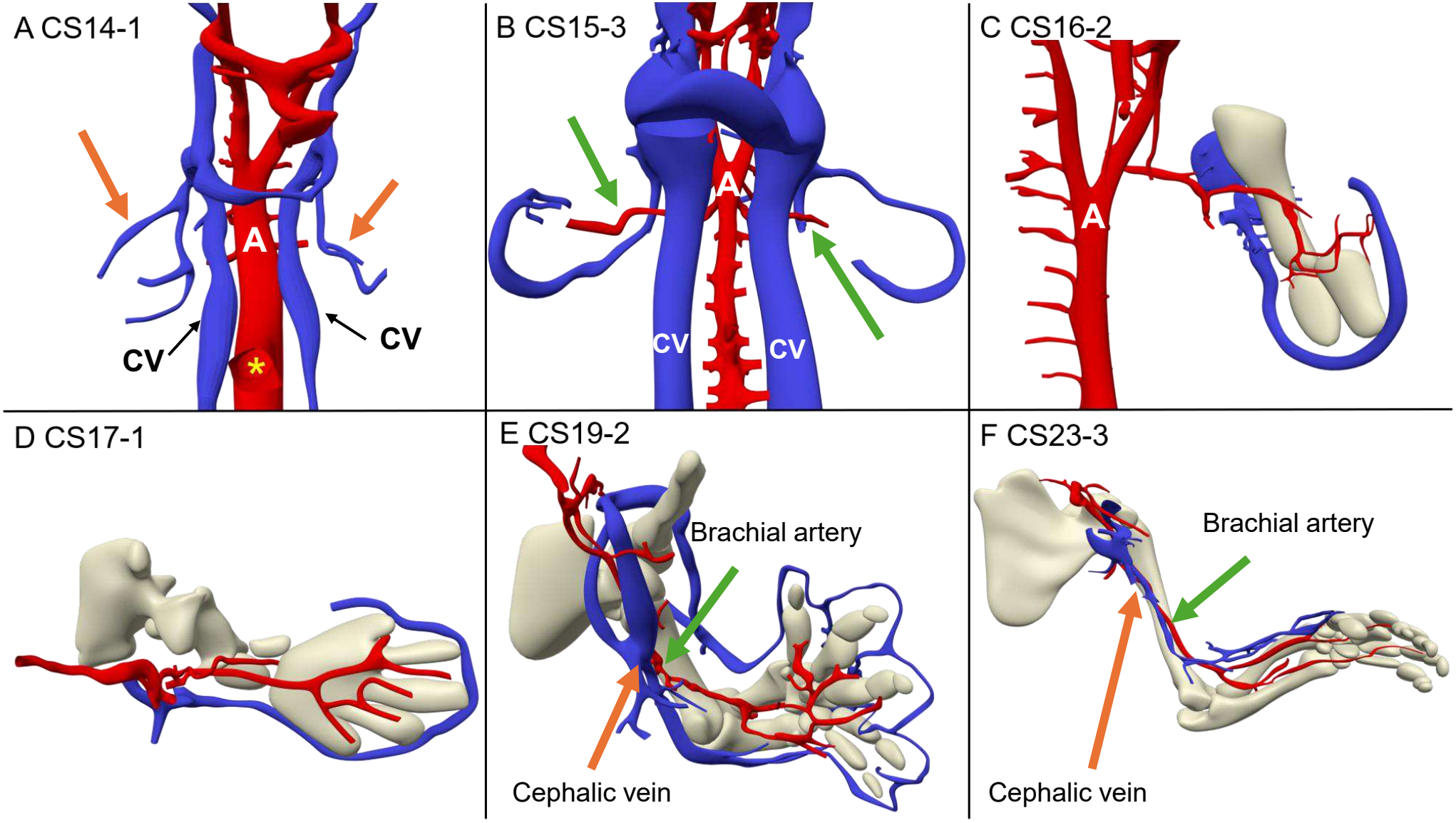
■ Bones, ■ Cen5-Cen6, ■ Cen8-Thn1, ■ Combination of Cen5-Thn1.

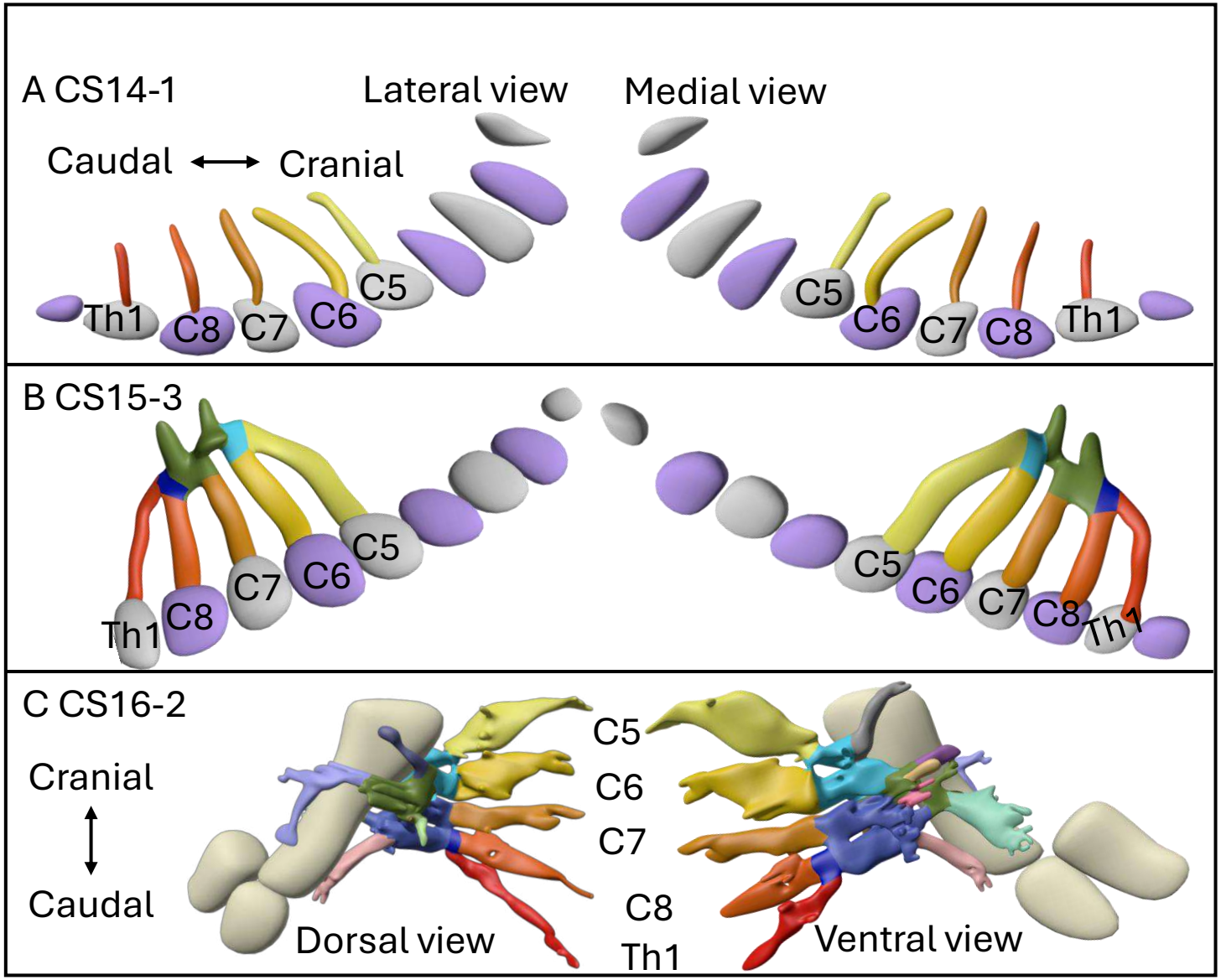
1

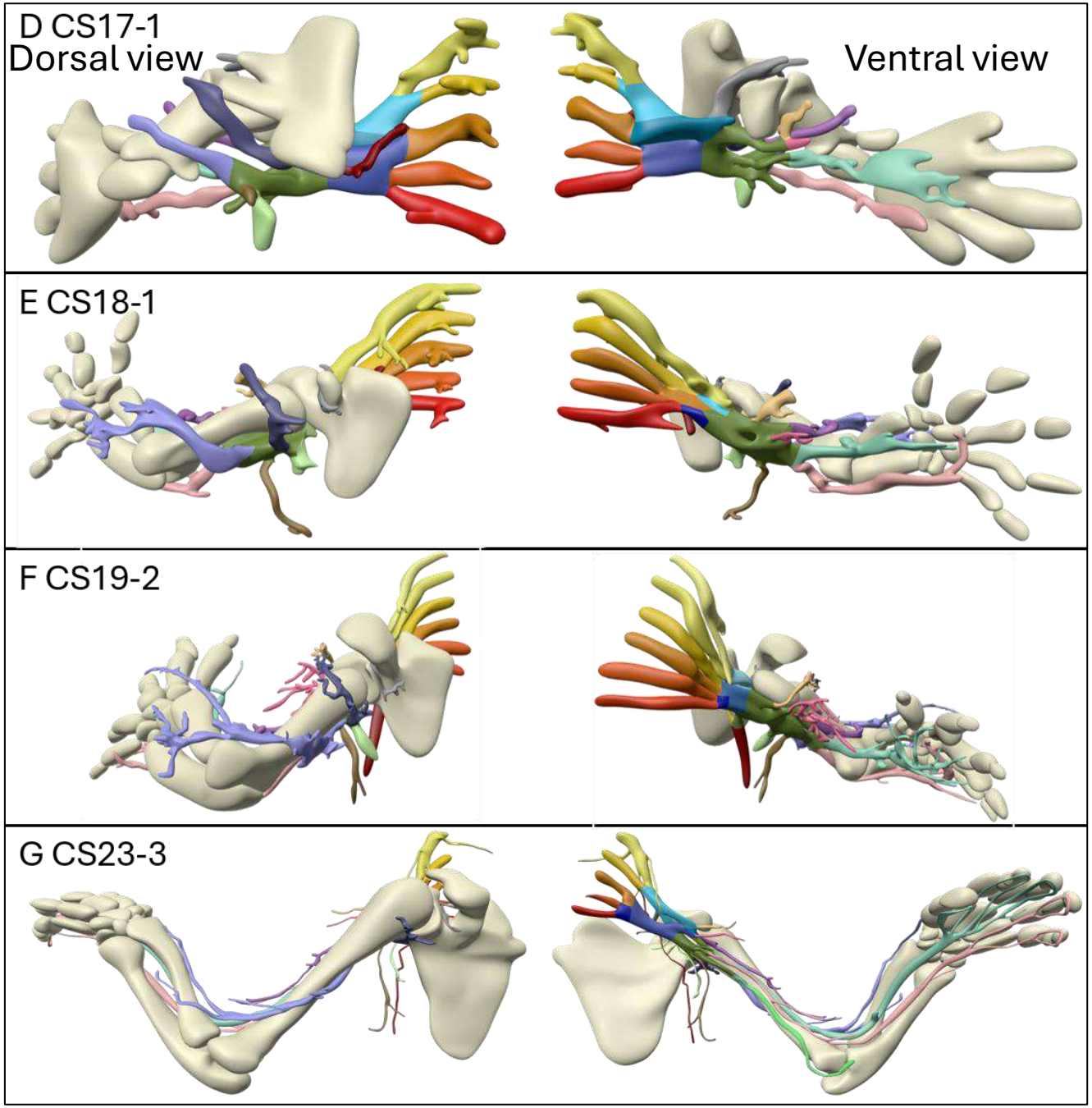

CS12-2 A1
NT
A
B1
MV
C1
26 pairs of somites
B
Pa
He
Cranial
Caudal
OC1
C5
Th1
A2
CS13-2
A
B2
A
C2
32 pairs of somites
Pa
B
He
Uc
OC1
C5
Th1
A3
CS14-4
B3
C3
Pa
B
He
Uc
D3
CS14-3
Cen5
Cen6
Cen7
Cen8
Thn1

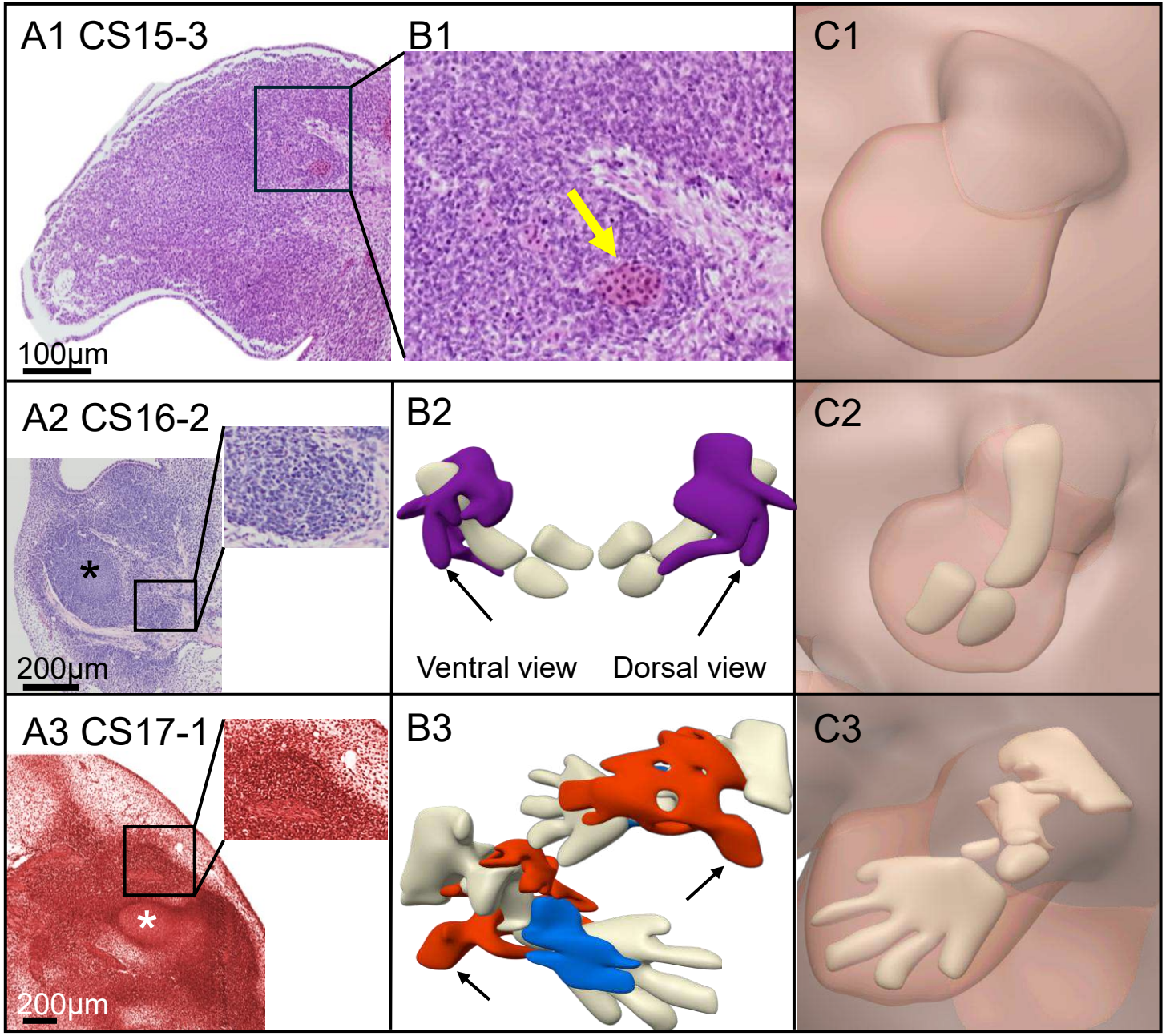
1

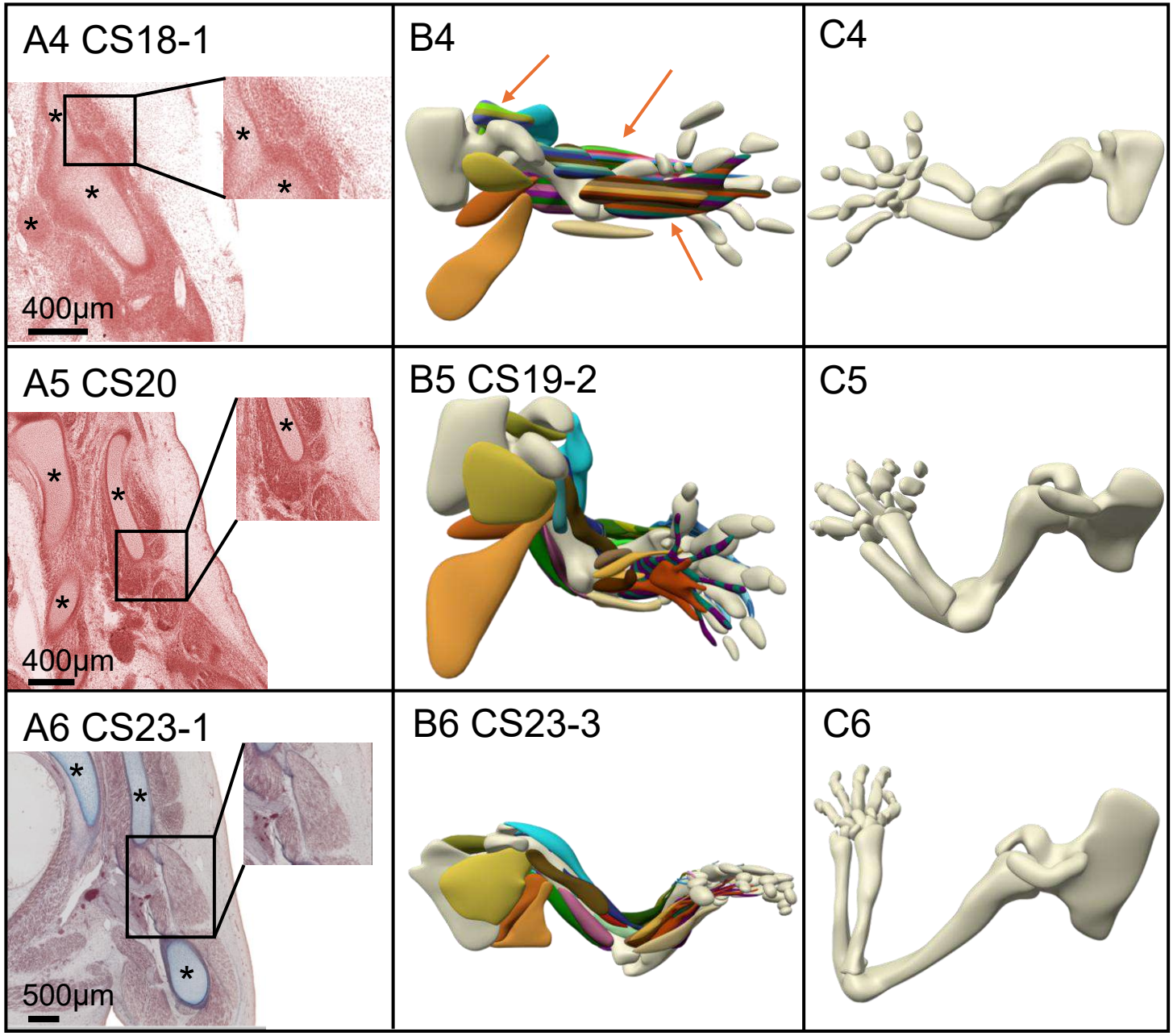

A4
CS15-3
B4
C4
Pa
B
He
Uc
D4
CS15-4
ST
MT
IT
A5
CS16-1
B5
C5
Pa
B
He
Uc
D5
Divisions
Sup
CS16-3
A6
CS17-1
B6
C6
B
He
Uc
D6
Ax
Mu
Ra
Me
Un
CS17-3


A CS14-1
A
CV
CV
*
B CS15-3
A
CV
CV
C CS16-2
A
D CS17-1
E CS19-2
Brachial artery
Cephalic vein
F CS23-3
Brachial artery
Cephalic vein

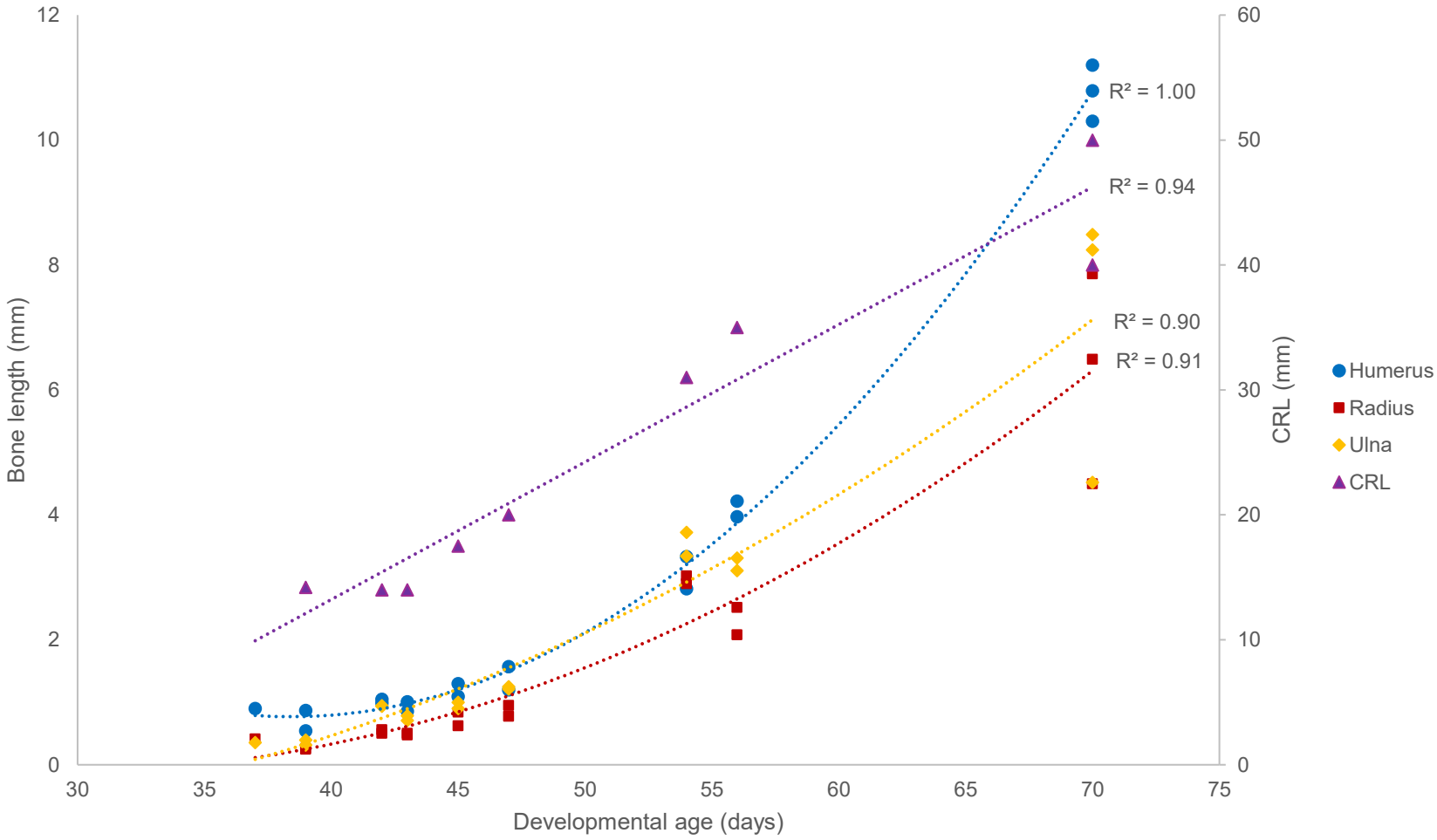

A CS14-1
Lateral view
Medial view
Caudal
Cranial
Th1
C8
C7
C6
C5
C5
C6
C7
C8
Th1
B CS15-3
Th1
C8
C7
C6
C5
C5
C6
C7
C8
Th1
C CS16-2
Cranial
Caudal
Dorsal view
C5
C6
C7
C8
Th1
Ventral view

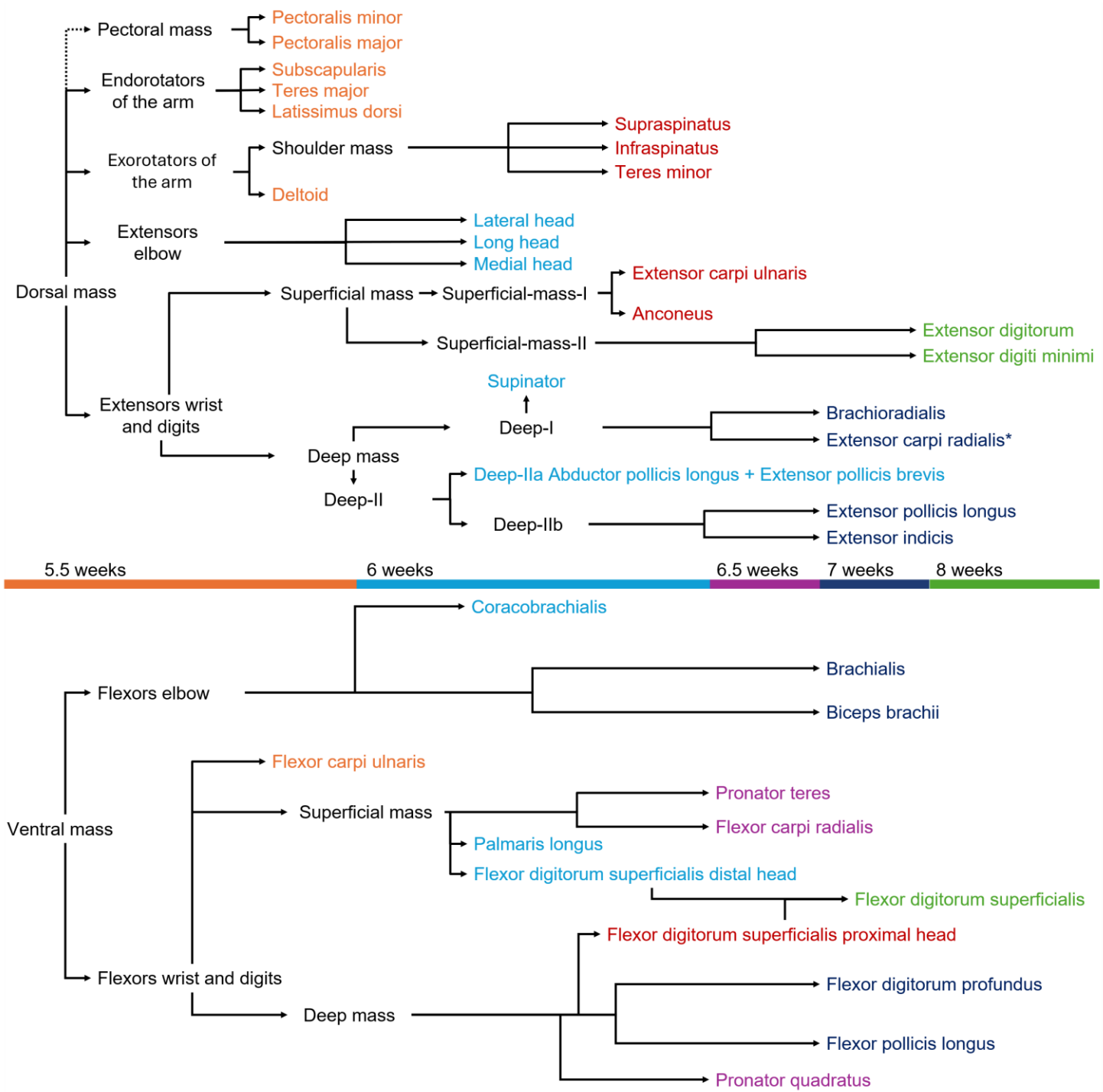

D CS17-1
Dorsal view
Ventral view
E CS18-1
F CS19-2
G CS23-3

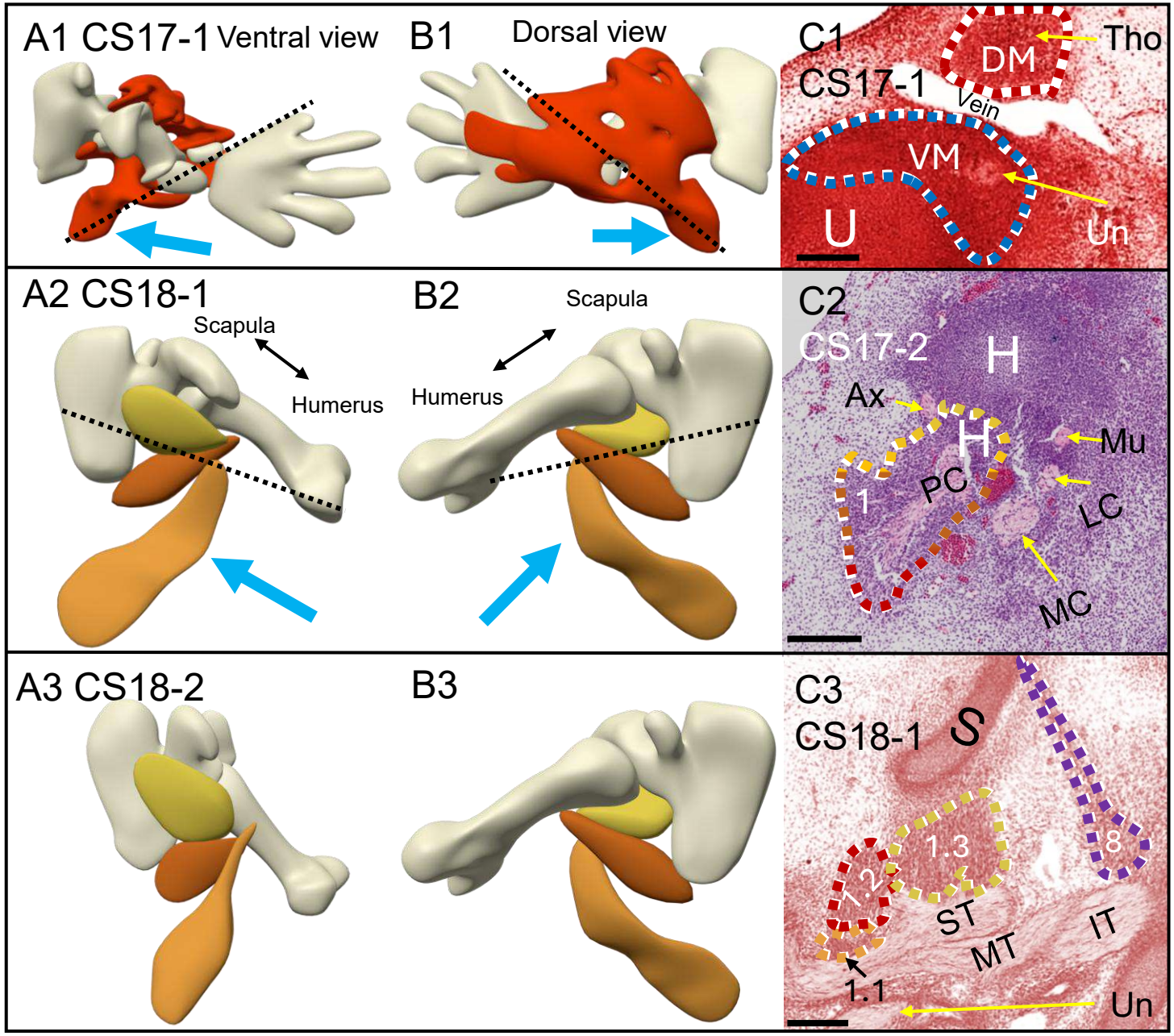

A1 CS15-3
B1
C1
100μm
A2 CS16-2
B2
C2
200μm
Ventral view
Dorsal view
A3 CS17-1
B3
C3
200μm

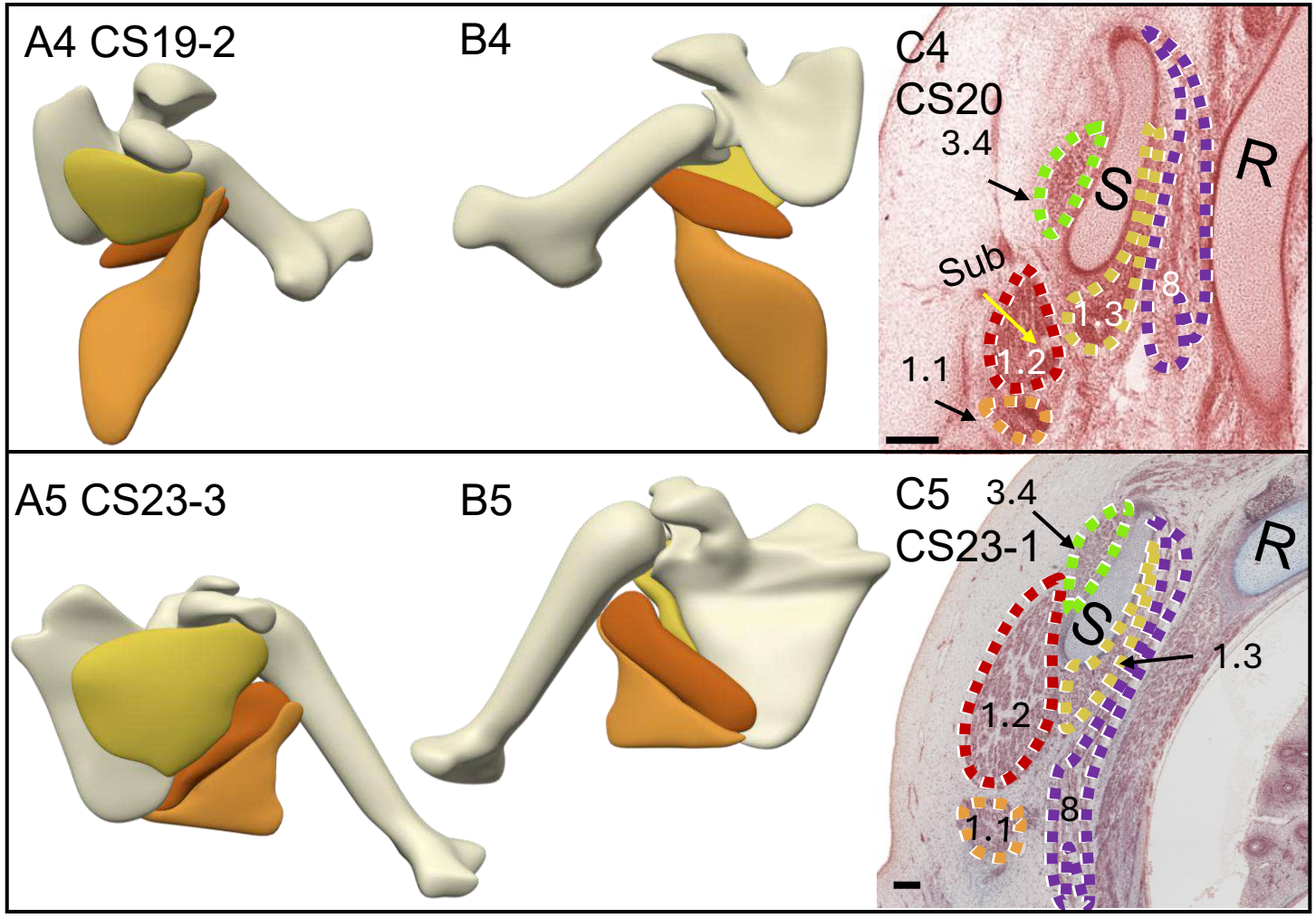

A4 CS18-1
400μm
B4
C4
A5 CS20
400μm
B5 CS19-2
C5
A6 CS23-1
500μm
B6 CS23-3
C6

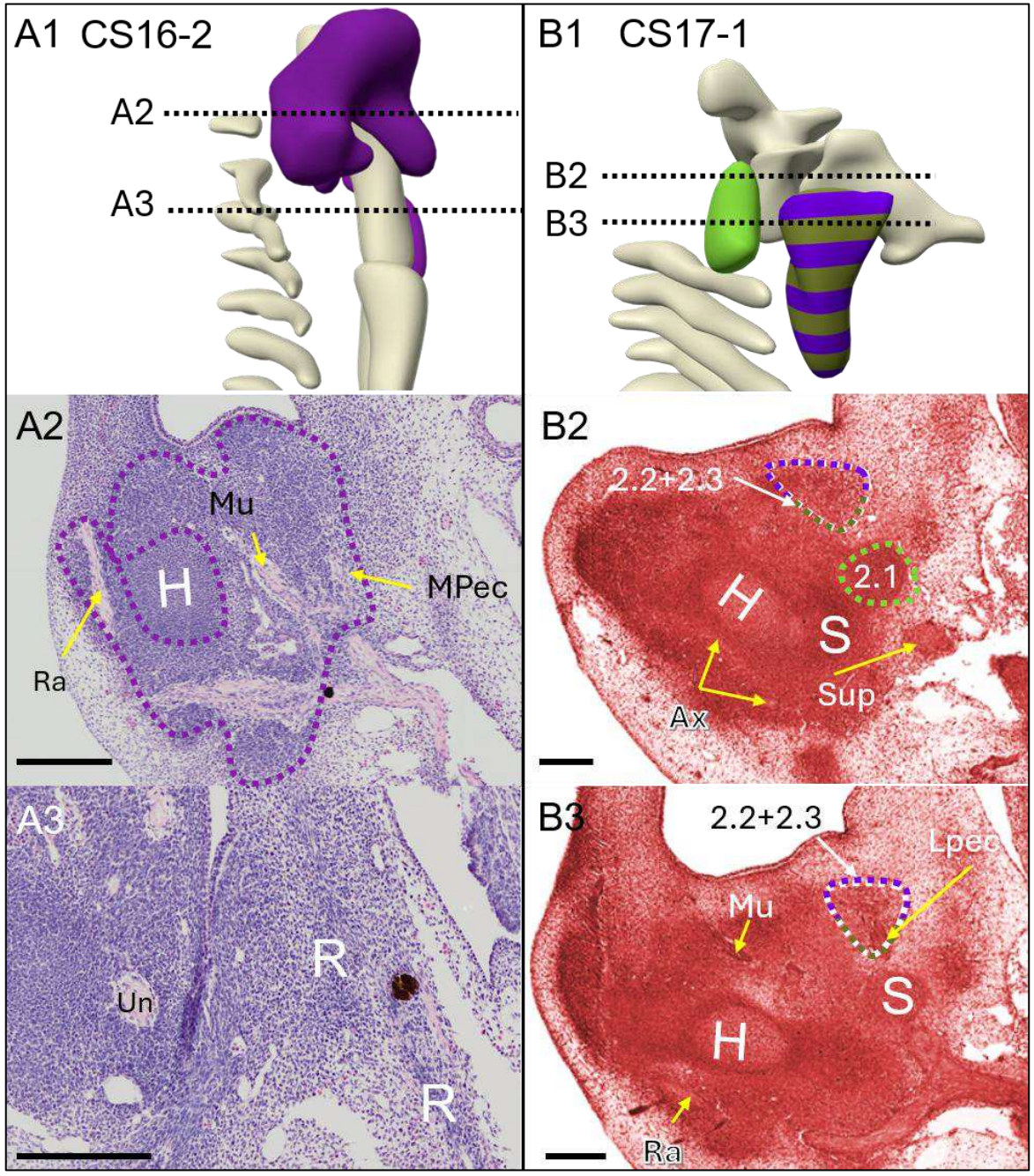
5

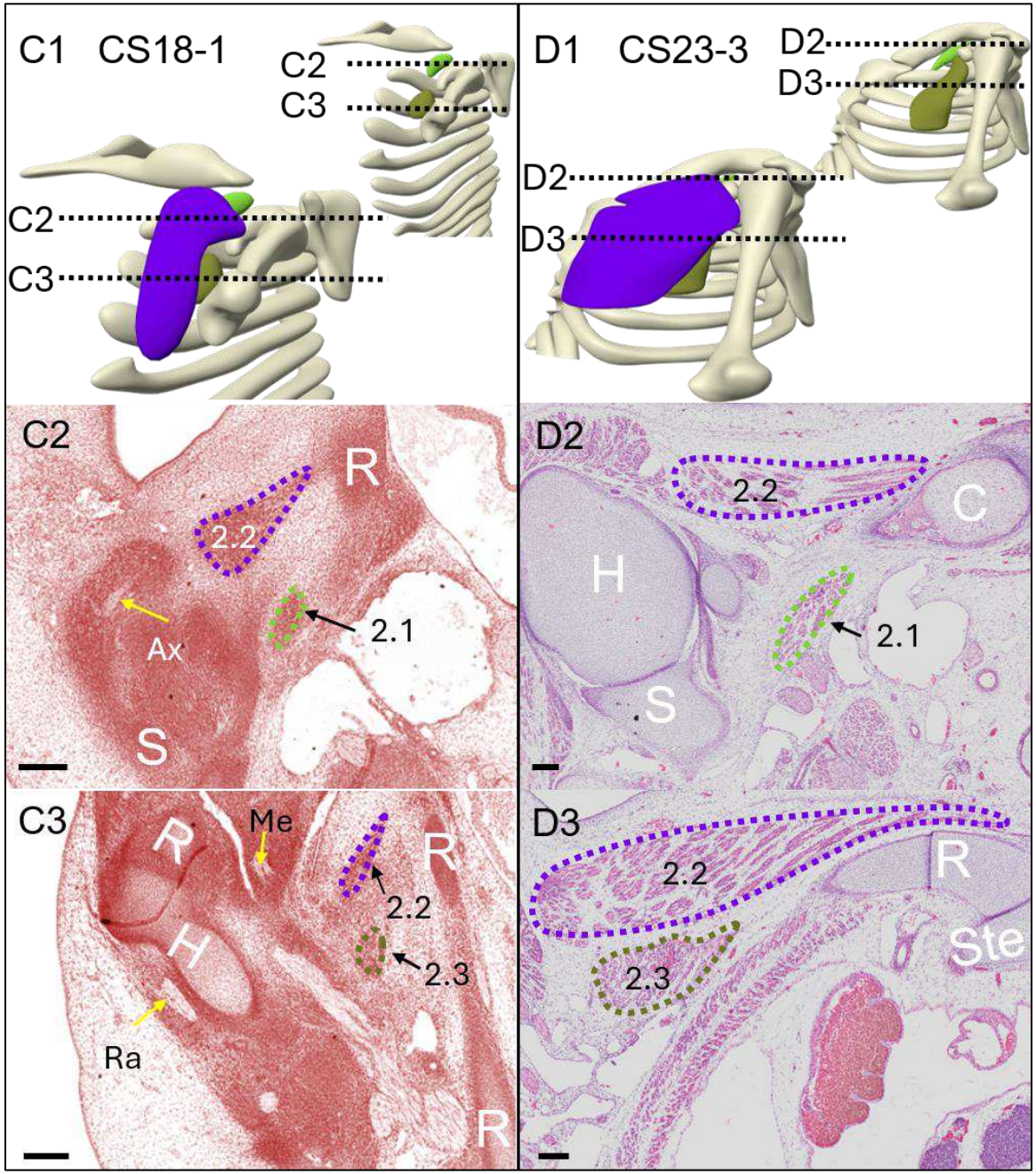

Bone length (mm)
CRL (mm)
Developmental age (days)
R² = 1.00
R² = 0.94
R² = 0.90
R² = 0.91
Humerus
Radius
Ulna
CRL
0
2
4
6
8
10
12
0
10
20
30
40
50
60
30
35
40
45
50
55
60
65
70
75

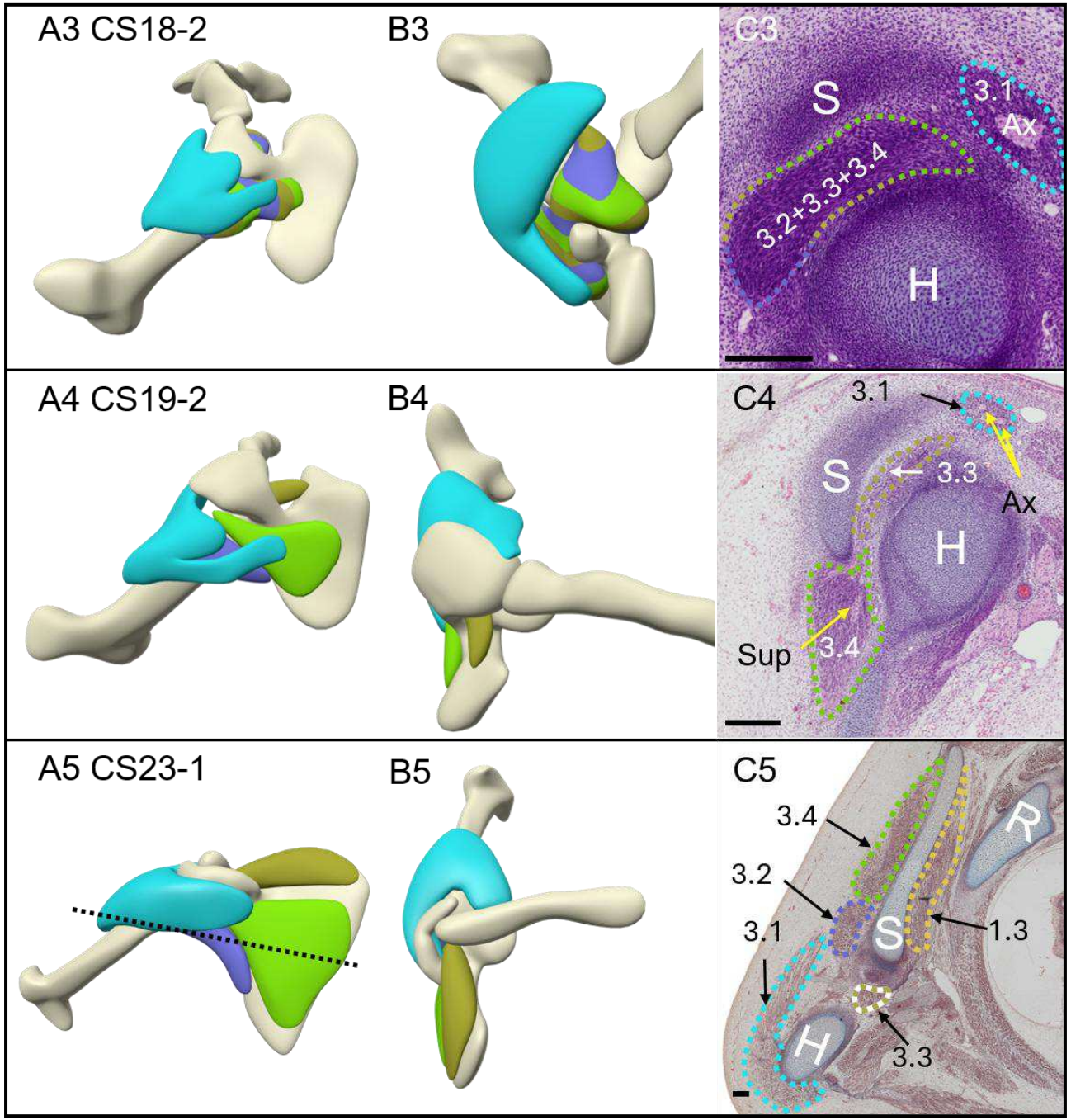

Pectoral mass
Pectoralis minor
Pectoralis major
Endorotators of the arm
Subscapularis
Teres major
Latissimus dorsi
Exorotators of the arm
Shoulder mass
Supraspinatus
Infraspinatus
Teres minor
Deltoid
Extensors elbow
Lateral head
Long head
Medial head
Dorsal mass
Superficial mass
Superficial-mass-I
Extensor carpi ulnaris
Anconeus
Superficial-mass-II
Extensor digitorum
Extensor digiti minimi
Supinator
Extensors wrist and digits
Deep-I
Brachioradialis
Extensor carpi radialis*
Deep mass
Deep-IIa Abductor pollicis longus + Extensor pollicis brevis
Deep-II
Deep-IIb
Extensor pollicis longus
Extensor indicis
5.5 weeks
6 weeks
6.5 weeks
7 weeks
8 weeks
Coracobrachialis
Flexors elbow
Brachialis
Biceps brachii
Flexor carpi ulnaris
Superficial mass
Pronator teres
Flexor carpi radialis
Ventral mass
Palmaris longus
Flexor digitorum superficialis distal head
Flexor digitorum superficialis
Flexor digitorum superficialis proximal head
Flexors wrist and digits
Deep mass
Flexor digitorum profundus
Flexor pollicis longus
Pronator quadratus

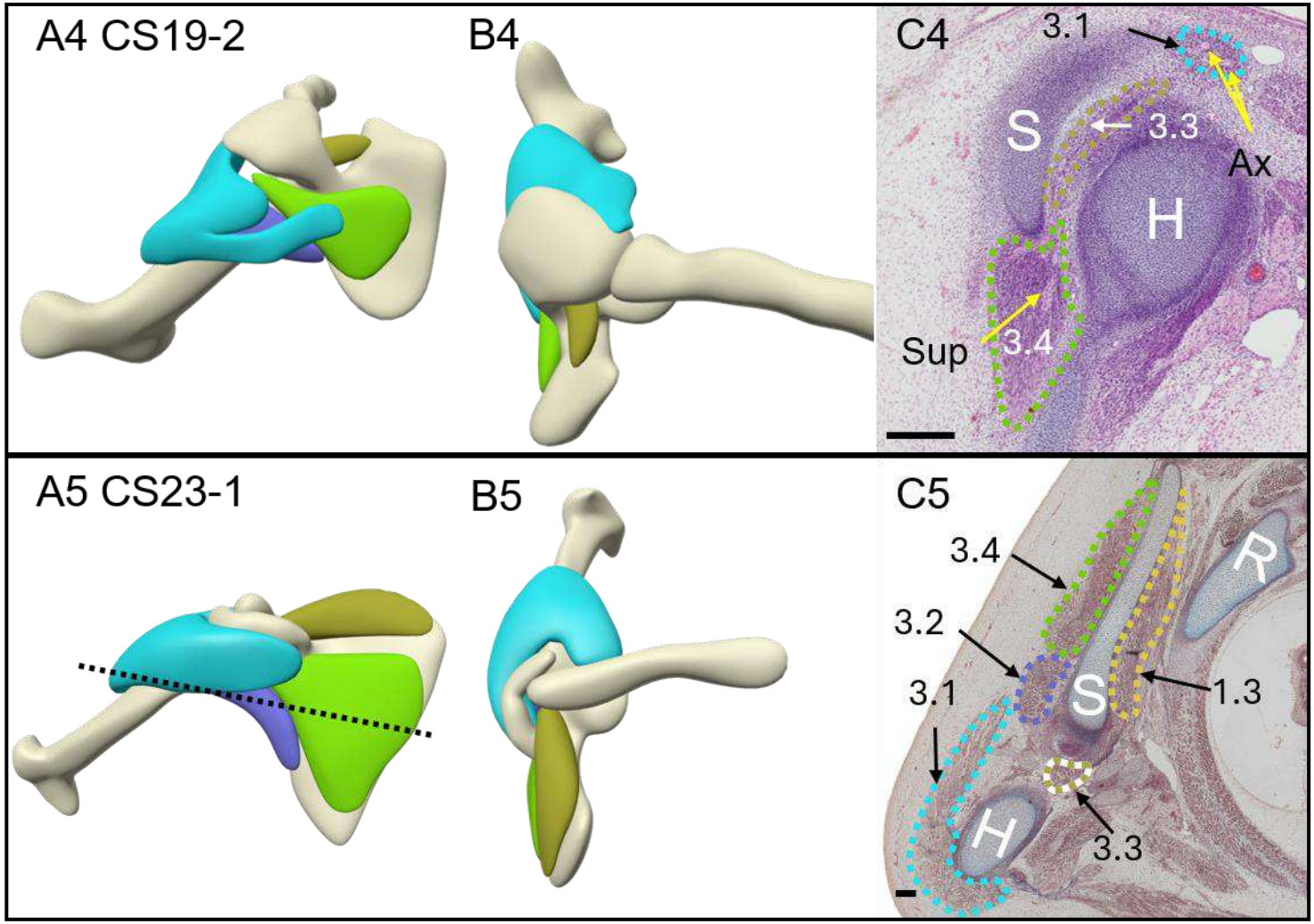

A1 CS17-1 Ventral view
B1 Dorsal view
C1
CS17-1
DM
Tho
Vein
VM
U
Un
A2 CS18-1
Scapula
Humerus
B2
Scapula
Humerus
C2
CS17-2
H
Ax
H
Mu
1
PC
LC
MC
A3 CS18-2
B3
C3
CS18-1
S
1.3
8
1.2
ST
MT
IT
1.1
Un

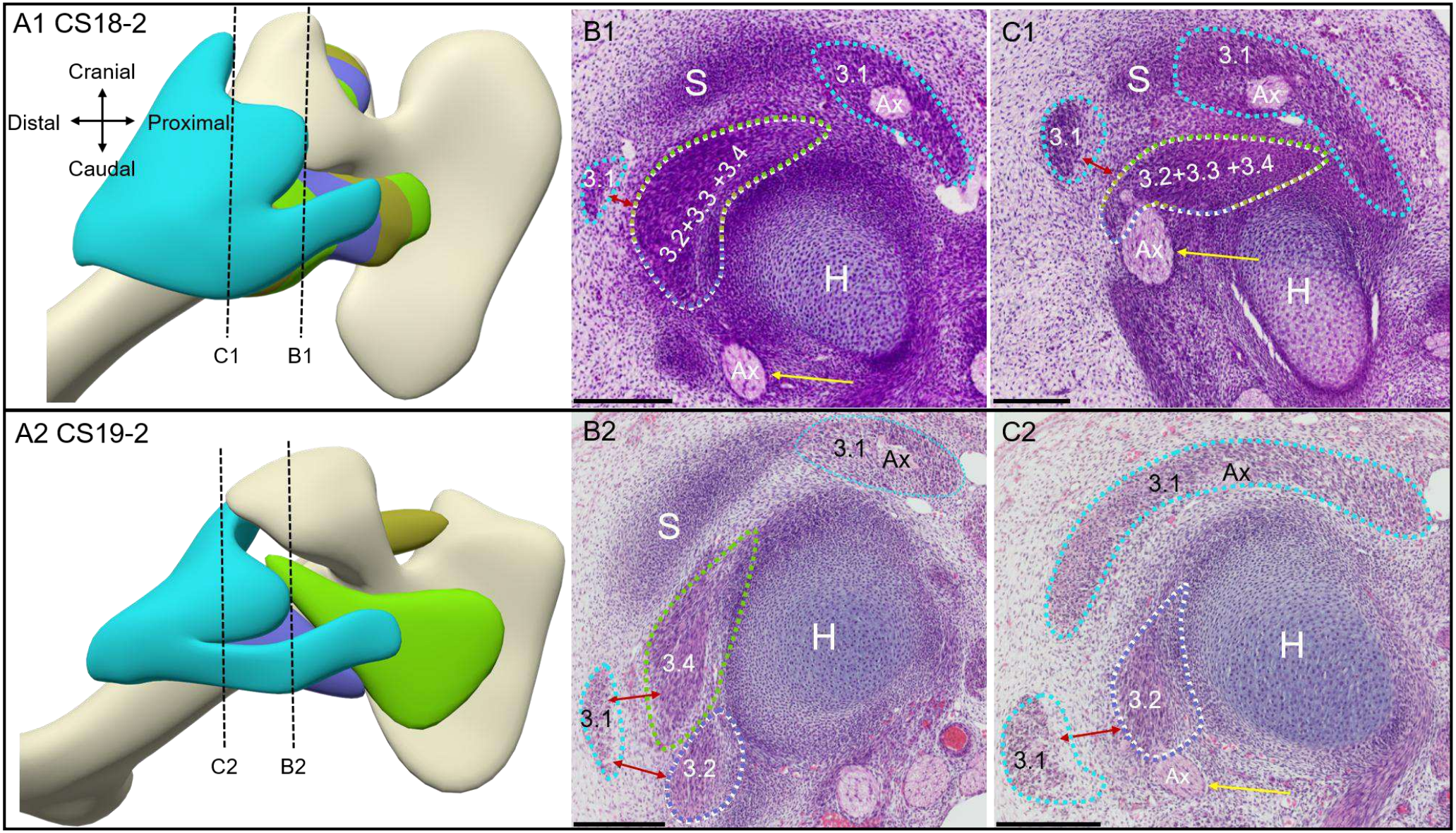

A4 CS19-2
B4
C4
CS20
3.4
S
R
Sub
8
1.3
1.1
1.2
A5 CS23-3
B5
C5
3.4
CS23-1
R
S
1.3
1.2
1.1
8

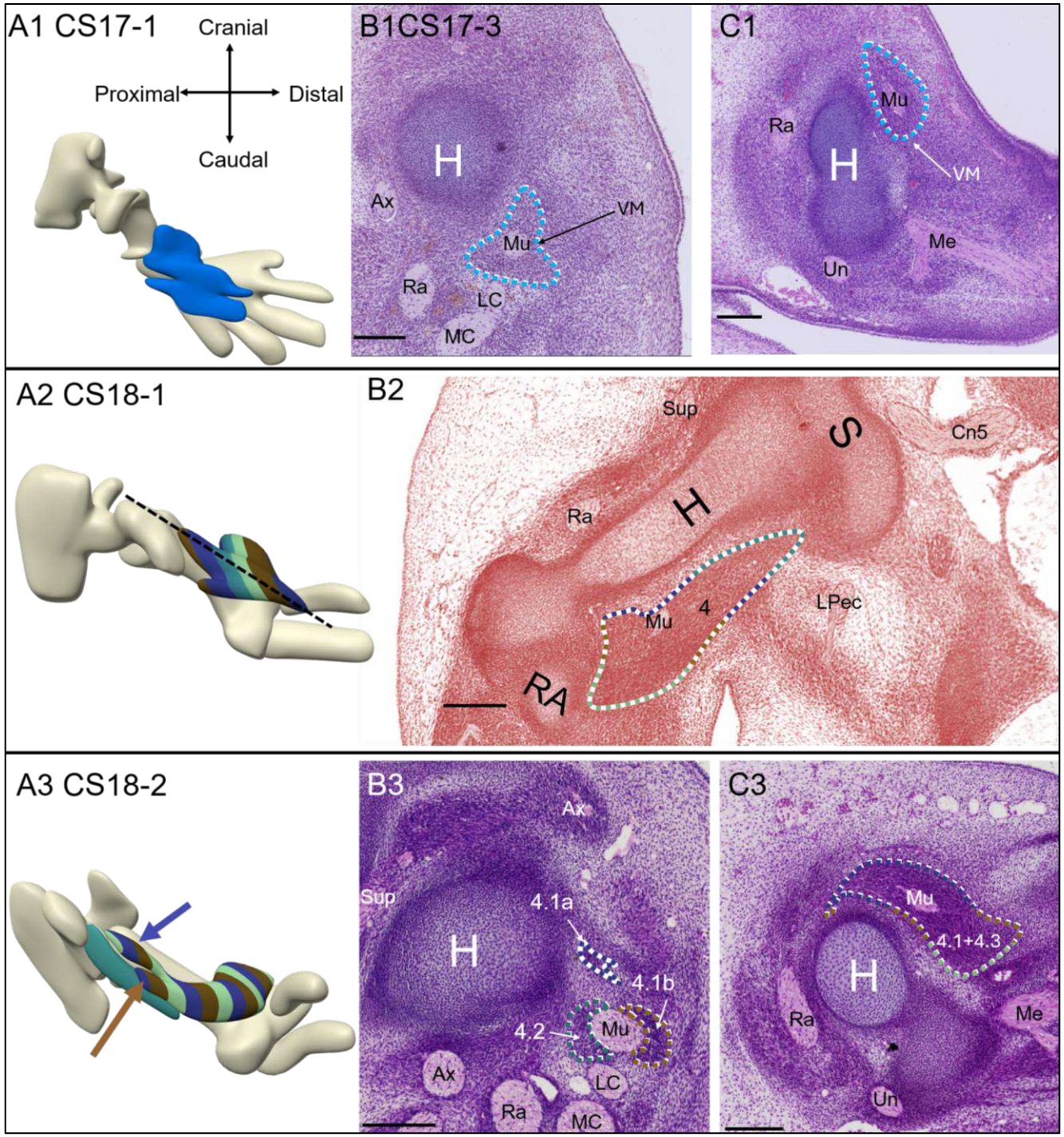

A1 CS16-2
A2
A3
B1 CS17-1
B2
B3
A2
Mu
H
MPec
Ra
B2
2.2+2.3
2.1
H
S
Sup
Ax
A3
R
Un
R
B3
2.2+2.3
Lpec
Mu
S
H
Ra

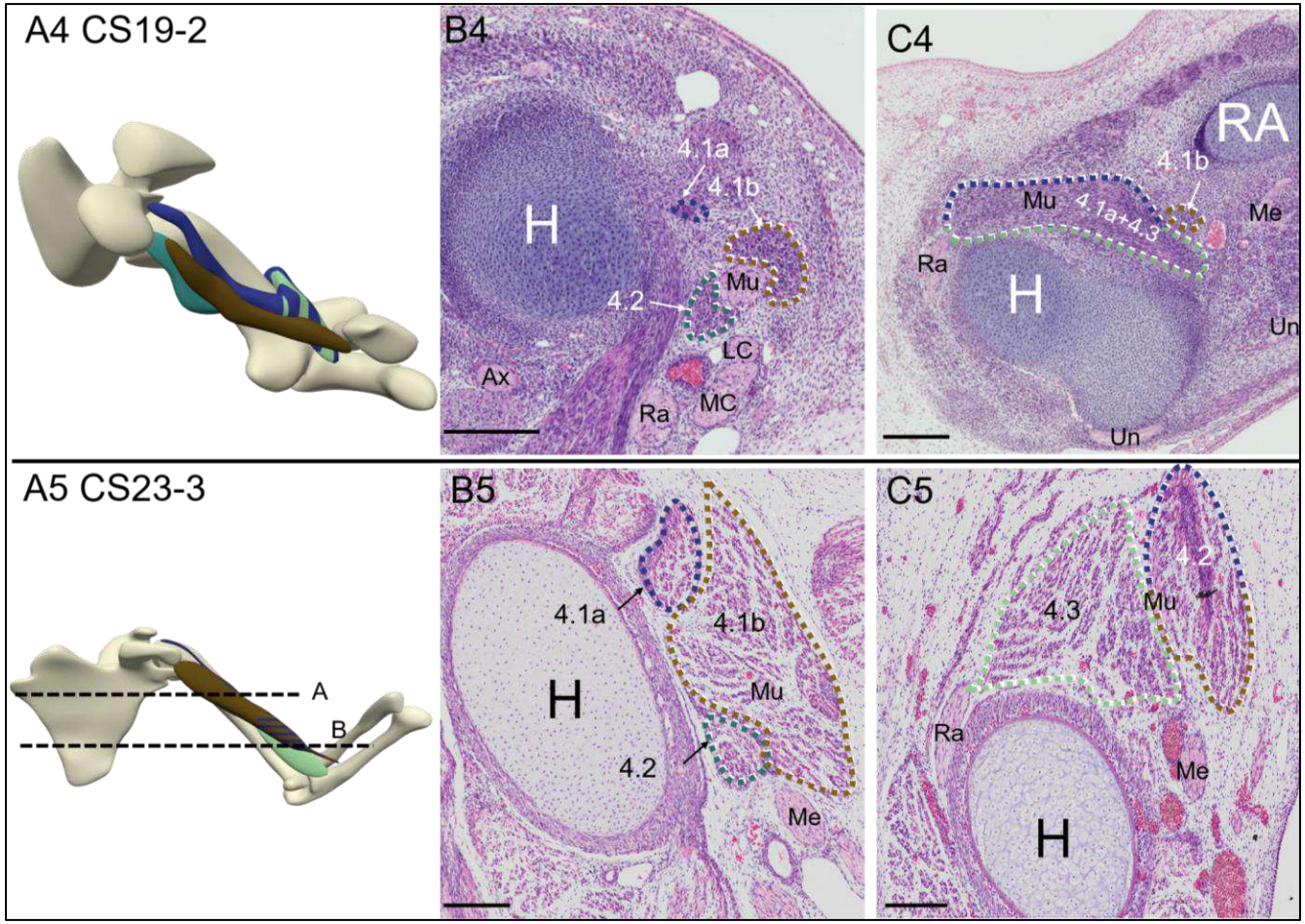

C1 CS18-1
C2
C3
C2
C3
D1 CS23-3
D2
D3
D2
D3
C2
R
2.2
2.1
Ax
S
D2
2.2
C
H
2.1
S
C3
R
Me
R
2.2
H
2.3
Ra
R
D3
2.2
R
Ste
2.3

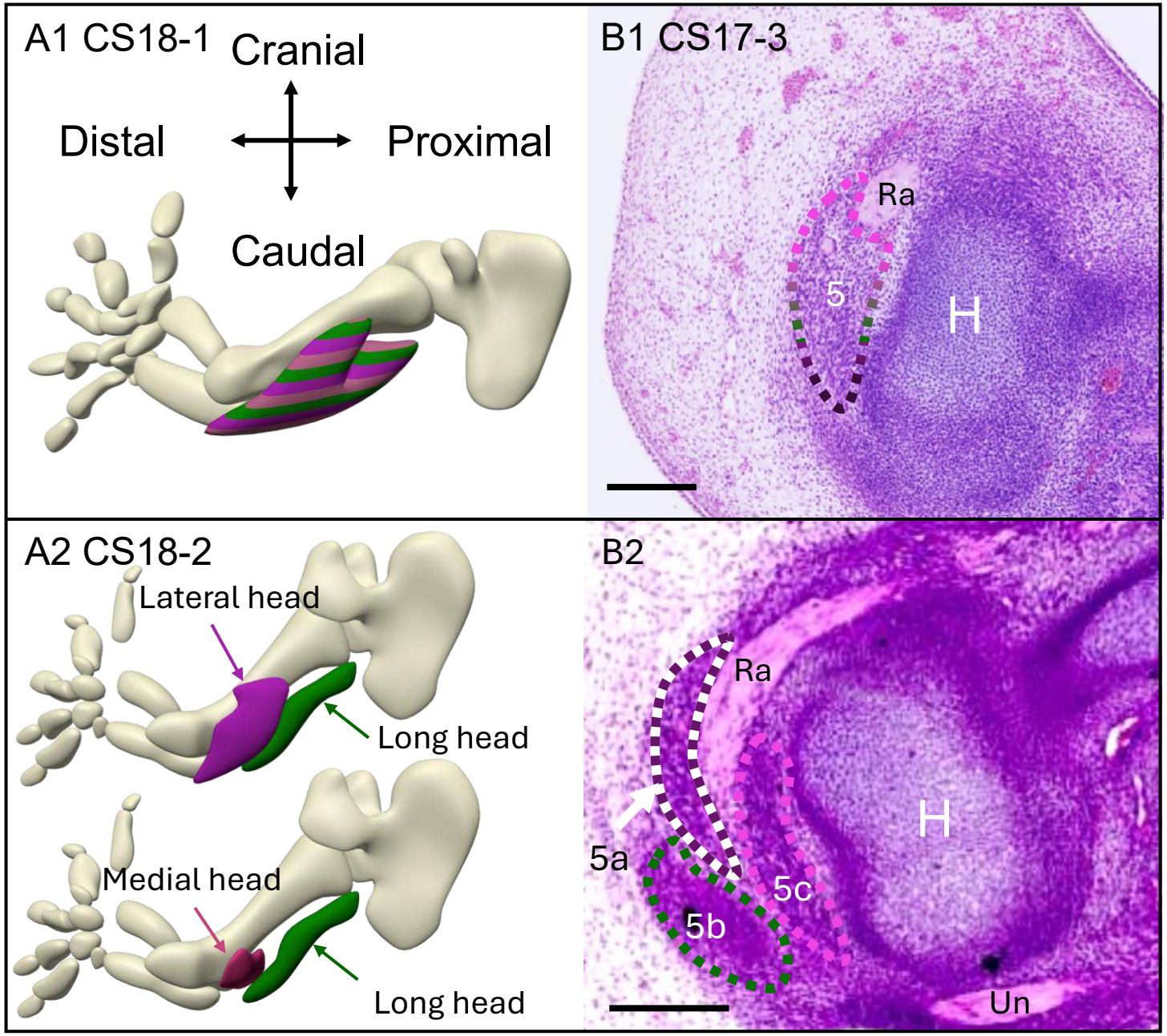

A3 CS18-2
B3
C3
S
3.1
Ax
3.2+3.3+3.4
H
A4 CS19-2
B4
C4
3.1
S
3.3
Ax
H
Sup
3.4
A5 CS23-1
B5
C5
3.4
R
3.2
3.1
S
1.3
H
3.3

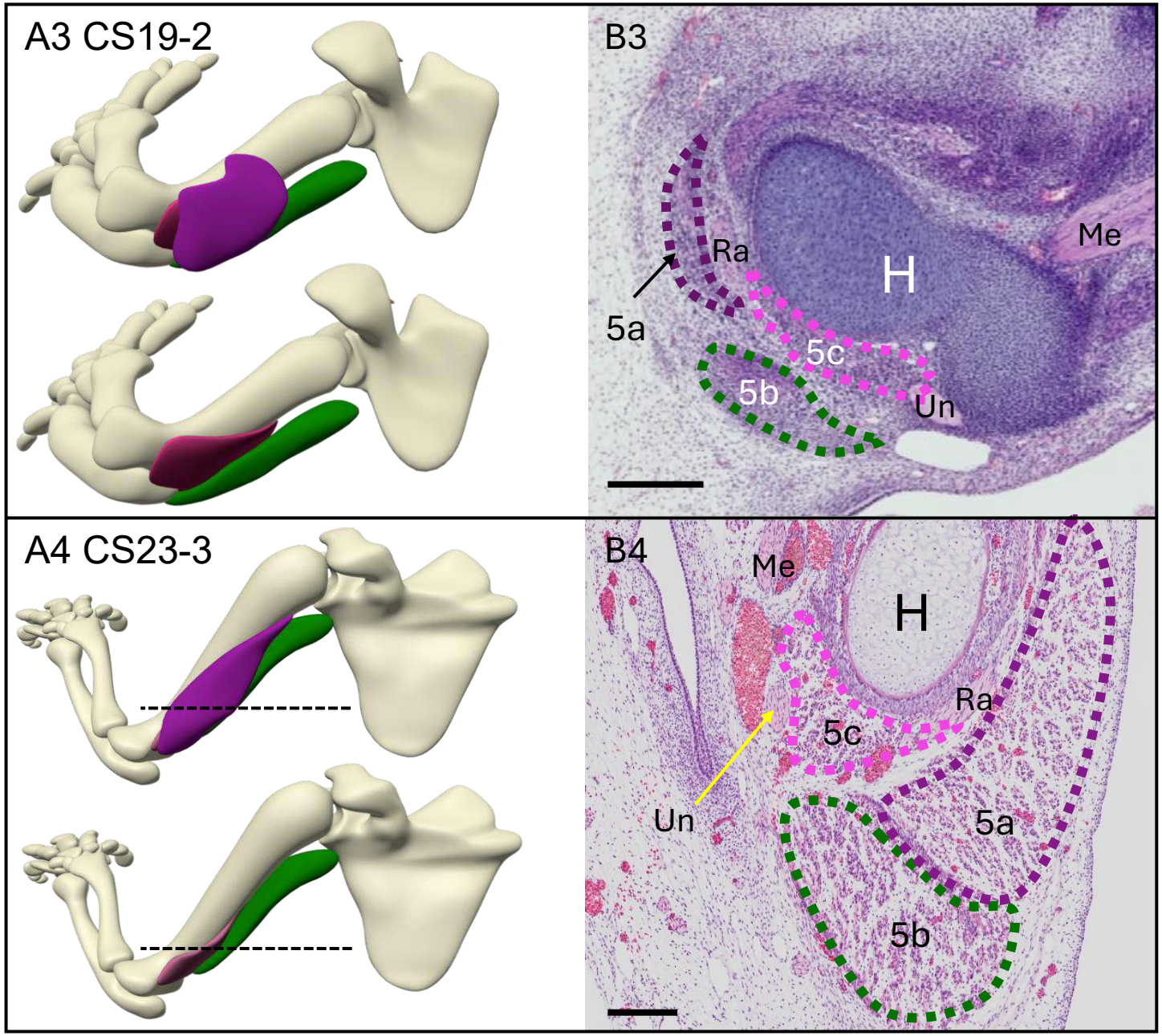

A4 CS19-2
B4
C4
3.1
S
3.3
Ax
H
Sup
3.4
A5 CS23-1
B5
C5
3.4
R
3.2
S
1.3
3.1
H
3.3

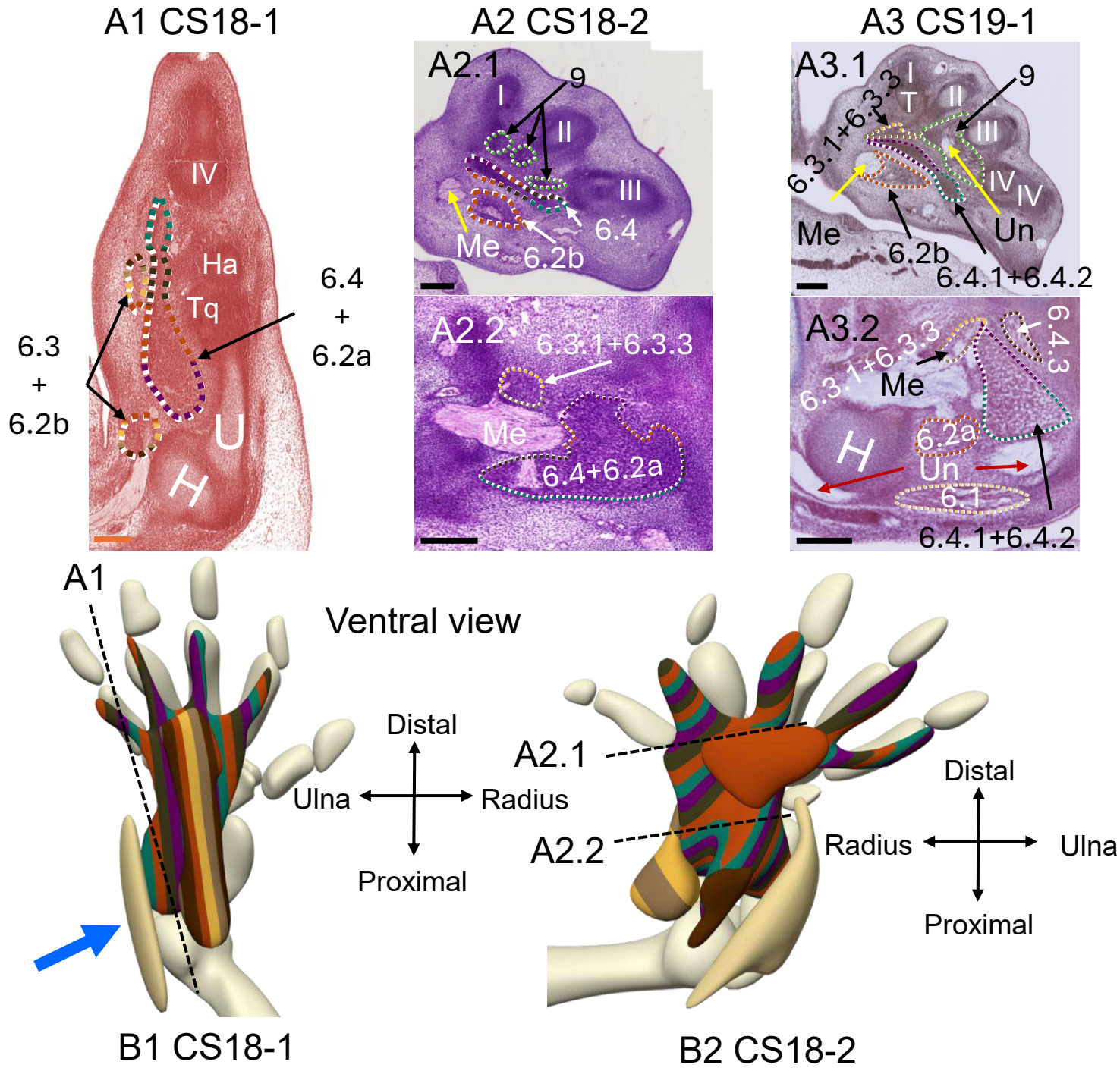

A1 CS18-2
Cranial
Distal
Proximal
Caudal
C1
B1
B1
S
3.1
Ax
3.1
3.2+3.3 +3.4
H
Ax
C1
S
3.1
Ax
3.1
3.2+3.3 +3.4
Ax
H
A2 CS19-2
C2
B2
B2
3.1
Ax
S
H
3.4
3.1
3.2
C2
3.1
Ax
H
3.2
3.1
Ax

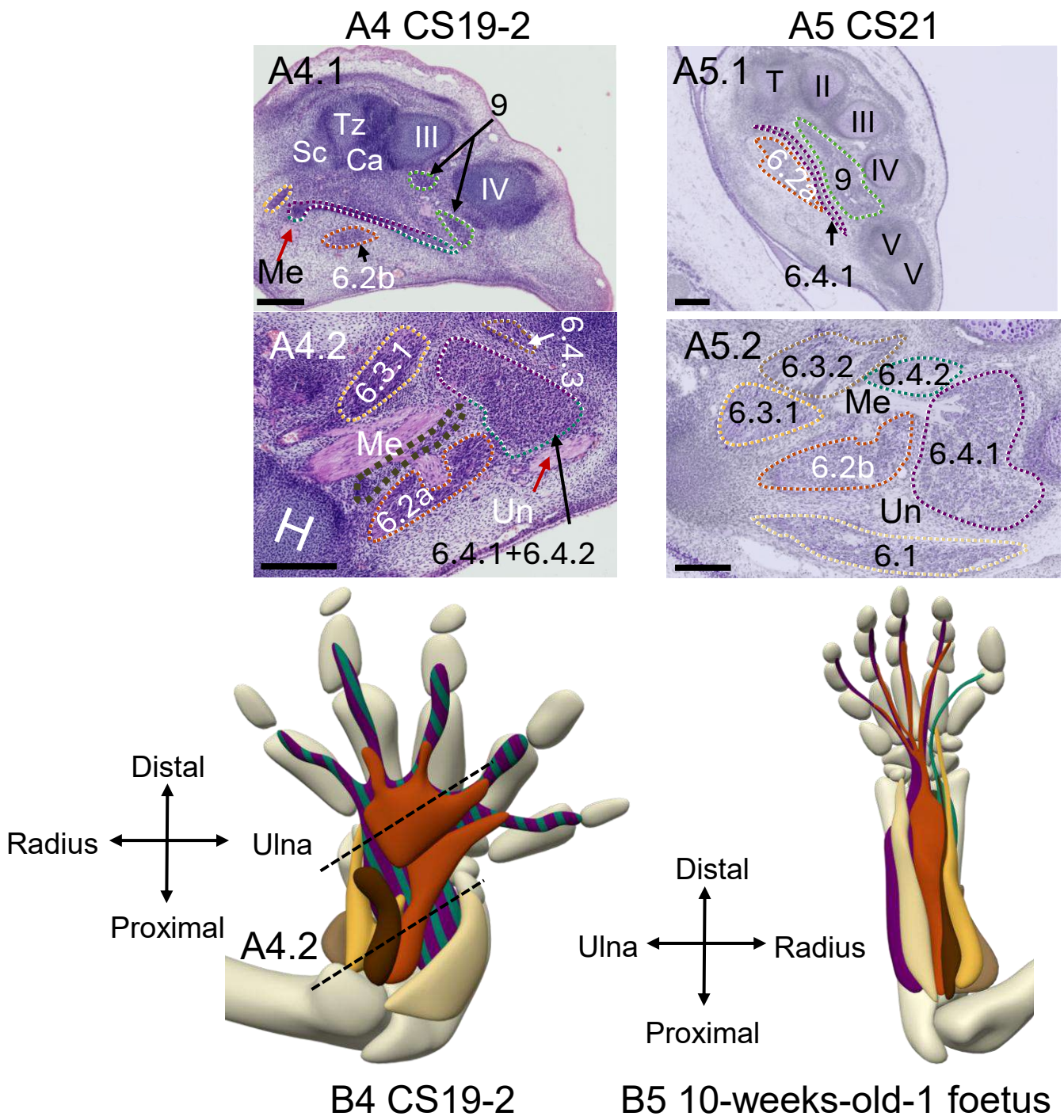

A1 CS17-1
Cranial
Proximal
Distal
Caudal
B1CS17-3
H
Ax
VM
Mu
Ra
LC
MC
C1
Mu
Ra
H
VM
Me
Un
A2 CS18-1
B2
Sup
S
Cn5
Ra
H
Mu
4
LPec
RA
A3 CS18-2
B3
Ax
Sup
4.1a
H
4.1b
4.2
Mu
Ax
LC
Ra
MC
C3
Mu
4.1+4.3
H
Ra
Me
Un

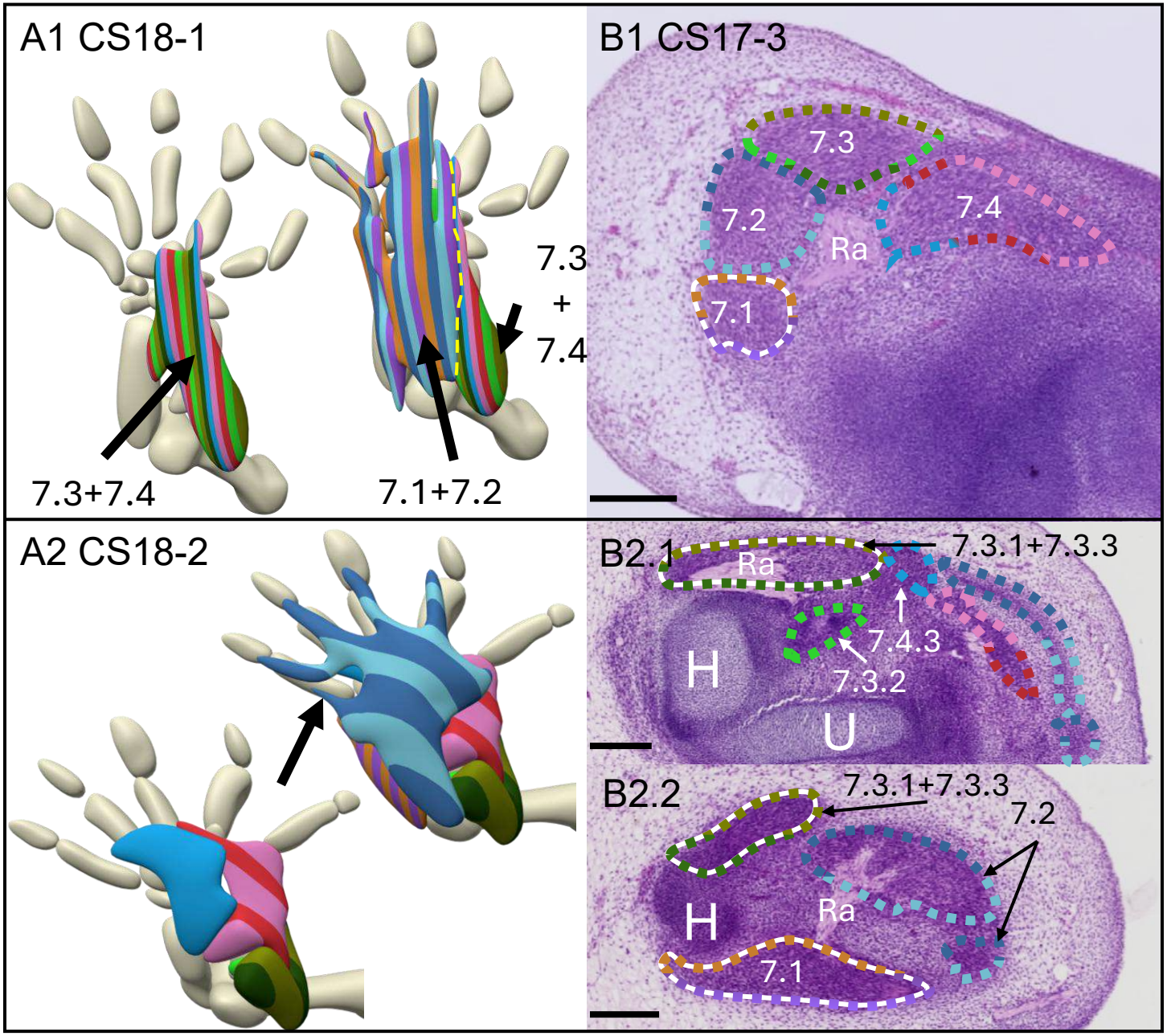

A4 CS19-2
B4
C4
4.1a
4.1b
H
Mu
4.2
LC
Ax
Ra
MC
RA
Mu
4.1a+4.3
Me
Ra
H
Un
Un
A5 CS23-3
B5
C5
A
B
4.1a
4.1b
H
Mu
4.2
Me
4.2
4.3
Mu
Ra
Me
H

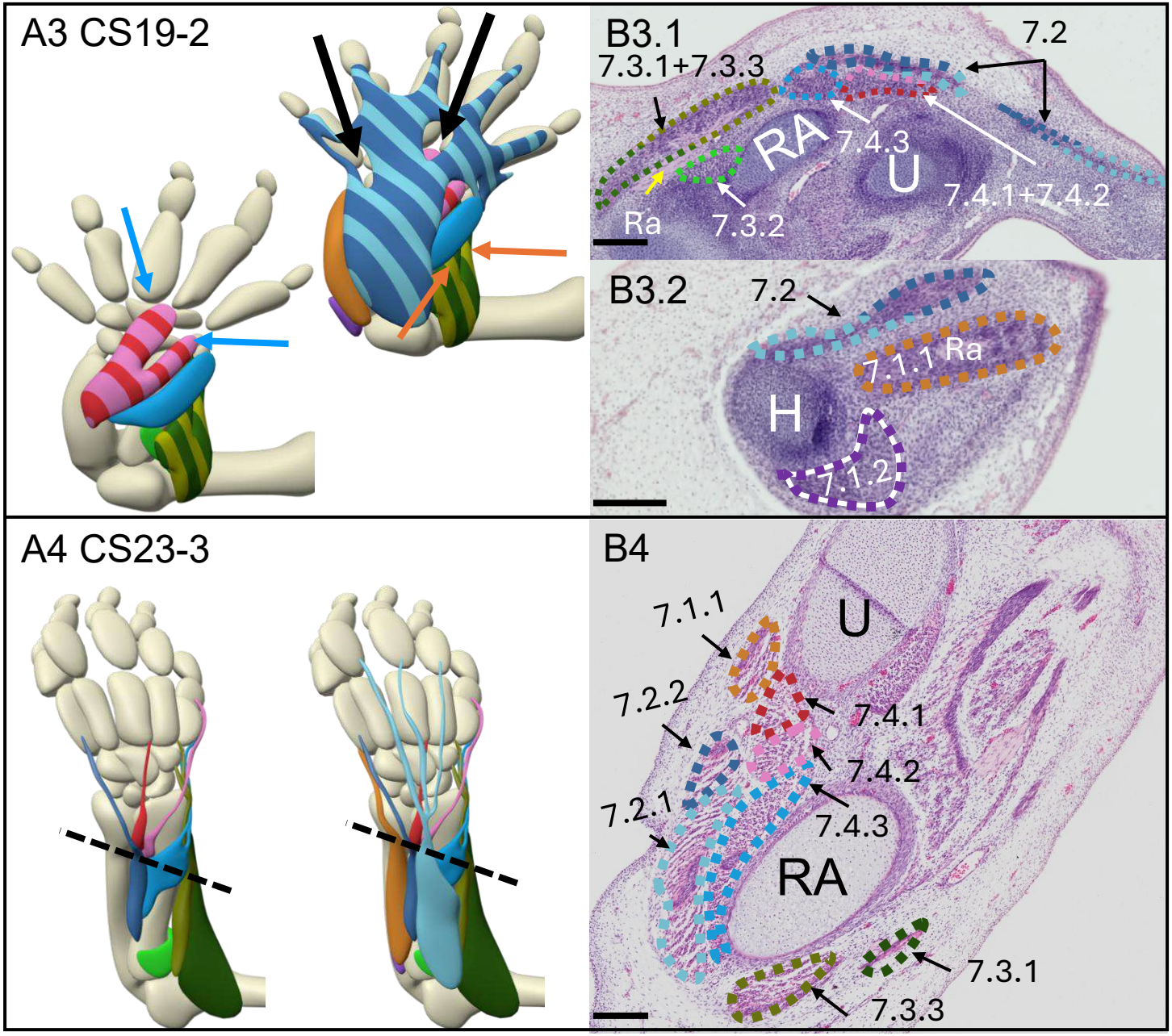

A1 CS18-1
Cranial
Distal
Proximal
Caudal
B1 CS17-3
Ra
5
H
A2 CS18-2
Lateral head
Long head
Medial head
Long head
B2
Ra
H
5a
5c
5b
Un

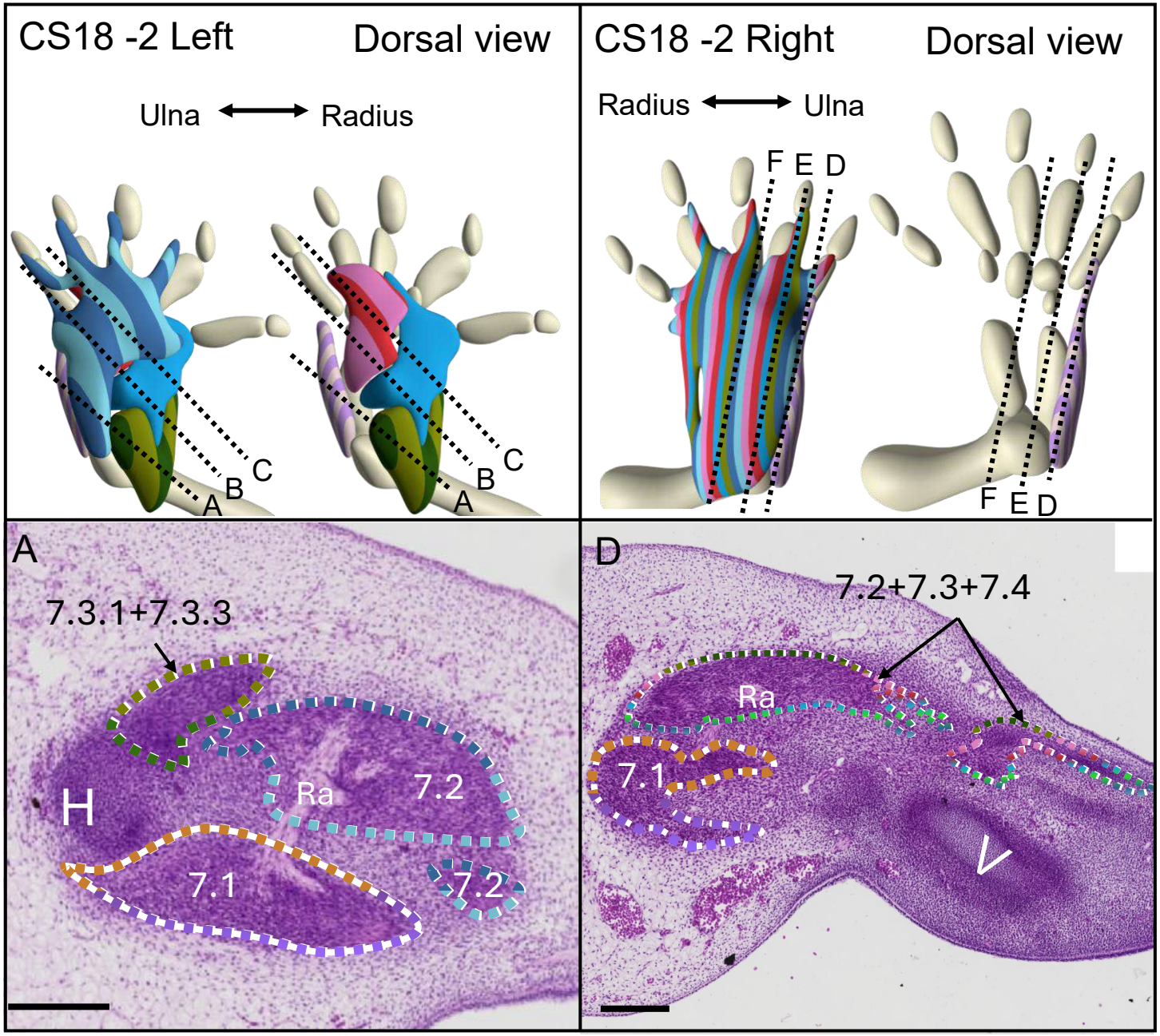

A3 CS19-2
B3
Ra
H
Me
5a
5c
5b
Un
A4 CS23-3
B4
Me
H
Ra
5c
Un
5a
5b

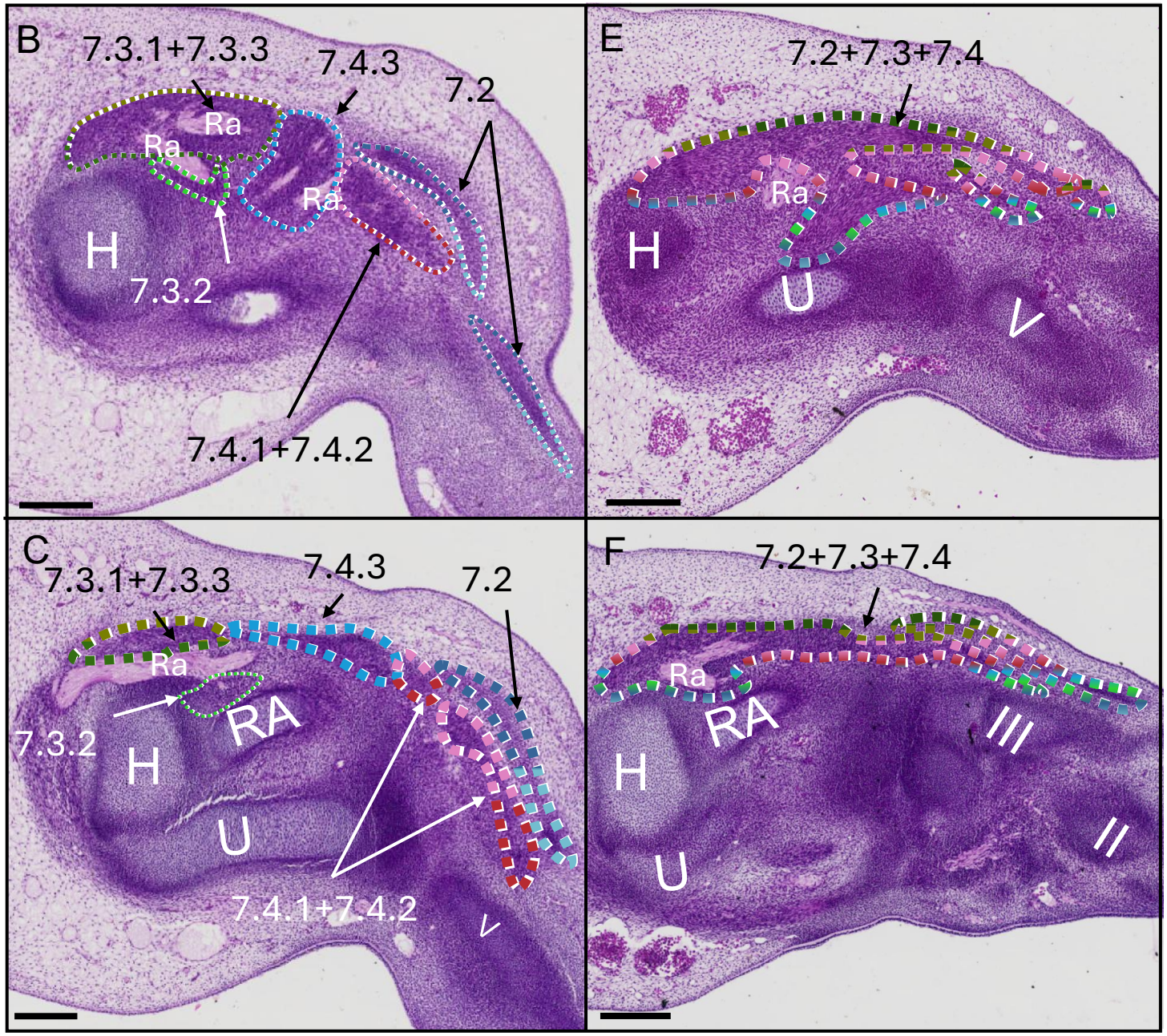

A1 CS18-1
A2 CS18-2
A3 CS19-1
IV
Ha
Tq
U
H
6.3
+
6.2b
6.4
+
6.2a
A2.1
I
9
II
III
6.4
Me
6.2b
A2.2
6.3.1+6.3.3
Me
6.4+6.2a
A3.1
I
T
II
9
III
6.3.1+6.3.3
IV
IV
Me
6.2b
Un
6.4.1+6.4.2
A3.2
6.3.1+6.3.3
6.4.3
Me
6.2a
H
Un
6.1
6.4.1+6.4.2
A1
Ventral view
Distal
Ulna
Radius
Proximal
A2.1
A2.2
Distal
Radius
Ulna
Proximal
B1 CS18-1
B2 CS18-2


A4 CS19-2
A5 CS21
A4.1
Tz
Sc
Ca
III
9
IV
Me
6.2b
A5.1
T
II
III
6.2b
9
IV
V
6.4.1
V
A4.2
6.3.1
6.4.3
Me
6.2a
Un
H
6.4.1+6.4.2
A5.2
6.3.2
6.4.2
6.3.1
Me
6.2b
6.4.1
Un
6.1
Distal
Radius
Ulna
Proximal
A4.2
Distal
Ulna
Radius
Proximal
B4 CS19-2
B5 10-weeks-old-1 foetus

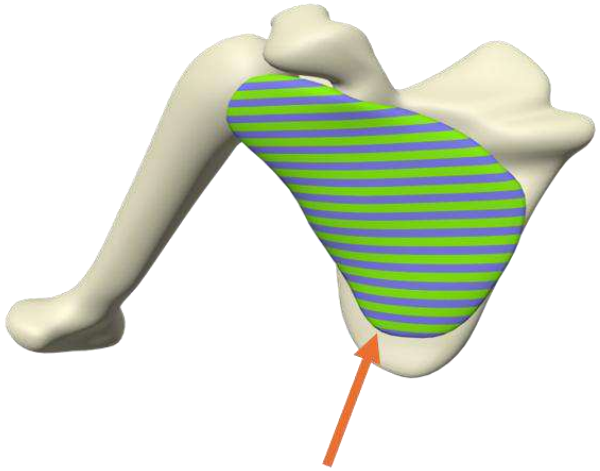

A1 CS18-1
7.3+7.4
7.1+7.2
7.3
+
7.4
B1 CS17-3
7.3
7.2
Ra
7.4
7.1
A2 CS18-2
B2.1
Ra
7.3.1+7.3.3
7.4.3
7.3.2
H
U
B2.2
7.3.1+7.3.3
7.2
H
Ra
7.1


A3 CS19-2
B3.1
7.3.1+7.3.3
7.2
RA
7.4.3
U
7.4.1+7.4.2
Ra
7.3.2
B3.2
7.2
7.1.1 Ra
H
7.1.2
A4 CS23-3
B4
7.1.1
U
7.2.2
7.4.1
7.4.2
7.2.1
7.4.3
RA
7.3.1
7.3.3


CS18 -2 Left
Dorsal view
Ulna
Radius
A
B
C
CS18 -2 Right
Dorsal view
Radius
Ulna
F E D
A
7.3.1+7.3.3
H
Ra
7.2
7.1
7.2
D
7.2+7.3+7.4
Ra
7.1
V

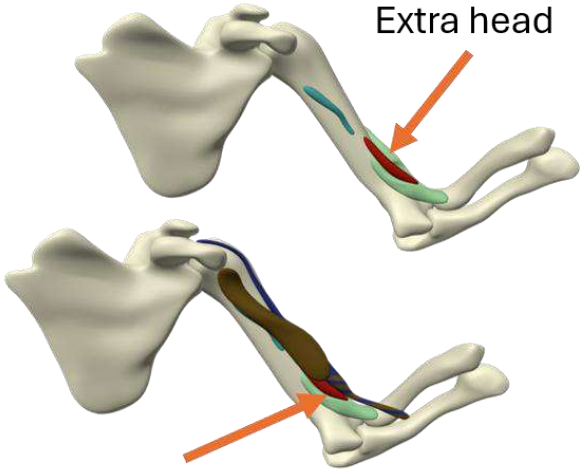

B
7.3.1+7.3.3
7.4.3
7.2
Ra
Ra
Ra
H
7.3.2
7.4.1+7.4.2
E
7.2+7.3+7.4
Ra
H
U
V
C
7.3.1+7.3.3
7.4.3
7.2
Ra
7.3.2
RA
H
U
7.4.1+7.4.2
V
F
7.2+7.3+7.4
Ra
RA
III
H
II
U

A1 Dorsal view

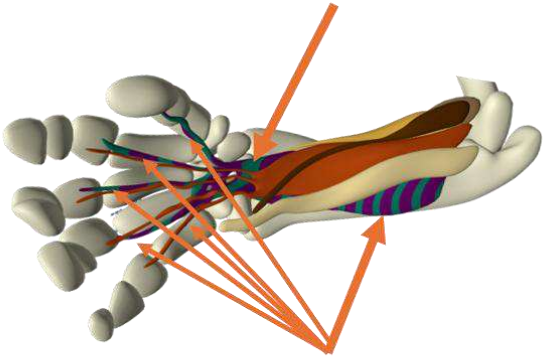


Infraspinatus +
teres minor

B1 Ventral view

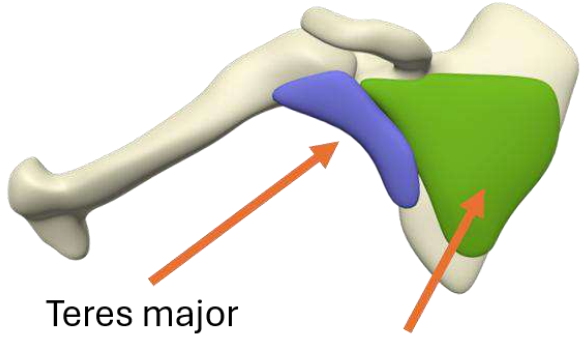


C1 Ventral view

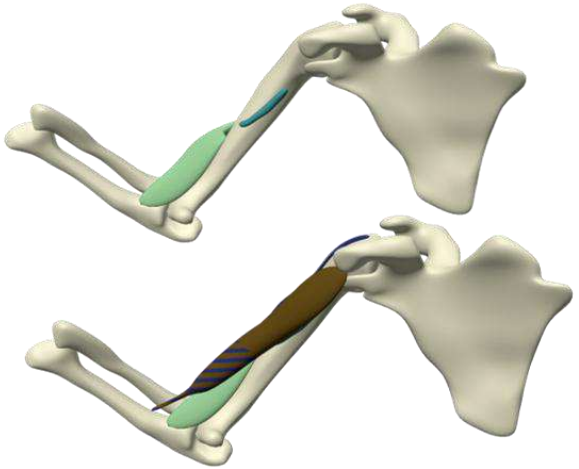


Flexor digitorum profundus
+ flexor pollicis longus

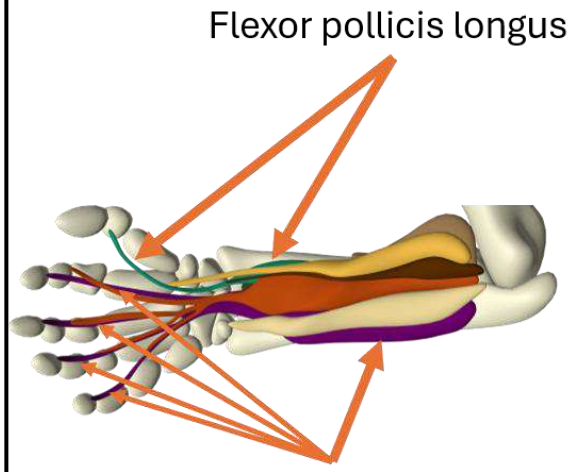
A2



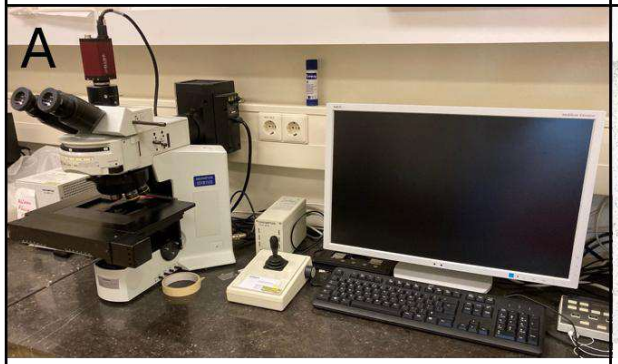
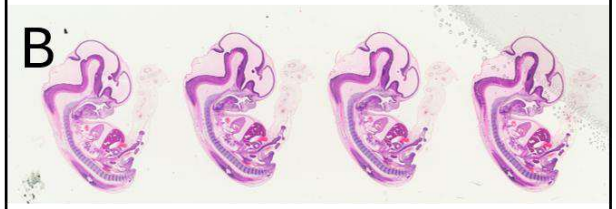
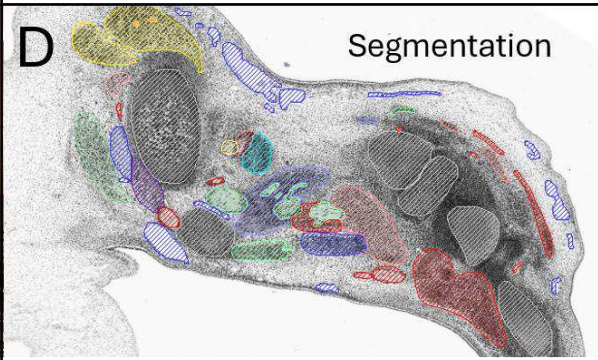
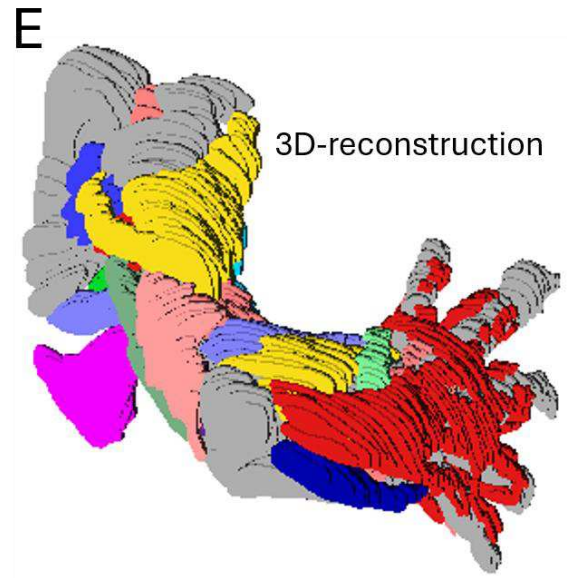
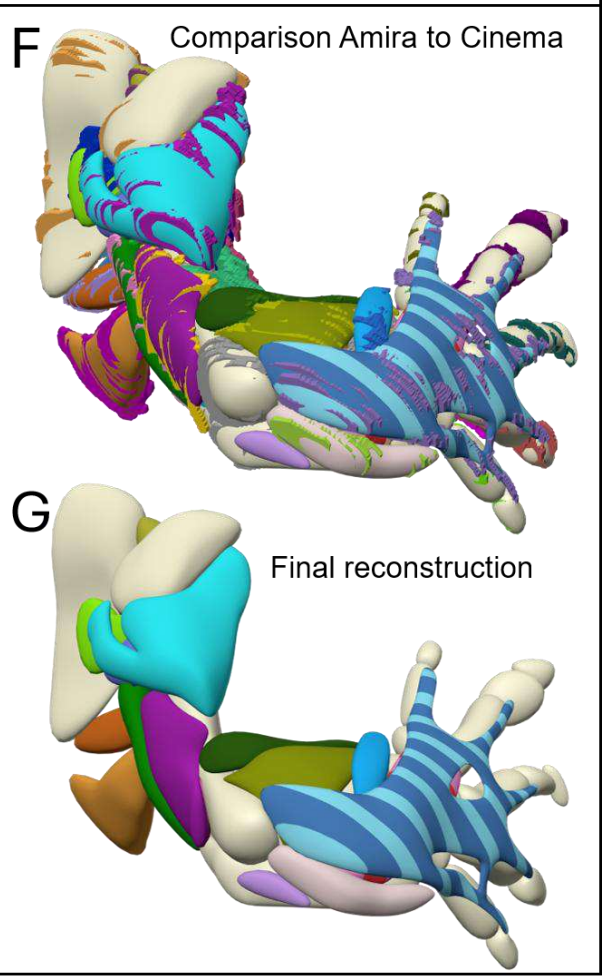
B2



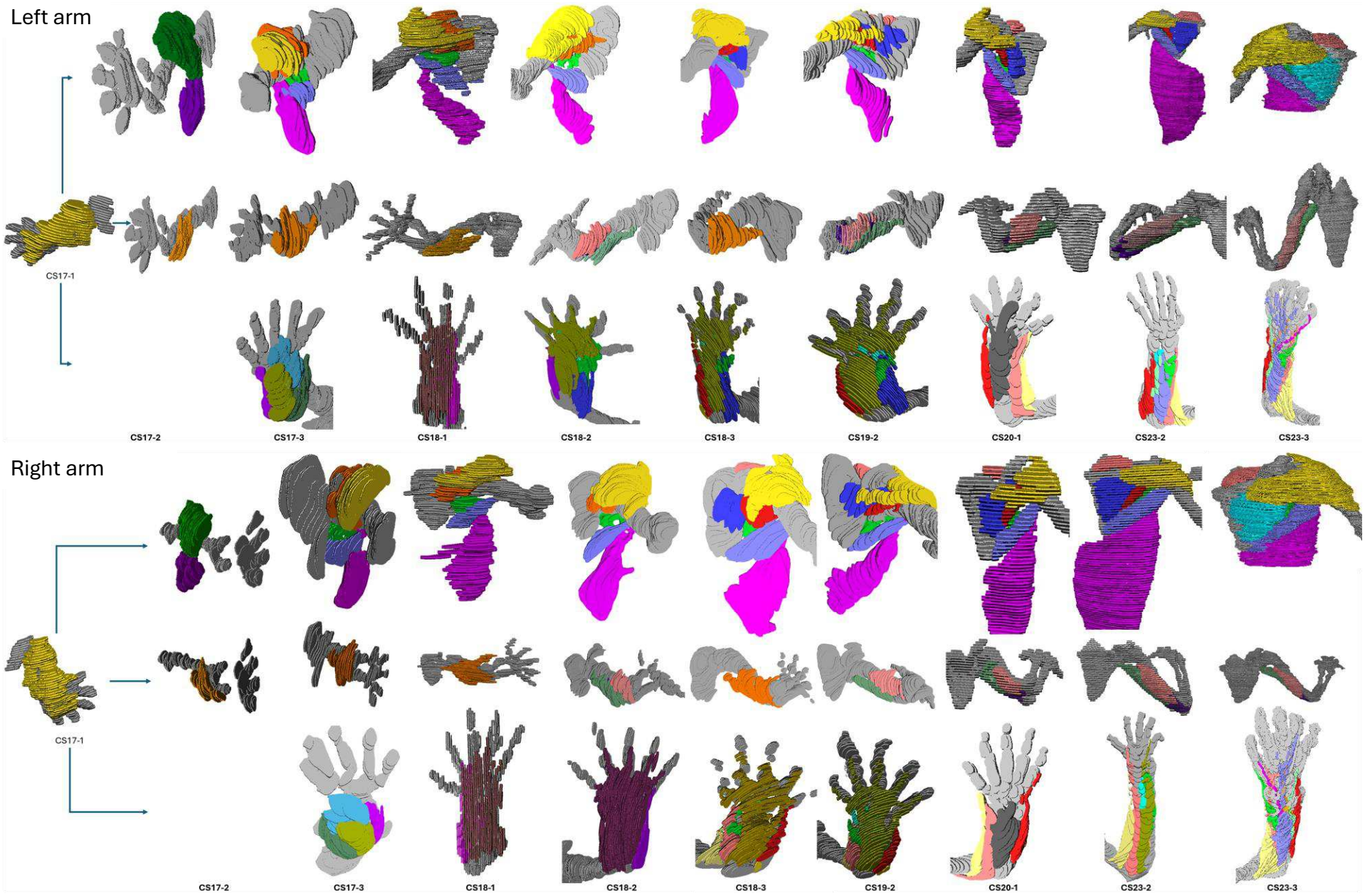
C2



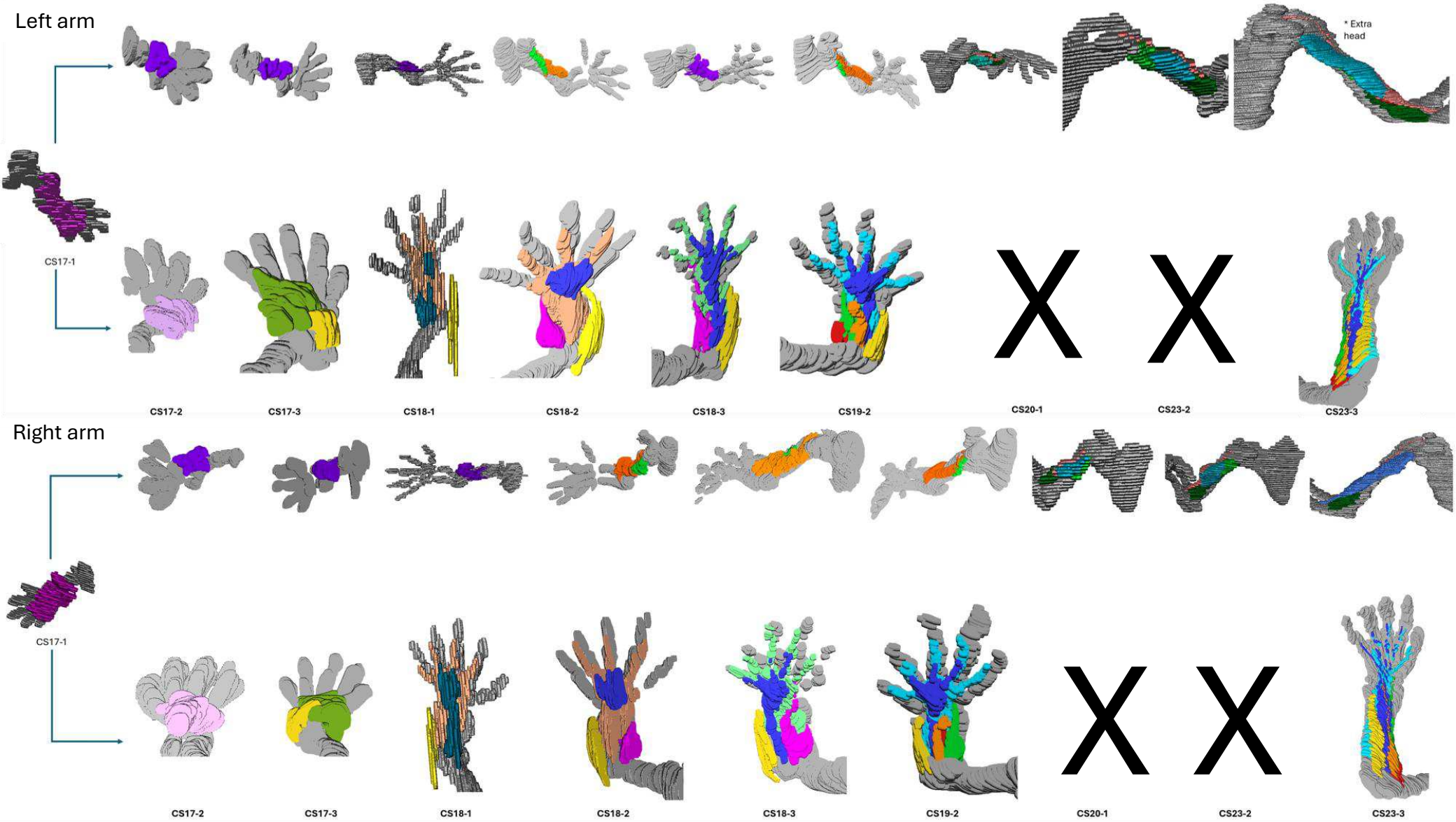
S1

1.Digitising histological sections	2. Reconstruction in Amira3D	3. Remodeling in Cinema4D
 Olympus BX61 scanning microscope  	 	

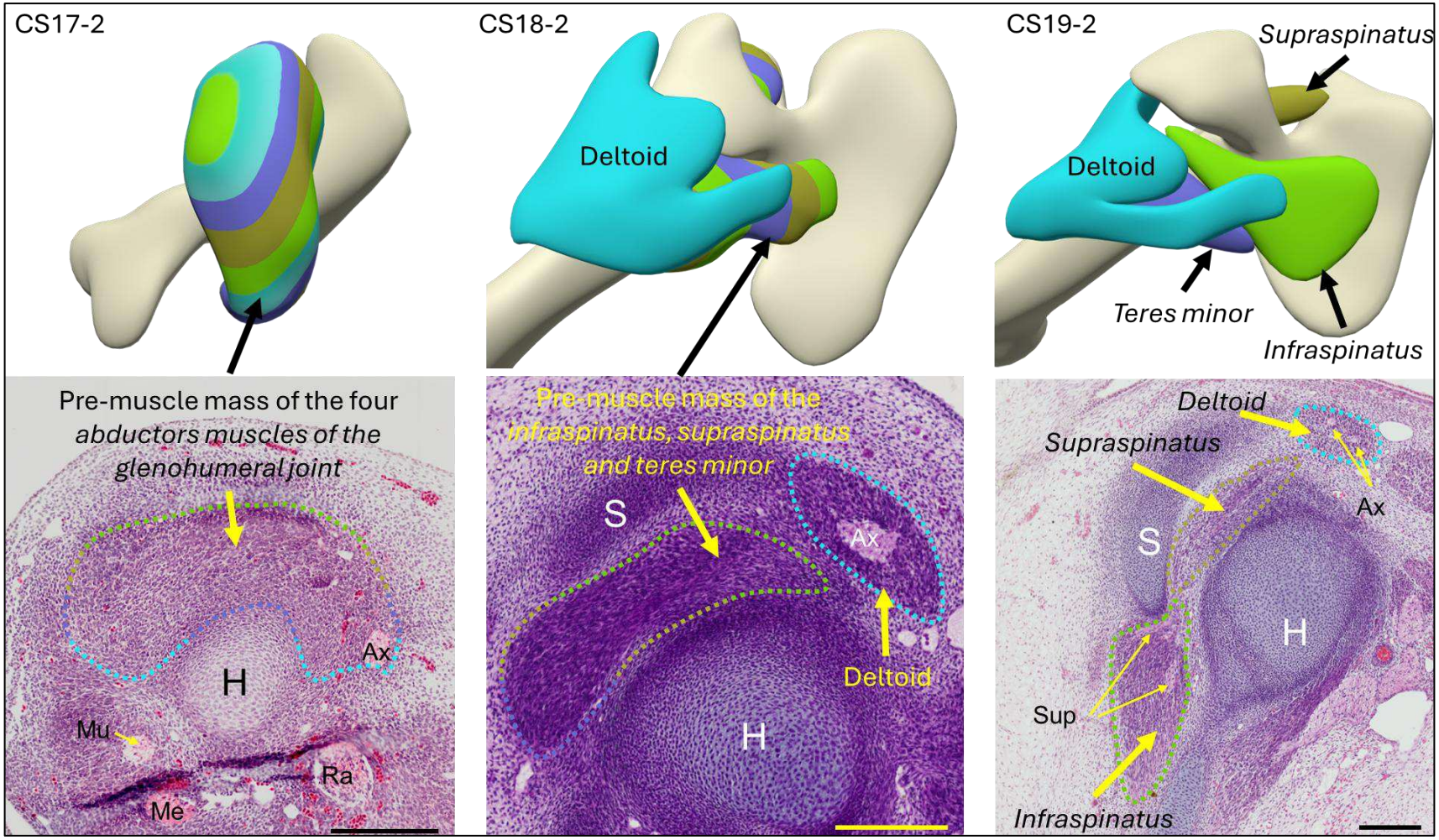
S2A


Left arm
CS17-1
CS17-2
CS17-3
CS18-1
CS18-2
CS18-3
CS19-2
CS20-1
CS23-2
CS23-3
Right arm
CS17-1
CS17-2
CS17-3
CS18-1
CS18-2
CS18-3
CS19-2
CS20-1
CS23-2
CS23-3

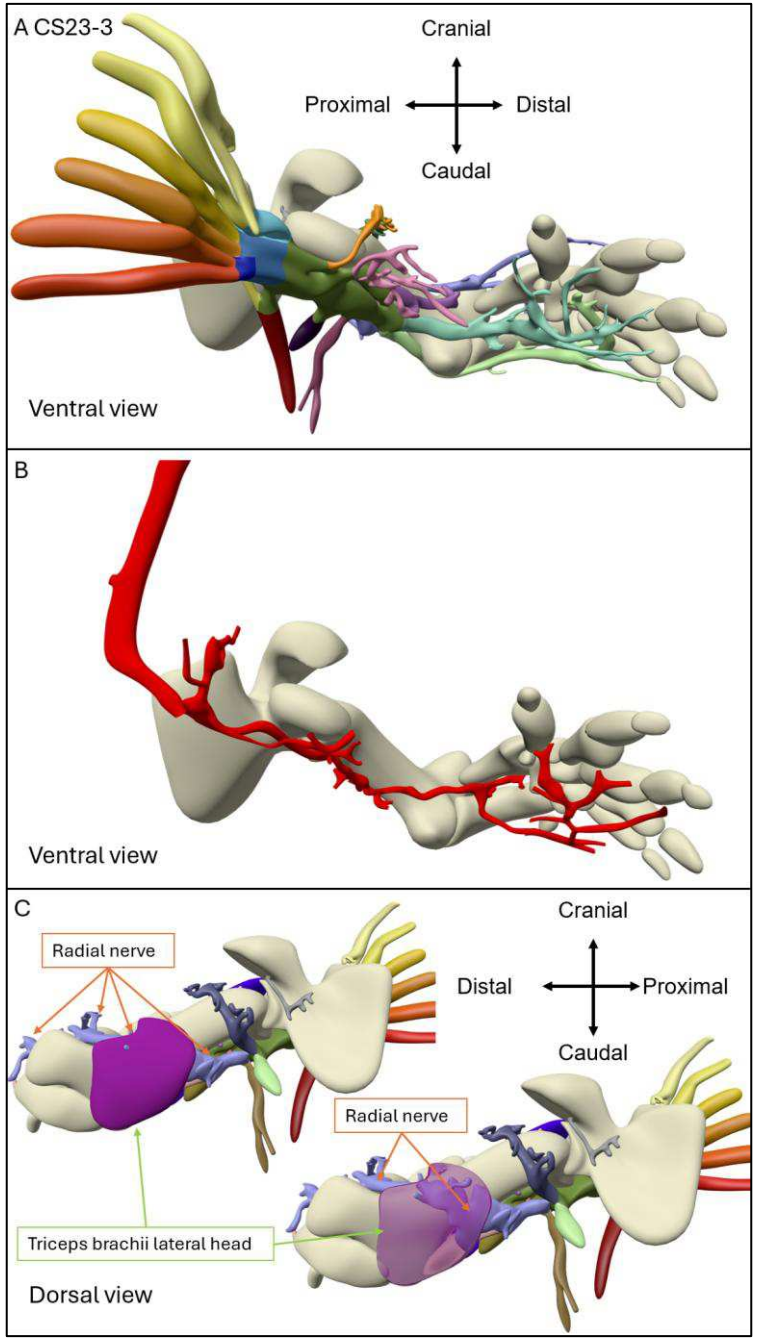
S2B


Left arm
* Extra head
CS17-1
CS17-2
CS17-3
CS18-1
CS18-2
CS18-3
CS19-2
CS20-1
CS23-2
CS23-3
Right arm
CS17-1
CS17-2
CS17-3
CS18-1
CS18-2
CS18-3
CS19-2
CS20-1
CS23-2
CS23-3

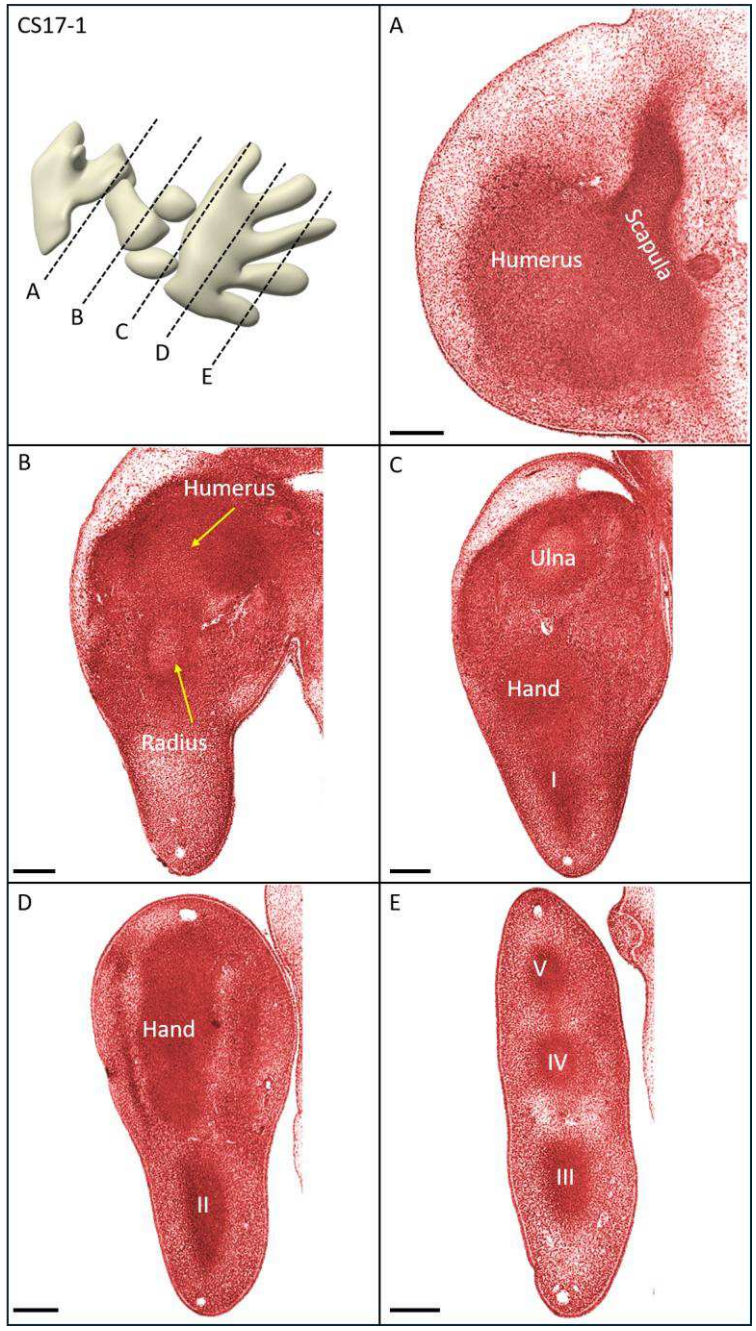
S3

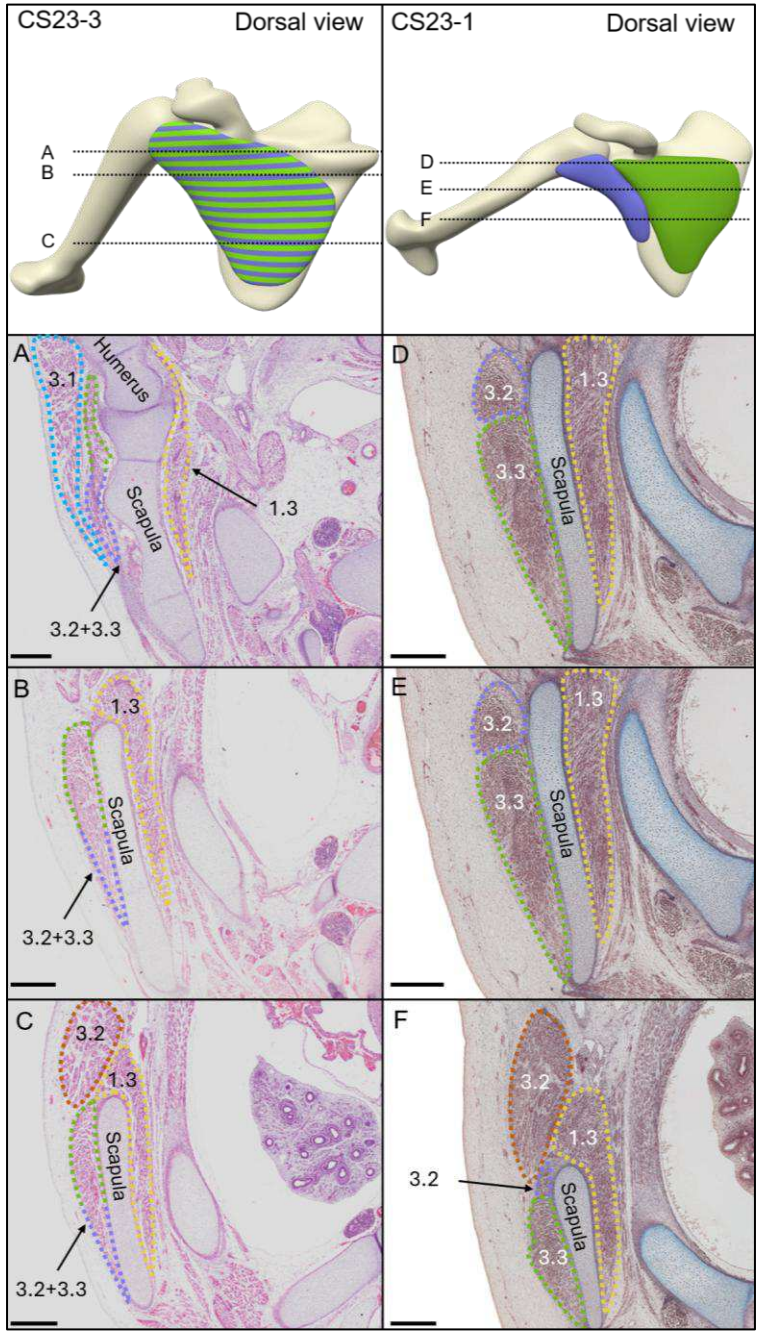

CS17-2
CS18-2
CS19-2
Deltoid
Supraspinatus
Deltoid
Teres minor
Infraspinatus
Pre-muscle mass of the four
abductors muscles of the
glenohumeral joint
H
Ax
Mu
Ra
Me
Pre-muscle mass of the
infraspinatus, supraspinatus
and teres minor
S
Ax
Deltoid
H
Deltoid
Supraspinatus
Ax
S
H
Sup
Infraspinatus

S4

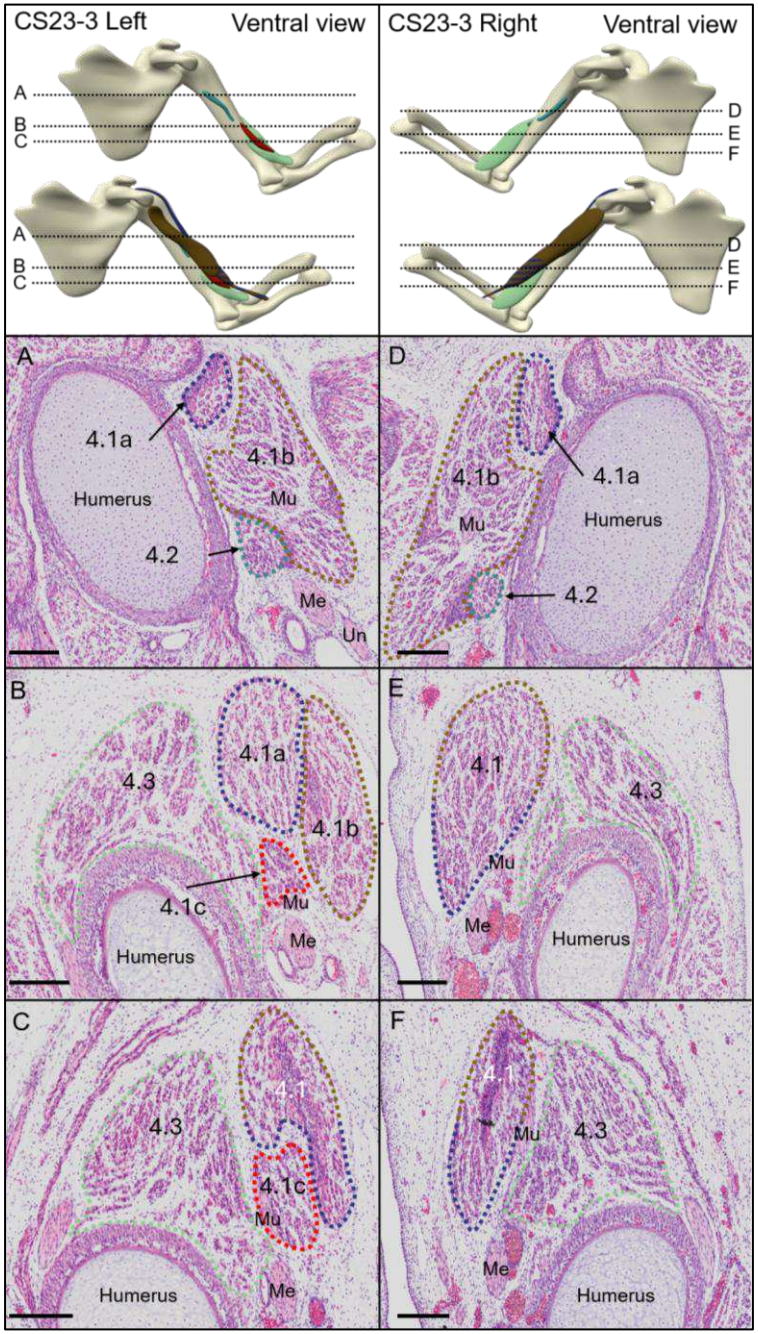

A CS23-3
Cranial
Proximal
Distal
Caudal
Ventral view
B
Ventral view
C
Radial nerve
Cranial
Distal
Proximal
Caudal
Radial nerve
Triceps brachii lateral head
Dorsal view

S11

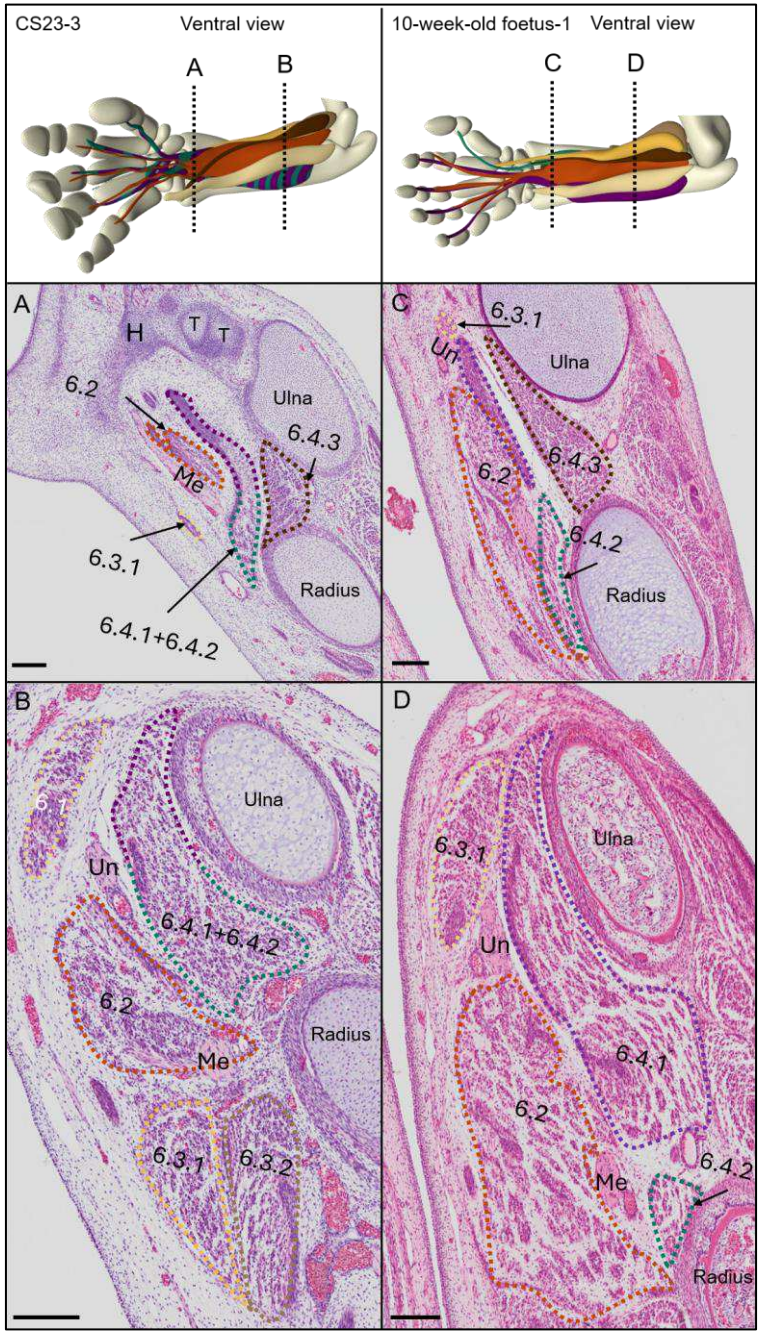

CS17-1
A
B
C
D
E
A
Humerus
Scapula
B
Humerus
Radius
C
Ulna
Hand
I
D
Hand
II
E
V
IV
III


CS23-3
Dorsal view
CS23-1
Dorsal view
A
B
C
D
E
F
A
3.1
Humerus
Scapula
1.3
3.2+3.3
D
3.2
1.3
3.3
Scapula
B
1.3
Scapula
3.2+3.3
E
3.2
1.3
3.3
Scapula
C
3.2
1.3
Scapula
3.2+3.3
F
3.2
1.3
3.2
Scapula
3.3

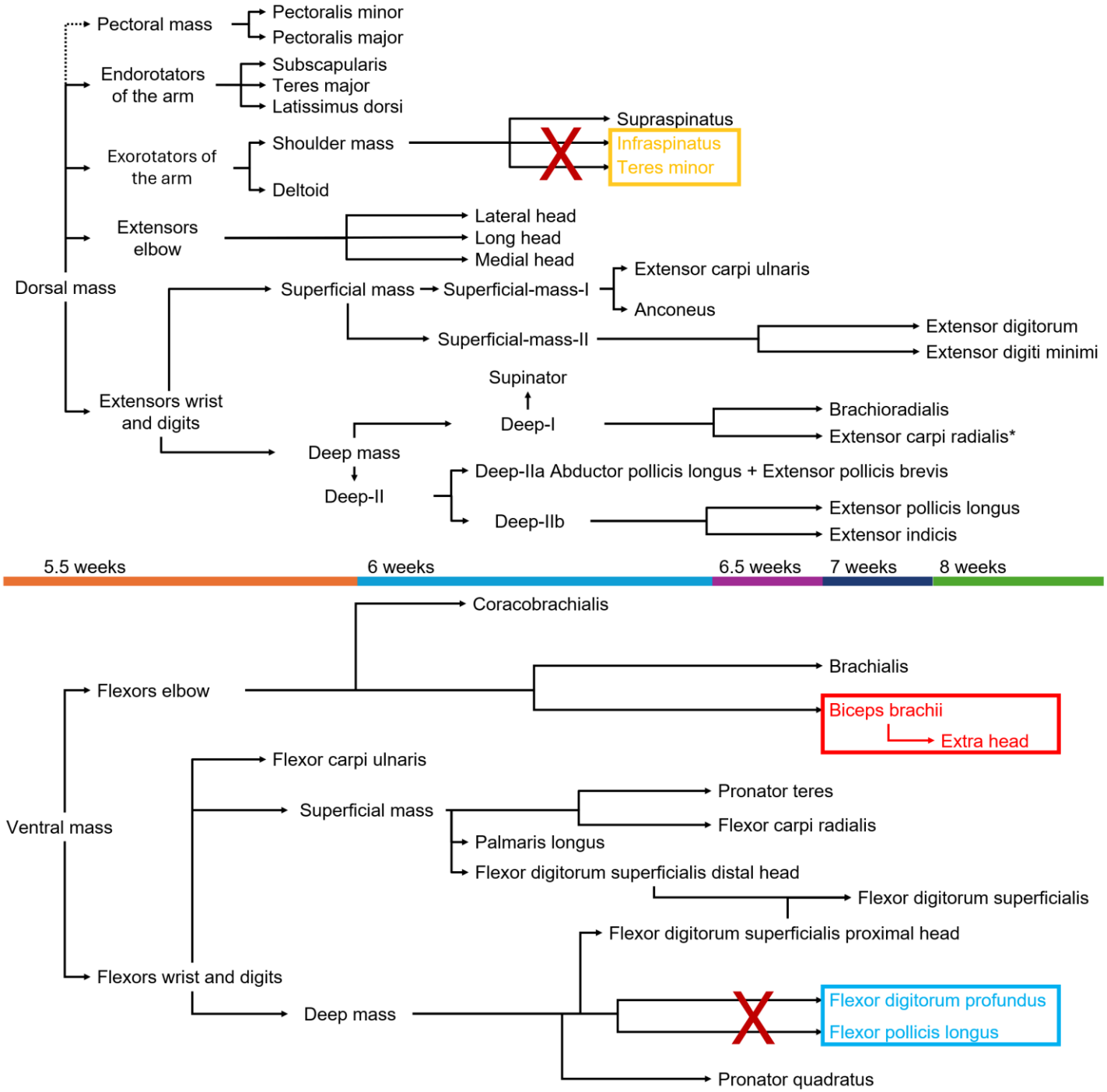
S13

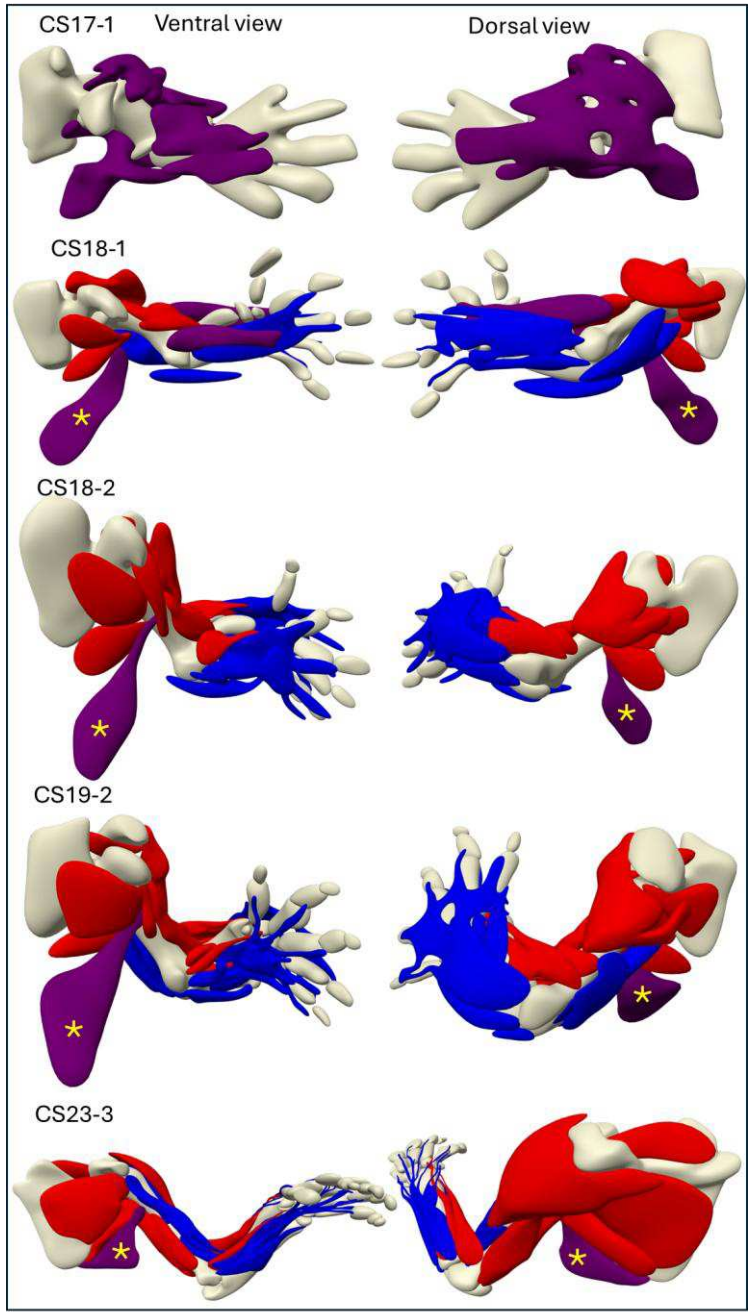

CS23-3 Left
Ventral view
CS23-3 Right
Ventral view
A
B
C
D
E
F
4.1a
4.1b
Mu
Humerus
4.2
Me
Un
4.3
4.1c
4.1
Me
Humerus

S14


CS23-3
Ventral view
A
B
10-week-old foetus-1
Ventral view
C
D
A
H
T
T
6.2
Ulna
6.4.3
Me
6.3.1
Radius
6.4.1+6.4.2
C
6.3.1
Un
Ulna
6.2
6.4.3
6.4.2
Radius
B
Ulna
Un
6.4.1+6.4.2
6.2
Radius
Me
6.3.1
6.3.2
D
6.3.1
Ulna
Un
6.4.1
6.2
6.4.2
Me
Radius

S15


Pectoral mass
Pectoralis minor
Pectoralis major
Endorotators of the arm
Subscapularis
Teres major
Latissimus dorsi
Exorotators of the arm
Shoulder mass
Deltoid
Supraspinatus
Infraspinatus
Teres minor
Extensors elbow
Lateral head
Long head
Medial head
Dorsal mass
Superficial mass
Superficial-mass-I
Extensor carpi ulnaris
Anconeus
Superficial-mass-II
Extensor digitorum
Extensor digiti minimi
Supinator
Extensors wrist and digits
Deep-I
Brachioradialis
Extensor carpi radialis*
Deep mass
Deep-II
Deep-IIa Abductor pollicis longus + Extensor pollicis brevis
Deep-IIb
Extensor pollicis longus
Extensor indicis
5.5 weeks
6 weeks
6.5 weeks
7 weeks
8 weeks
Coracobrachialis
Flexors elbow
Brachialis
Biceps brachii
Extra head
Flexor carpi ulnaris
Ventral mass
Superficial mass
Pronator teres
Flexor carpi radialis
Palmaris longus
Flexor digitorum superficialis distal head
Flexor digitorum superficialis
Flexor digitorum superficialis proximal head
Flexors wrist and digits
Deep mass
Flexor digitorum profundus
Flexor pollicis longus
Pronator quadratus


CS17-1
Ventral view
Dorsal view
CS18-1
CS18-2
CS19-2
CS23-3

Supplementary Files

This is a list of supplementary files associated with this preprint. Click to download.

- FigureS6.3DPDFofembryoCS171.pdf
- FigureS9.3DPDFofembryoCS192.pdf
- FigureS10.3DPDFofembryoCS233.pdf
- FigureS8.3DPDFofembryoCS182.pdf
- FigureS5.3DPDFofembryoCS162.pdf
- FigureS7.3DPDFofembryoCS181.pdf